UM-HSRI-PF-75-2

A Computer Model of Steady-State and Transient Traction Forces and Aligning Moment Developed by Pneumatic Tires

by

Bertil Koch

January 1975

Highway Safety Research Institute/University of Michigan

HIGHWAY SAFETY RESEARCH INSTITUTE
Institute of Science and Technology
Huron Parkway and Baxter Road
Ann Arbor, Michigan 48105

APR 11 1975 file w/ report

THE UNIVERSITY OF MICHIGAN

April 11, 1975

Mr. John C. Scowcroft, Manager
Vehicle Safety Research Department
Motor Vehicle Manufacturers Association
320 New Center Building
Detroit, Michigan 48202

Dear Mr. Scowcroft:

Enclosed are 50 copies of Interim Document 9, "A Computer Model of Steady-State and Transient Traction Forces and Aligning Moment Developed by Pneumatic Tires." This document is a detailed report on our development of a semi-empirical tire model with transient traction response capability. It is the final report on Project #1, "Investigate the Influence of Rates of Change of Slip (lateral and longitudinal) on the Traction Field of the Pneumatic Tire," of the HSRI tire traction research program for fiscal year 1975.

Sincerely,

John T. Tielking
Project Director

jn

BIBLIOGRAPHIC DATA SHEET	1. Report No. UM-HSRI-PF-75-2	2.	3. Recipient's Accession No.

4. Title and Subtitle
A COMPUTER MODEL OF STEADY-STATE AND TRANSIENT TRACTION FORCES AND ALIGNING MOMENT DEVELOPED BY PNEUMATIC TIRES

5. Report Date
January 1975

6.

7. Author(s)
J.B.C. Koch

8. Performing Organization Rept. No. UM-HSRI-PF-75-2

9. Performing Organization Name and Address
Highway Safety Research Institute
University of Michigan
Huron Parkway and Baxter Road
Ann Arbor, Michigan 48105

10. Project Task Work Unit No.
329180

11. Contract/Grant No.

12. Sponsoring Organization Name and Address
Motor Vehicle Manufacturers Association
320 New Center Building
Detroit, Michigan 48202

13. Type of Report & Period Covered

14.

15. Supplementary Notes

Tire Traction Characteristics Affecting Vehicle Performance: Interim Document 9

16. Abstracts

This document presents the final report on the development of a semi-empirical tire model which has the capability of simulating steady-state and transient traction forces and aligning moment in response to combined longitudinal and lateral wheel slip. The model recognizes the tire-road friction force as a function of local position and velocity of tread element sliding within the contact region. Examples of steady-state and transient response calculations are given. Pure-digital and analog-digital (hybrid) computer programs are included.

17. Key Words and Document Analysis. 17a. Descriptors

Friction
Tire Model
Tire Traction
Tire Transients
Hybrid Computer Model

17b. Identifiers/Open-Ended Terms

17c. COSATI Field/Group

18. Availability Statement	19. Security Class (This Report)	21. No. of Pages
UNLIMITED	UNCLASSIFIED	163
	20. Security Class (This Page) UNCLASSIFIED	22. Price

UM-HSRI-PF-75-2

A COMPUTER MODEL OF STEADY-STATE AND TRANSIENT TRACTION FORCES AND ALIGNING MOMENT DEVELOPED BY PNEUMATIC TIRES

J. Bertil C. Koch

Project 329180

Tire Traction Characteristics
Affecting Vehicle Performance

Interim Document 9

January 1975

Sponsored by

The Motor Vehicle Manufacturers Association

CONTENTS

CONTENTS (Continued)

1. SCOPE OF THIS REPORT

The activities reported in this document were aimed at extending existing mathematical models of tire dynamics based on the representation of the carcass as a beam on a foundation and supplied with rubber elements for the tread pattern. The parent concept, developed by Pacejka [1], is centered on the dynamic behavior of the tread element mass points as they pass through the contact patch at various conditions of slip. The assumption in the parent concept—that the friction forces in the contact patch depend on the velocity of sliding between the tread element and road—has been retained in the present extension.

In this work, special emphasis has been put on the extension of Pacejka's model to include transitional behavior, as in shimmy, allowing for partial or full sliding. This, in turn, makes it possible to obtain frequency responses for lateral force and aligning moment at any mean slip angle. The model can also calculate longitudinal and lateral forces and aligning moment in a combined transient steering and braking or driving maneuver.

The model was tested by using property data for an FR70-14 tire. This tire was designated R70B in the HSRI tire testing program, and some experimental steady-state data on it were available [2].

The report contains selected results from these computations consisting of steady-state tread element sliding velocity and deflection distributions in the contact patch together with beam deflection and slope distribution, also within the contact patch.

The resulting steady-state longitudinal and lateral forces and aligning moment are given at various combinations of slip numbers.

The frequency responses of lateral force and aligning moment for a free-rolling tire subject to steer angle oscillations at zero mean angle are also presented.

2. BACKGROUND

The pneumatic tire is no doubt one of the most complex dynamic components utilized by a road vehicle. The complexity presents serious obstacles to the development of realistic mathematical representations of tire dynamic performance. In the study of the dynamic behavior of a passenger car with the aid of mathematical models, it is most often sufficient to let the moving parts be represented by rigid masses acted upon by point loads supplied by spring forces and/or damping forces. The tire, in contrast, is a flexible structure acted upon by distributed forces where, under certain conditions, the distribution of structure mass has to be considered. The distributed traction forces acting on the tire in the area in contact with the road surface constitute in themselves a problem since they are related to the not yet fully understood phenomenon of friction between two surfaces in relative stiction or sliding.

This complexity of the dynamics of the pneumatic tire and the lack of electronic computers in the early days of theoretical tire research in the 30's and 40's, coupled with the then prevailing trial-and-error experimentation in tire and auto industry research, is a partial explanation why the progress of mathematical representation of the dynamics of the tire has been slow in the beginning. Thus, it took

25 years from the publication in 1930 by Fromm [3] of his findings on the "law of the sideslip," based on an un-extensible carcass, till Fiala [4] in 1954 published his work on lateral force and moment of a tire with the flexible carcass modeled like a beam on an elastic foundation and supplied with tread blocks.

Gradually a strong need arose in the vehicle dynamics groups within the aircraft and auto industry to obtain a deeper knowledge and better understanding in such matters as vehicle stability and control. Also, during the last decade or so, governmental legislative efforts in this country have started setting up special requirements for standards of stability and control of motor vehicles.

This all amounts to a substantial increase over the last twenty years or so of research activities in the field of tire dynamics. With this has followed a need to resort more extensively to the mathematical model of the vehicle system as a tool for making short-cuts in laboratory and on-the-road experiments.

No doubt the tire plays a very important role in establishing the steering characteristics of a vehicle. This has resulted in the development of many ingenious, yet over-simplifying, mathematical descriptions of tire dynamics. Not until the advent of electronic computers (analog and digital), however, has it been possible to realize more

elaborate mathematical representations of the highly complex tire structure. Thus we witness during the last fifteen years an increased activity in the theoretical study of various aspects of tire dynamics. Some outstanding contributions to these efforts related to the phenomenon of shimmy are worth mentioning here.

The first theories on shimmy of modern wheel suspensions and tires were made by Wylie in 1939 [5] and by Kantrowitz in 1940 [6]. Their findings were based on a beam approximation of the carcass. In 1941, v.Schlippe and Dietrich [7] published their work that was to become a cornerstone in future developments on tire dynamics encountered in wheel shimmy. They added to the beam theory a finite contact length.

The tire shimmy theories have been extended over the years by, among others, Saito [8] and Segel [9].

All the previous works on shimmy have ignored the explicit treatment of the tread rubber. It was not until 1966 that Pacejka [10] added tread elements to the carcass in the fashion introduced by Fiala in 1954.

Among the areas of dynamics of the pneumatic tire that are receiving increasing consideration is the nature of the generation of the traction forces that are developed by the rolling tire in the interface between tire and road surface

in response to steady-state longitudinal and lateral slip and various oscillating slip modes. An understanding of the nature of these forces and the ability to predict them by calculations based on construction data and some basic physical properties of the tire and friction functions for the tire-road interface is the goal of these activities.

3. GENERAL ASSUMPTIONS

The carcass of the tire, which is assumed massless, is represented in the model by a laterally flexible cylindrical beam (tread base) on a foundation (tire walls). The tread rubber is assumed to consist of separate blocks. These blocks are represented by circumferentially interspaced tread elements attached to the beam. The elements contain mass. Due to lateral forces transferred through the tread elements in the contact patch and reactions in the foundation along the circumference of the beam, the beam deflects laterally without tilting. The calculation of its lateral deflection is based on the assumption that the cylindrical beam is circular. This implies that the effect on the lateral stiffness of the flattening of the curved beam in the contact area due to vertical load is disregarded. As an extension to this work, experimentally obtained Green-functions of the kind obtained by Savkoor [11] for the lateral deflection of a flattened tire subject to a lateral force can be used in lieu of the beam equation.

Longitudinal forces in the contact patch will rotate the circumferentially inextensible beam on the foundation and also translate the circular beam, allowing for a longitudinal translation of the contact patch.

The tread pattern is assumed to consist of individual rubber blocks that are discontinuous in the circumferential

direction. These blocks are replaced in the model by infinitely thin lugs across the width of the tire with a constant circumferential spacing of the elements. The elements deflect longitudinally and laterally when they are subject to traction forces in the contact patch. The deflections in the two directions are assumed to be independent of each other. The distribution and deflection of tread elements when braking and cornering is schematically given in Figure 3.1 (p. 9).

The mass of a tread element is assumed concentrated at its outer end. In order to allow longitudinal and lateral displacement of the element masses, they are attached to the belt by independent linear springs and dampers in the two directions. Since the motions of the tread elements are affected by inertia forces, they can vibrate with tire squeal frequency when the net damping exerted on them is small enough.

Since the beam is massless, the inertia forces on the beam at vibrational modes are missing, rendering the results only of a theoretical value at higher frequencies.

The distribution of vertical pressure in the contact patch is assumed laterally uniform and to have the function of a fourth-order parabola in the longitudinal sense. This seems a reasonable approximation according to Borgmann [12].

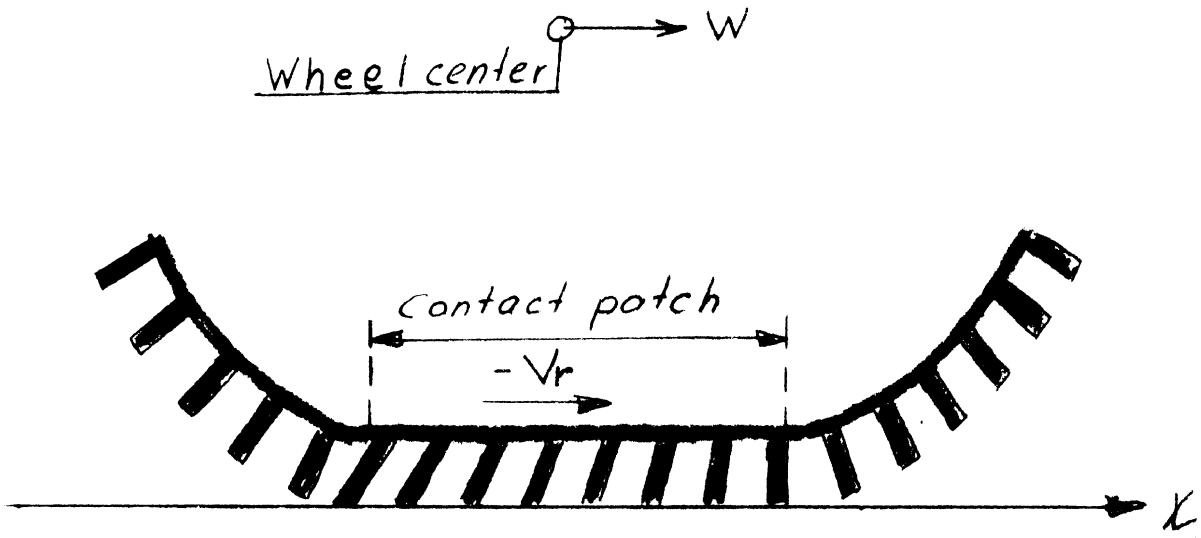

Longitudinal Deflection of
Elements When Braking

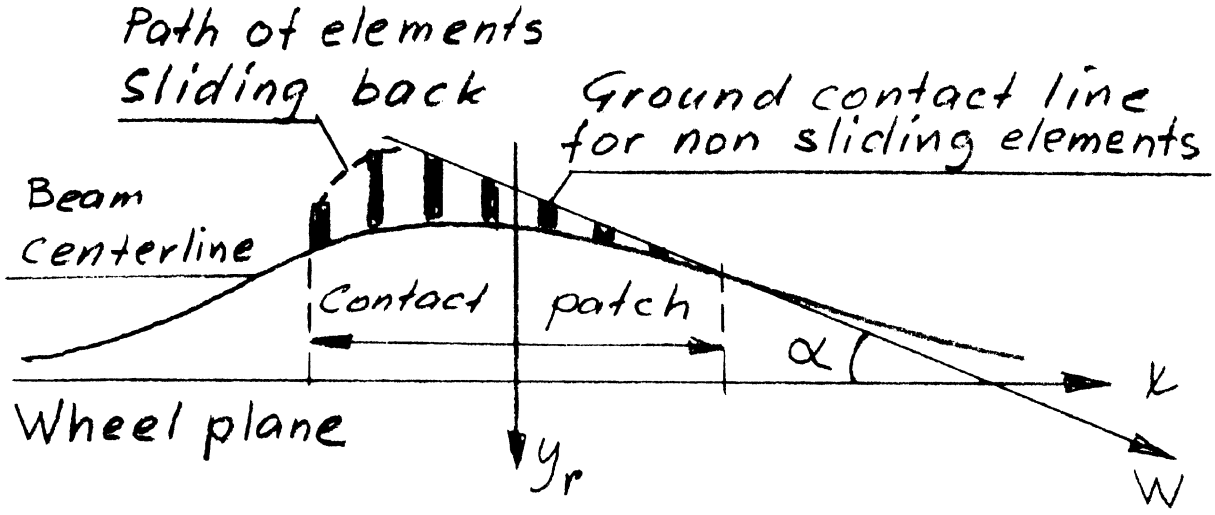

Lateral Deflection of Elements
And Beam When Cornering

Figure 3.1. Schematic of Deflection of Discontinuous Row of Infinitely Thin Elements.

The traction force on an element in the contact patch is determined by the normal contact pressure and the sliding-velocity-dependent friction coefficient. Due to the special character of this relationship at small sliding velocities, a relationship with a finite friction coefficient at zero velocity has been applied in this work.

The present study concerns three degrees of freedom of motion of the wheel (the mounting rim). These are rotation about the wheel spin axis, yawing motion about a vertical axis through the wheel center, and lateral translation of the wheel plane. Wheel camber is not considered.

4. MODEL DEVELOPMENT

4.1 GENERAL INFORMATION

The unloaded tire is assumed to exhibit a plane of symmetry, called the wheel plane, at right angles to the wheel axle (spin axis). The wheel center is located by the intersection of the spin axis with the wheel plane. A reference system, x_w, y_w (Fig. 4.1, p. 13), on the surface of the road is related to the steady-state motion of the wheel. The x_w-axis is in the intersection of the wheel plane and the road pointing in the direction of the wheel plane component of the steady-state translatory forward velocity of the wheel. The y_w-axis coincides with the projection of the wheel axis on the ground. Its direction is to the right when facing in the direction of the x_w-axis.

In the steady-state mode, the x_w, y_w system has a translatory velocity W relative to ground. The angle, α, between W and the x_w-axis is referred to as the slip angle.

In the free-rolling mode the longitudinal position of the midpoint of the contact patch is assumed to lie on the y_w-axis. Due to steady-state longitudinal forces, this center gets shifted a disance U_c along the x_w-axis. A coordinate system, x_r, y_r, is now defined with the x_r-axis coinciding with the x_w-axis and the origin at $x_w = U_c$.

This system has the property at steady-state that the x_r-axis lies in the wheel plane and the y_r-axis divides

longitudinally the length 2a of the contact patch into two equally long parts.

With reference to Figure 4.2, the transient motions of the wheel plane are introduced by the rotation $\alpha_y(t)$ and translation $y_L(t)$ of the wheel plane fixed system, x_t, y_t. It is understood that the rotation and translation are such that they give rise only to small increments (to the steady-state slip angle) of local slip angle along the contact patch. It is observed that a rotation of the wheel plane about the z_w-axis at a longitudinal slip will produce both a rotation of the x_t, y_t system as well as a translation.

Transients in the wheel plane are caused by changes of the x_w-component of W and/or the rotational velocity of the wheel.

The lateral deflection of the beam centerline relative to the wheel plan is $v_c(x)$, where x is the distance in the wheel plane from the origin of x_r or y_t.

4.2 EQUATIONS DESCRIBING TREAD ELEMENT MOTION

The translatory velocity, W, of the wheel gives rise to a lateral slip speed, V_{cy}, of the wheel plane.

$$V_{cy} = W \cdot \sin \alpha \tag{1}$$

The longitudinal speed, V_x, of the wheel center is given by

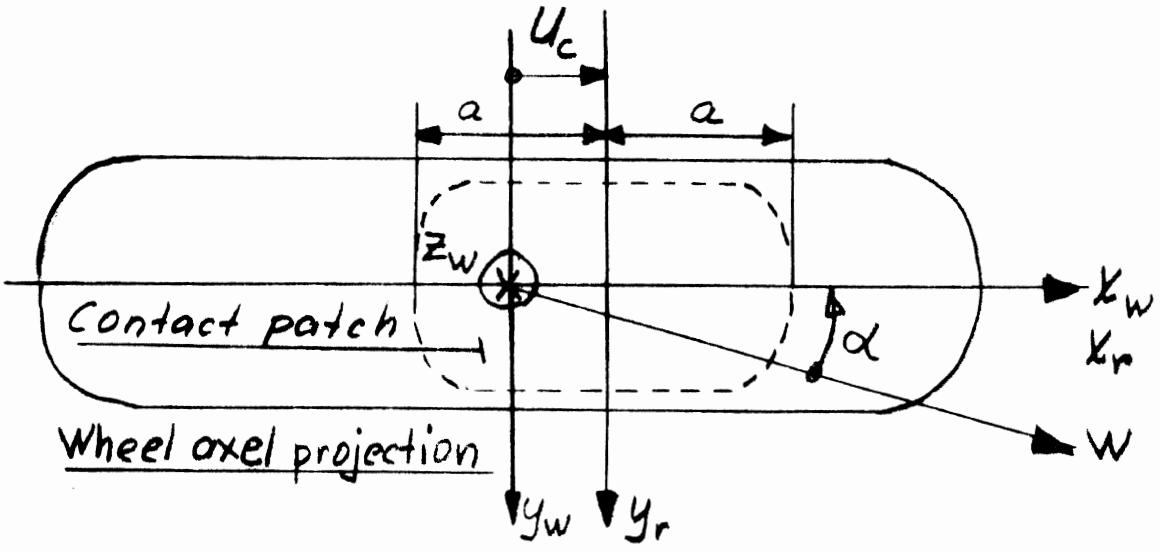

Figure 4.1 Coordinate Systems x_w, y_w, and x_r, y_r on the Road Surface for Steady-State Motion.

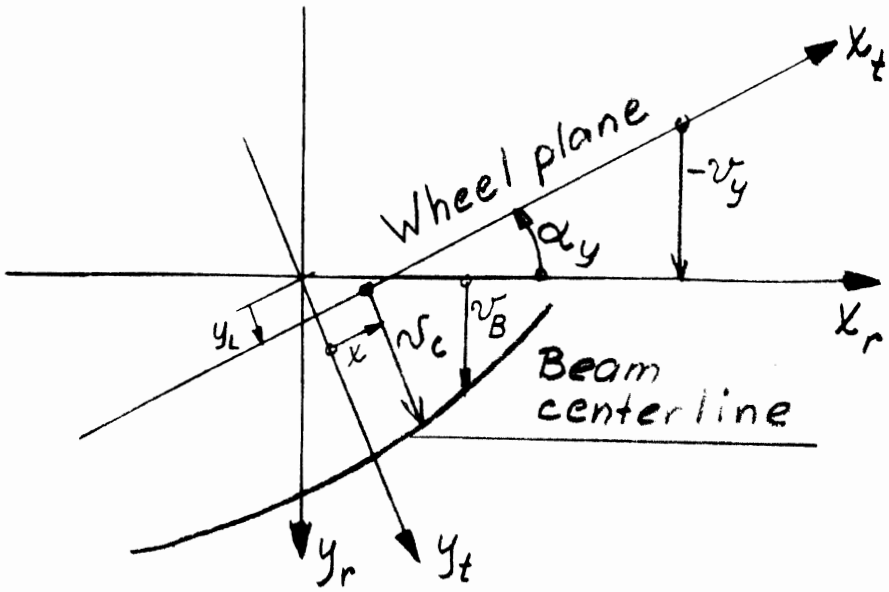

Figure 4.2. Coordinate System x_t, y_t for Transient Motion.

$$V_x = W \cdot \cos \alpha \qquad (2)$$

Introducing S_x as longitudinal slip, the longitudinal slip speed, V_{cx}, of the belt in the contact area is given by

$$V_{cx} = S_x \cdot V_x = S_x \cdot W \cdot \cos \alpha \qquad (3)$$

Free-rolling is indicated by $S_x = 0$ and locked-wheel braking by $S_x = 1$. Driving is obtained for negative S_x values.

A point on the belt travels through the contact patch at a speed, $\dot{x}$, given by the negative rolling speed, V_r.

$$\dot{x} = - V_r \quad \text{with} \quad V_r = V_x - V_{cx} \qquad (4)$$

The location, x, of a point on the beam relative to the x_r origin is then

$$x = a - V_r \cdot (t-t_o) \qquad (6)$$

where a is the contact patch half length and t_o the time for the entry of an element at $x = a$.

The tread elements are regarded as infinitely thin lateral lugs. Per unit circumferential length, this tread rubber has a mass density of nominal m_n, longitudinal and

lateral spring constant rates of k_x and k_y, and damping constant rates of c_x and c_y.

The mass is assumed concentrated at the outer periphery of the tread surface. Since the mass, m_n, is distributed along the thickness of the tread, an effective mass, m, has to take the place of m_n in the concentrated mass at the periphery according to a relation given in Appendix E.

Let u(x) and v(x) denote the longitudinal and lateral displacement of an element relative to its undeflected position on the belt centerline as it moves from entry to exit of the contact patch (Fig. 4.3). Since the x_r, y_r system has a steady-state translation relative to an inertia system, the equations of motion for an element written in the x_r, y_r system will take the form

$$m\ddot{x}_r + c_x \cdot \dot{u} + k_x \cdot u = q_x = m\ddot{x}_r + q'_x \tag{6}$$

$$m\ddot{y}_r + c_y \cdot \dot{v} + k_y \cdot v = q_y = m\ddot{y}_r + q'_y \tag{7}$$

where

$$\begin{aligned} v &= y_r - v_c & u &= x_r - x \\ \dot{v} &= \dot{y}_r - \dot{v}_c & \dot{u} &= \dot{x}_r - \dot{x} \end{aligned} \tag{8}$$

and q_x and q_y are the components of friction force on the element due to its speed of sliding over the road surface. The q'_x and q'_y are the forces that act on the beam.

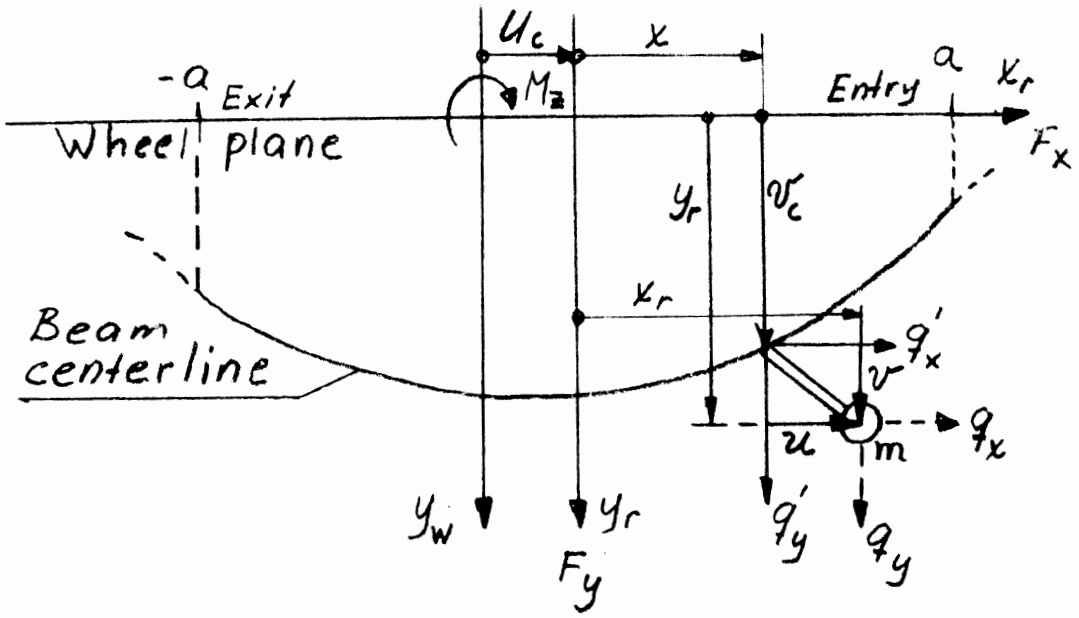

Figure 4.3. Moment, Forces and Deflections for Element Dynamics at Steady State.

For the longitudinal component, V_{sx}, of sliding velocity of an element we have

$$V_{sx} = V_{cx} + \dot{u} \tag{9}$$

For the lateral component, V_{sy}, the slope of the beam due to the lateral force distribution has to be included in the derivation

$$V_{sy} = V_{cy} + \dot{v}_c + \dot{v} = V_{cy} + \dot{y}_r \tag{10}$$

In the steady-state $\dot{v}_c$ is obtained from

$$\dot{v}_c(x) = \frac{dv_c}{dt} = \frac{dv_c}{dx}\,\frac{dx}{dt} = v_c' \cdot \dot{x} \tag{11}$$

Here v_c' is the slope of the deflected beam. The $\dot{x}$ is given in (4) as

$$\dot{x} = - V_r \tag{12}$$

Hence

$$\dot{v}_c = - V_r \cdot v_c' \tag{13}$$

The resultant sliding velocity, V_s, is now given by

$$V_s = \sqrt{V_{sx}^2 + V_{sy}^2} \tag{14}$$

The sliding velocity gives the friction coefficient, μ

$$\mu = \mu(V_s) \tag{15}$$

which in turn with the vertical pressure intensity, q_z, gives the resultant friction intensity, q.

$$q = \mu(V_s) \cdot q_z \tag{16}$$

Appendix A deals with considerations on the choice of $\mu(V_s)$ function.

The resultant components of friction force are proportional to and opposing the sliding velocity components, thus:

$$q_x = - q \cdot \frac{V_{sx}}{V_s} \tag{17}$$

$$q_y = - q \cdot \frac{V_{sy}}{V_s} \tag{18}$$

The distribution of forces $q_x'(x)$ and $q_y'(x)$, which are obtained from the element deflections as they move along the contact patch, are integrated to give the longitudinal force, F_x, and the lateral force, F_y, acting on the wheel at longitudinal slip, S_x, and slip angle, α.

$$F_x = \int_{-a}^{a} q'_x \, dx \tag{19}$$

$$F_y = \int_{-a}^{a} q'_y \, dx \tag{20}$$

For the M_{zy} part of the aligning torque, M_z, the integral takes the following form:

$$M_{zy} = \int_{-a}^{a} (-q'_x \cdot v_c + q'_y \cdot x)dx + U_c \cdot F_y \tag{21}$$

Note that this contribution, M_{zy}, to the aligning moment is obtained under the assumption of an infinitely thin tire. Without a lateral force distribution, this component is zero. In Section 4.4 will be given the contribution, M_{zx}, by longitudinal forces due to a finite tire width.

With K_L denoting the spring constant for the longitudinal deflection, U_c, of the beam at the point of action of a circumferential force, F_x, we have the following relationship:

$$U_c = F_x/K_L \tag{22}$$

making

$$U_c \cdot F_y = F_x \cdot F_y/K_L \tag{23}$$

Since a knowledge of the lateral force distribution $q'_y(x)$ in (7) is needed to obtain the beam deflection $v_c(x)$, and since its derivative $v'_c(x)$ is implicit in (7) and (9), an iterative process is necessary to obtain the steady-state equilibrium solution.

The way to obtain this solution will be described in the next section on the transient mode of the tire. The mechanism developed for this case will also yield the steady-state solution.

4.3 EQUATIONS FOR NON-STEADY SLIP

4.3.1 YAWING OSCILLATIONS OF THE WHEEL PLANE. Superimposed on a steady-state rolling at a slip angle of α is a small amplitude sinusoidal yawing oscillation of the wheel plane about the x_r, y_r origin. The x_r, y_r system stays at the mean slip angle, α. The system x_t, y_t follows the wheel plane (see Fig. 4.2).

The angle, α_y, of the yawing motion is given by

$$\alpha_y = \alpha_{Ay} \cdot \sin(\omega t) \tag{24}$$

where α_{Ay} is the oscillation amplitude and ω is the circular frequency in rad/sec.

Due to the oscillation, the functions v and $\dot{v}$ in (8) obtain additional terms v_y and $\dot{v}_y$ and become

$$v = y_r - (v_c + v_y) \tag{25}$$

$$\dot{v} = \dot{y}_r - (\dot{v}_c + \dot{v}_y) \tag{26}$$

The deflection v_c varies now not only with x but also with time. The time derivative, $\dot{v}_c$, is therefore to be taken as the total derivative.

$$\dot{v}_c = \left(\frac{\partial v_c}{\partial t}\right)_x + \left(\frac{\partial v_c}{\partial x}\right)_t \frac{dx}{dt} = (\dot{v}_c)_x - V_r \cdot (v_c')_t$$

For v_y and $\dot{v}_y$ we obtain the following relations

$$v_y(x) = - \alpha_y \cdot x \tag{27}$$

$$\dot{v}_y(x) = - \dot{\alpha}_y \cdot x - \alpha_y \cdot \dot{x} \tag{28}$$

Making use of (12) will change (28) into

$$\dot{v}_y(x) = - \dot{\alpha}_y \cdot x + \alpha_y \cdot V_r \tag{29}$$

4.3.2 TRANSLATORY OSCILLATIONS OF THE WHEEL PLANE. Relative to the origin of the x_r, y_r system, the wheel plane performs lateral displacements, y_L, given by

$$y_L = y_{AL} \cdot \sin(\omega t) \tag{30}$$

where ω is not necessarily the same as in (24). The additional terms for v and $\dot{v}$ take here the form y_L and $\dot{y}_L$, hence for combined transitional motions we have

$$\left.\begin{aligned} v &= y_r - (v_c + v_y + y_L) = y_r - v_B \\ \dot{v} &= \dot{y}_r - (\dot{v}_c + \dot{v}_y + \dot{y}_L) = \dot{y}_r - \dot{v}_B \end{aligned}\right\} \qquad (31)$$

where v_B indicates the total deflection from the y_r-axis of the element basepoint on the belt.

In order to save calculation time, the element basepoint functions v_B and $\dot{v}_B$ in (31) are given a linear approximation within each section. The derivation of their sectionwise linear approximations for v_c, v_y, y_L and their first derivatives is given in Appendix C.

The choice of the value of N depends on the rate of change of such functions as $\dot{v}_y$, $\dot{y}_L$, and $\dot{V}_r$. A value of N = 20 has been used throughout this report.

The time required for the elements to travel through a section is given by

$$\Delta t = \frac{2a}{V_r \cdot N}$$

This Δt is used to increment t in (24) or (30). This scheme is also used for obtaining the steady-state solution for a certain slip angle, α.

When obtaining steady-state solutions the beam deflection velocity $(\dot{v}_c)_x$ is neglected. Rapid convergence to the steady-state from arbitrary initial conditions results.

For the transient motions the $(\dot{v}_c)_x$ has to be retained. This causes instability which has been cured by a scheme described in Appendix C.

4.4 CONTRIBUTION TO TRANSIENT ALIGNING MOMENT DUE TO FINITE WIDTH OF CONTACT PATCH

The yawing motion of a tire of finite width gives rise to longitudinal deflections of the tread elements. These deflections are antisymmetric across the width of the contact patch and give, therefore, rise to a component, M_{zx}, of the aligning moment.

We will here assume that the longitudinal deflections of the elements will be so small that sliding can be ignored. This is a reasonable approximation when the wheel is free rolling and the oscillation amplitude is small.

A derivation of the M_{zx} component of the aligning moment was first given by Pacejka [10]. Expressed in the cycle frequency, ω, this can, according to Phillips [16], be written as follows:

$$M_{zx} = \frac{2b^2 \cdot a \cdot k_x}{3\,\bar{\omega}_a} \alpha_{Ay} \left\{ \left[\bar{\omega}_a - \sin \bar{\omega}_a \cdot \cos \bar{\omega}_a \right] \sin (\omega t) + \sin^2 \bar{\omega}_a \cdot \cos (\omega t) \right\}$$

In addition to previously defined quantities, b stands for contact patch half width and $\bar{\omega}_a$ is given by

$$\bar{\omega}_a = \omega \frac{a}{\bar{W}}$$

4.5 ITERATIVE PROCESS FOR FINDING v_c AND q'_y

The contact length, 2a, is divided up in N equal sections. Since the sections are traversed from x = a to x = -a, section nr 1 starts at x = a and section nr N ends at x = -a. Infinitely thin tread elements with a spacing of 2a/N are followed as their attachment points on the beam move from section to section along the contact patch (Fig. 3.1). As an old element leaves the contact patch at the exit end (x = -a), a new one enters at the entry (x = a). During the passage of elements through their respective sections, the beam deflects with the speed $(\dot{v}_c)_x$. The N lateral force distributions, q'_{yn}, obtained within each one of the sections are integrated yielding N point loads, $q(x_i)$, assumed located at the center $x = x_i$ of each section.

$$q(x_i) = \int_{x_i - 2a/N}^{x_i + 2a/N} q'_{yn}\, dx$$

$$x_i = a - \frac{2a}{N}(i - 1 + .5)$$

These N point loads are used to calculate the deflection $v_c(x)$ and the slope $v_c'(x)$ for the passage of the elements through their next consecutive sections, and so on.

The calculations of $v_c(x)$ and $v_c'(x)$ due to the point loads are based on the equation for deflection of a point loaded beam under tension on an elastic foundation. Details of these calculations are given in Appendix B.

5. MODEL IMPLEMENTATION

The model has been mechanized for both pure digital and hybrid (digital plus analog) computation. The digital programming language is FORTRAN IV.

The digital version is implemented on a Digital Equipment PDP 11/45, making use of the interactive integration system program FORMIC[1]. This FORMIC program is readily transferable to other types of computers.

The hybrid version combines the PDP 11/45 and an Applied Dynamics AD/4 analog computer. The analog is used mainly to perform the integrations for the tread element dynamics, bringing down the solution time considerably compared to the pure digital. Thus the time required in the hybrid program for an element to pass through the whole length of a 20-section contact patch is ~ 12.5 sec. at time scale 100. In the pure digital program this requires ~ 220 sec., resulting in a time ratio of ~ 17.5.

Appendix G contains an introductory presentation of FORMIC together with the FORTRAN programs for the digital and hybrid versions and an analog patching diagram for the hybrid version.

---

[1]Developed by Saab-Scania AB, Sweden.

6. RESULTS

6.1 OBTAINING A STEADY-STATE SOLUTION

The steady-state solution at a certain combination of longitudinal and lateral slip can be obtained from arbitrary initial conditions. Mostly these are taken to be the undeflected state of beam and elements with the slip numbers set at their desired values. A heavily damped steady-state solution is obtained by neglecting the deflection velocity, $\partial v_c/\partial t$, of the beam. The distance traveled by the tire to obtain a steady state is, under these circumstances, slightly more than the length of the contact patch. Note that this damping is a property of the mathematical solution technique and not one of the beam, which in the case of steady-state solutions is undamped.

The development of a steady-state solution of lateral element deflection (which is, except for the small damping force, directly proportional to the force intensity distribution) is shown in Figure 6.1 on page 30 for $\alpha° = 4°$ for the first 12 steps of the computation. Figure 6.1 also shows the final deflection after more than 20 steps. The gradual build-up to a final deflection by each one of the 20 elements within the contact patch is clearly seen in Figure 6.1.

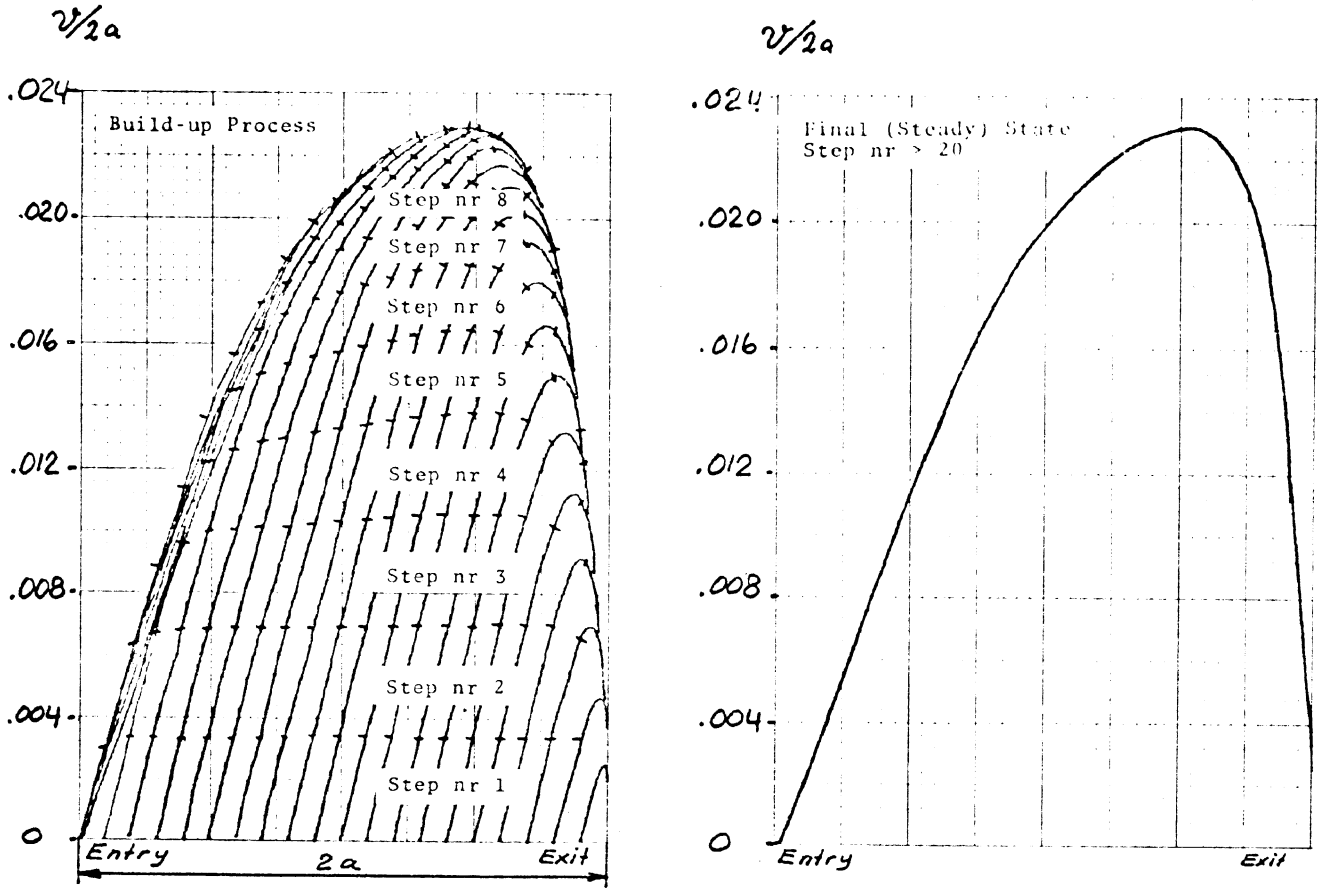

Figure 6.1 Stepwise Build-up of Steady-State Lateral Element Deflection Ratio v/2a (left) and Final Steady-State (right) at $\alpha° = 4$.

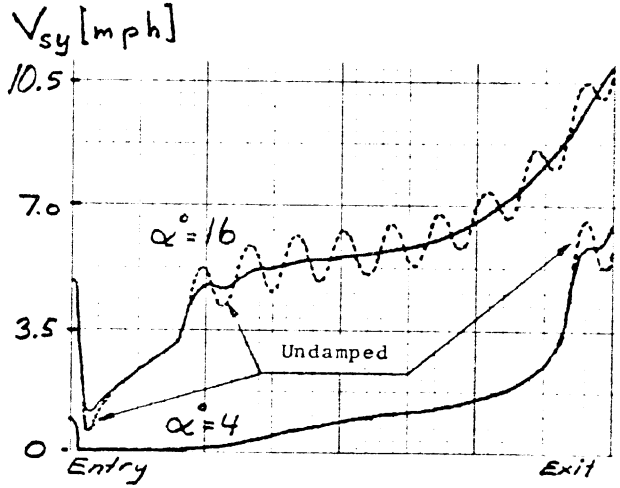

Figure 6.2 Final State of Lateral Sliding Velocity Distribution V_{sy} at $\alpha° = 4$ and 16 With and Without Element Damping. Traveling Speed 20 mph.

In step 1, the slopes of the element deflection (gradient of lateral force intensity) are determined solely by the slip angle. As the beam gradually gets deflected, in the successive steps, the slope of the beam affects the situation and lowers the force gradient in the entry part of the contact patch. At the rear, the sliding back due to decreasing normal pressure is noted.

Close observation (fine resolution on a CRT) reveals the gradual deflection of the elements as they enter into the contact patch. This is, of course, due to the time necessary to accelerate the mass of the element away from the equatorial line of the beam. The gradual build-up of the vertical load intensity adds to this effect.

The steady-state shape of the distribution of sliding velocity at 20 mph traveling speed for $\alpha^\circ = 4$ is given in Figure 6.2. Here three ranges of interest present themselves. The first is at the entry into the contact patch. Here the sliding velocity, which starts with a value determined by the slip angle and the slope of the beam at the entry point, very rapidly goes down to zero; i.e., there is stiction of the element to the road surface. The stiction range prevails until the deflection force of the element overcomes the friction force. Then the last range starts where the element rebounds toward the beam in a fashion determined to a large extent by the decreasing vertical pressure at the

patch exit. The rebound has the natural frequency of the element and an amplitude that is governed by the damping in the element and the negative slope of the $\mu(V_s)$ curve in unison. The oscillations spread over a larger portion of the contact patch as the slip angle increases, and become more marked when the damping coefficient, c_y, is reduced to zero. This is also shown in Figure 6.2 for $\alpha° = 4$ and 16. The oscillation frequency is ~770 Hz compared to the theoretical 745 of Appendix E. Figure 6.3 contains a plot of the fourth-order vertical pressure distribution parabola used in this investigation.

The graphs shown of the course to a steady-state solution have been obtained with the final parameter values for beam and elements given in Appendix E.

6.2 STUDY OF TIRE PARAMETER EFFECTS ON CORNERING STIFFNESS (SLOPE, $dF_y/d\alpha$, AT THE ORIGIN)

The assumed shape of the $\mu(V_s)$ curve has practically no effect on the course of the $F_y(\alpha)$ relation for small angles, making it essentially linear in the range $-1 < \alpha° < 1$. In Figure 6.4 is shown the effects on F_y at $\alpha° = 1$ of changing individually the beam parameters EI, K, and N by the factors 10, 2, .5, .2 from their nominal values. In the same figure is also shown the effect of varying the tread element spring constant, k_y, by the factors 1.8 to .6 from its nominal value.

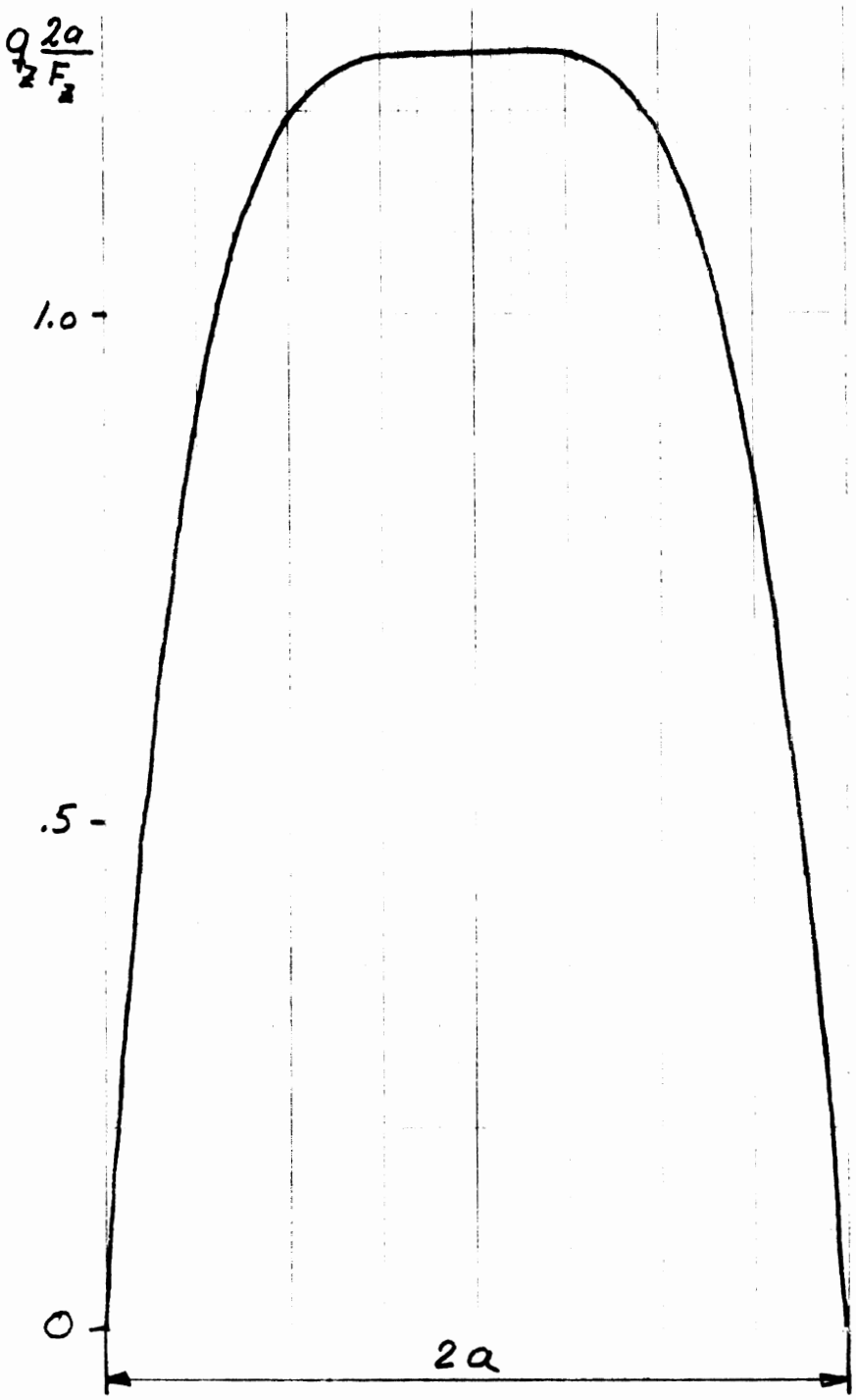

Figure 6.3. Shape of 4th Order Vertical Pressure Distribution.

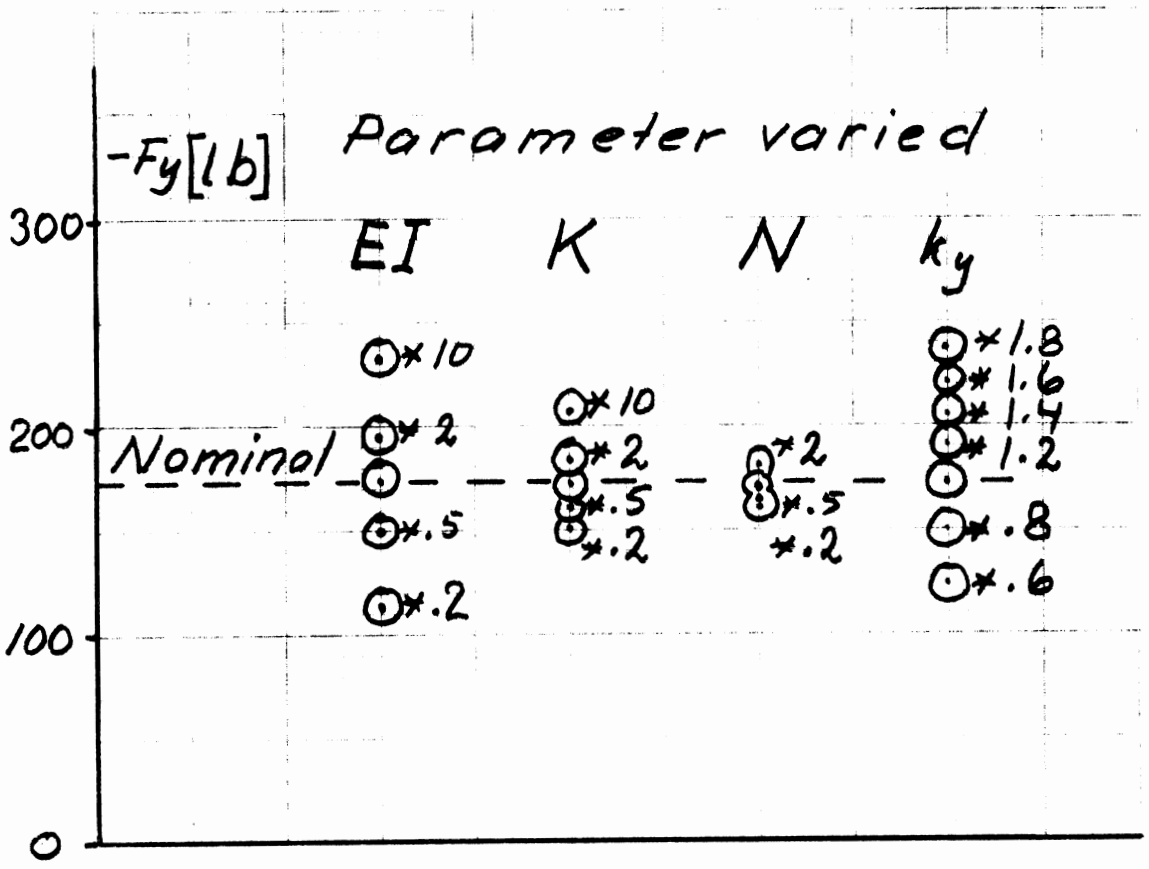

Figure 6.4 The Effect on the Lateral Force F_y at Slip Angle $\alpha° = 1$ of Variation of Beam Parameters EI, K and N and Element Lateral Spring Constant k_y.

Since the effect of changing the element spring constant is more pronounced than a change in any of the other parameters and in view of the uncertainty of its derivation, it seems justifiable to put all the adjustment on this parameter in order to obtain the same cornering stiffness as that obtained on the mobile tire tester [2]. All the other constants have been kept at their calculated values.

Figure 6.5 shows the effect the variation of EI has on the lateral deflection of the tread elements and, hence, the intensity of lateral force. Notice particularly that the effect of a weakening of the beam stiffness makes the force intensity more and more concave, until it even shows a change of sign in the forward part of the contact patch.

Figure 6.5 also shows the corresponding course of slope of the beam inside the contact patch. From this figure the explanation to the change in sign of the lateral force intensity is to be found in the increase of steepness of the slope at the entry region of the contact patch.

This is clarified in Figure 6.6 where, at a small slip angle ($\alpha^\circ = 1$), the non-sliding ground contact line of the elements is drawn from the entry point of the beam at three different values of stiffness.

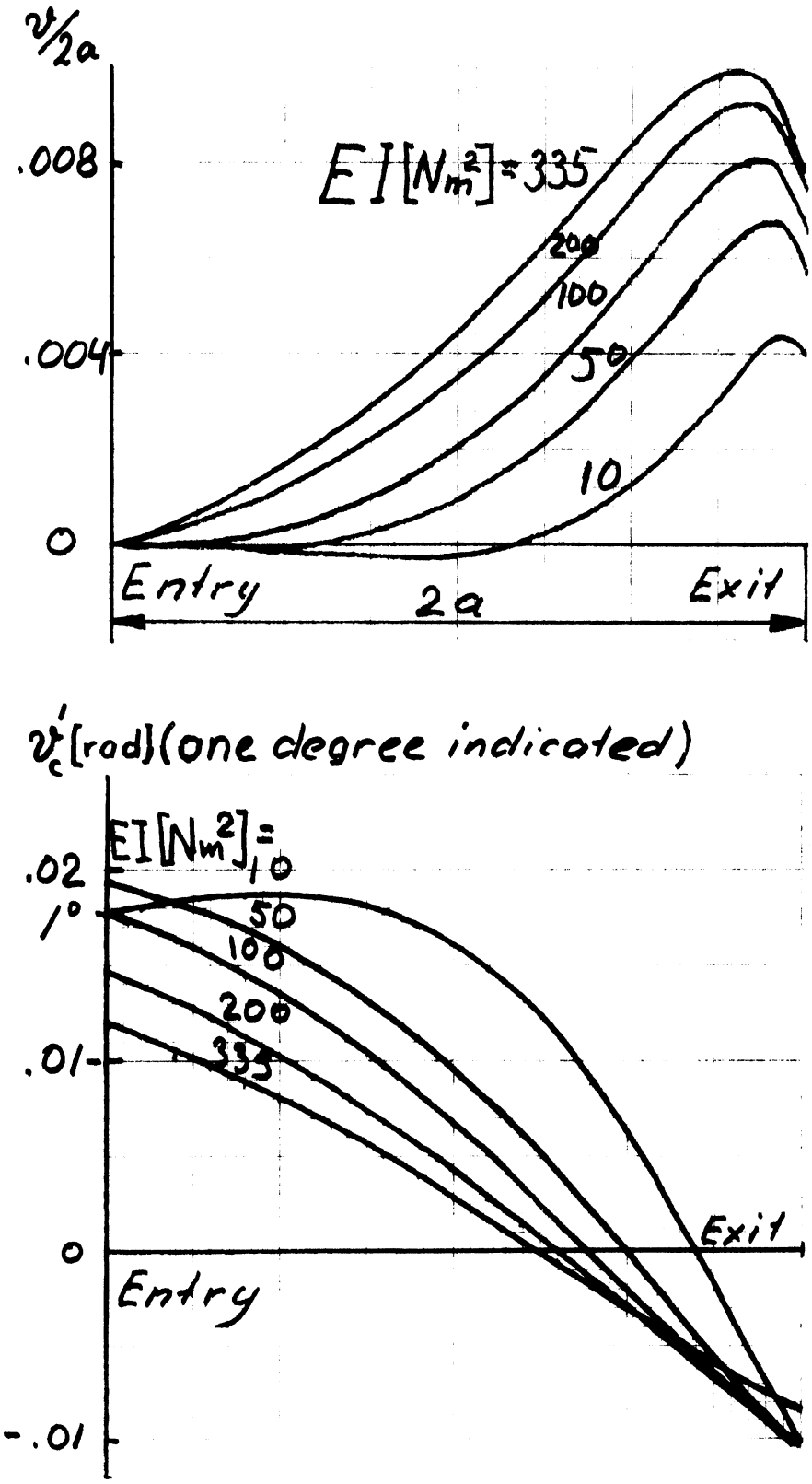

Figure 6.5 Lateral Element Deflection Ratio v/2a (top) and Beam Centerline Slope v_c' (bottom) at $\alpha° = 1$ for Beam Stiffness EI = 10-335Nm^2 and Tension N = 1000N.

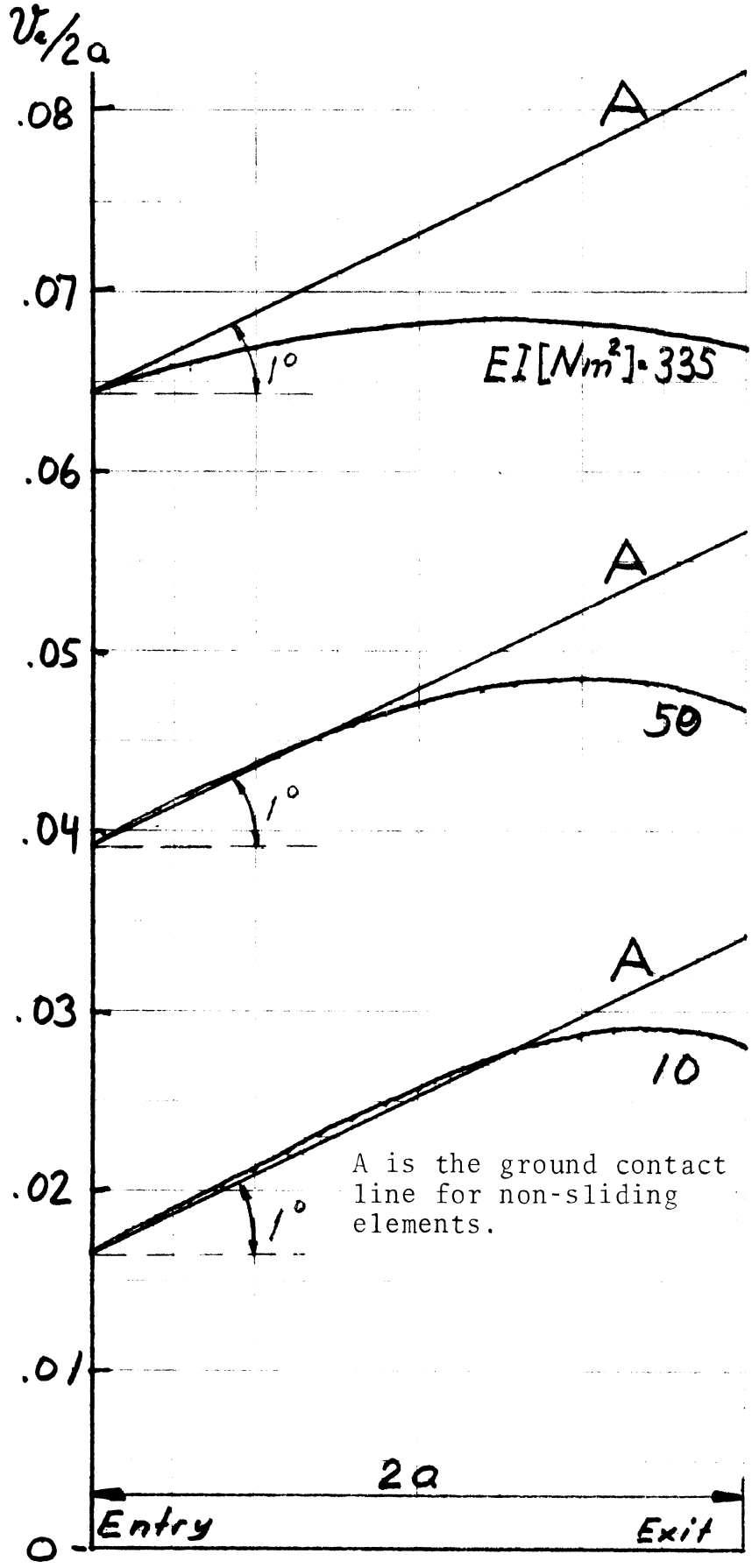

Figure 6.6 Lateral Relative Beam Centerline Deflection Ratio $v_c/2a$ at $\alpha° = 1$ for Beam Stiffness EI = 10,50,335 Nm^2 and Tension N = 1000N.

6.3 FRICTION CURVE PARAMETERS

The next step was to find, under an assumed analytical representation (Fig. A6) of the $\mu(V_s)$ curve, the parameter values that made a best fit to the experimentally obtained $F_y(\alpha)$ relation at 20 mph.

By varying the parameters μ_{po}, μ_{p1} (defined in Appendix A) for the parabola and the limit plateau (μ_{pt}) to give experimentally obtained F_y values at $\alpha° = 4, 8, 12$, and 16, it was possible to settle on a set of parameters that give a good fit for the whole experimental range $\alpha° = 0 - 16$.

Figure 6.7 shows the μ_{po}-μ_{p1} parameter relation for the α-range with $\mu_{pt} = 1.11$. It turns out that $\mu_{pt} = 1.11$, $\mu_{po} = .21$, and $\mu_{p1} = 1.35$ is the optimal combination. Figure 6.8 gives the resultant fit with experimental data points indicated.

The decline of the $\mu(V_s)$ curve for large values of V_s does not influence the F_y versus α curve to any noticeable degree for slip angles < 16° at 20 mph. The hyperbolic part of the $\mu(V_s)$ curve was therefore obtained from an equivalent fitting operation of the $F_x(S_x)$ relation for $.5 \lesssim S_x \lesssim .8$. The parameter values for the hyperbola settled on are: $\mu_H = 1.4$, $\mu_{AS} = .7$, and $V_{AS} = -.255 \cdot W_{Ref}$ where W_{Ref} is defined in Appendix F.

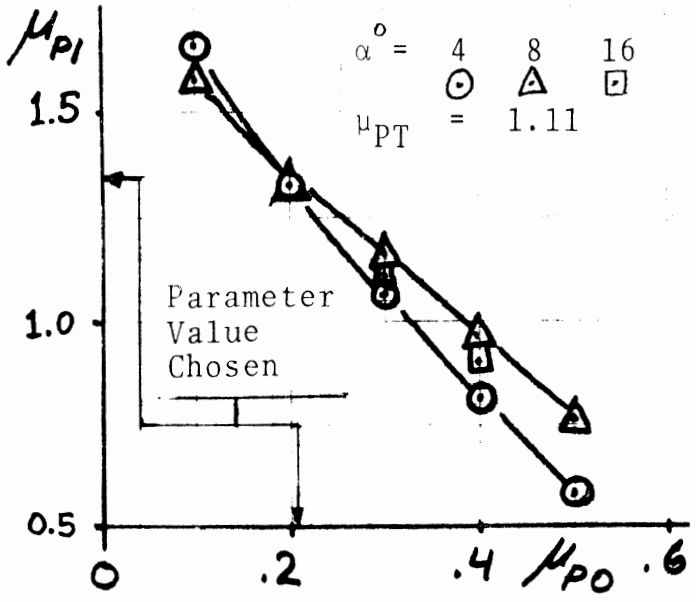

Figure 6.7. Establishing Best Fit Parameter Values for the $\mu(V_S)$ function.

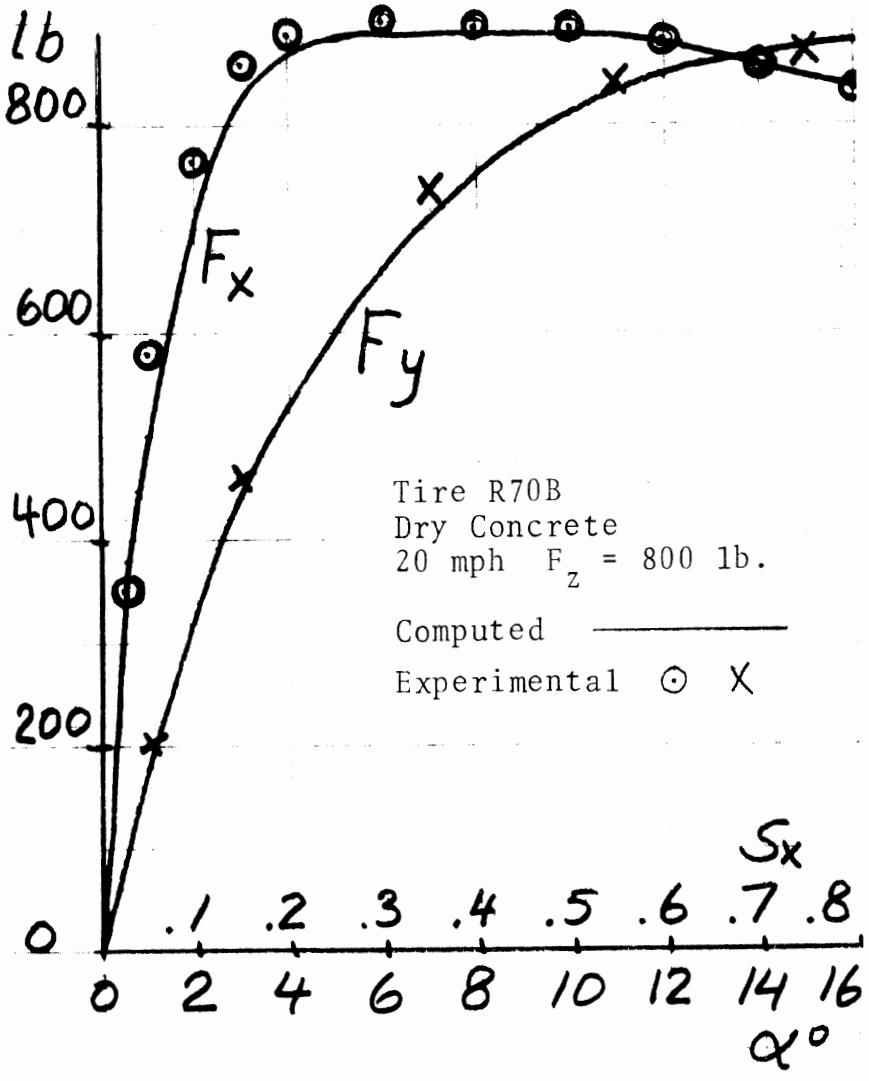

Figure 6.8 Comparison Between Computed $F_x(S_x)$ and $F_y(\alpha)$ Functions and Experimental Data.

The $\mu(V_s)$ curve thus arrived at, and used for the main part of the results presented in the rest of this report, is shown in Figure 6.9 and in Figure 6.12 (top-left).

As can be seen from Figure 6.8, the fit for the $F_y(\alpha)$ function is good, whereas the fit for the $F_x(S_x)$ function is not good in the range $.05 < S_x < .2$. No doubt a more detailed representation of the $\mu(V_s)$ curve and a more elaborate simultaneous fitting procedure for the two functions will improve this situation.

6.4 STEADY-STATE DISTRIBUTION OF SLIDING VELOCITY AND ELEMENT DEFLECTION AT VARIOUS SLIP VALUES

In Figure 6.9 are compiled the distribution of element sliding velocity and deflection intensity in the lateral direction for the free-rolling tire at slip angles $\alpha° = 1, 2, 4, 8, 12, 16$.

Perhaps the most interesting feature of the graphs on sliding velocity are the gradual decrease of the range of no sliding with increasing slip angle. The non-sliding region vanishes at a value of $\alpha° \simeq 6.2$. The initial sliding velocity at its entry point is of course determined by the slip angle and beam slope conditions at this point. The higher the slip angle, the earlier in the contact patch will occur the start of sliding after stiction (or increase of sliding velocity after an initial decrease). This is, of course, a result of the fact that the lateral force intensity,

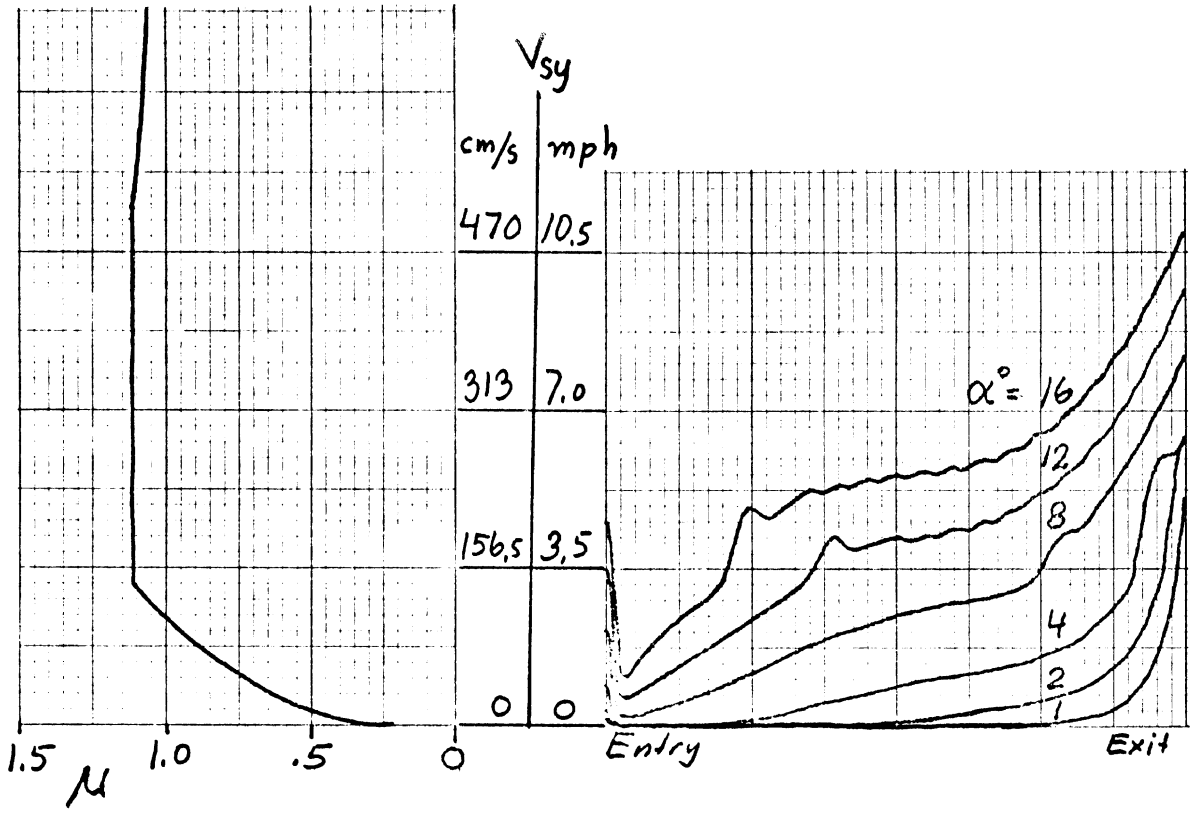

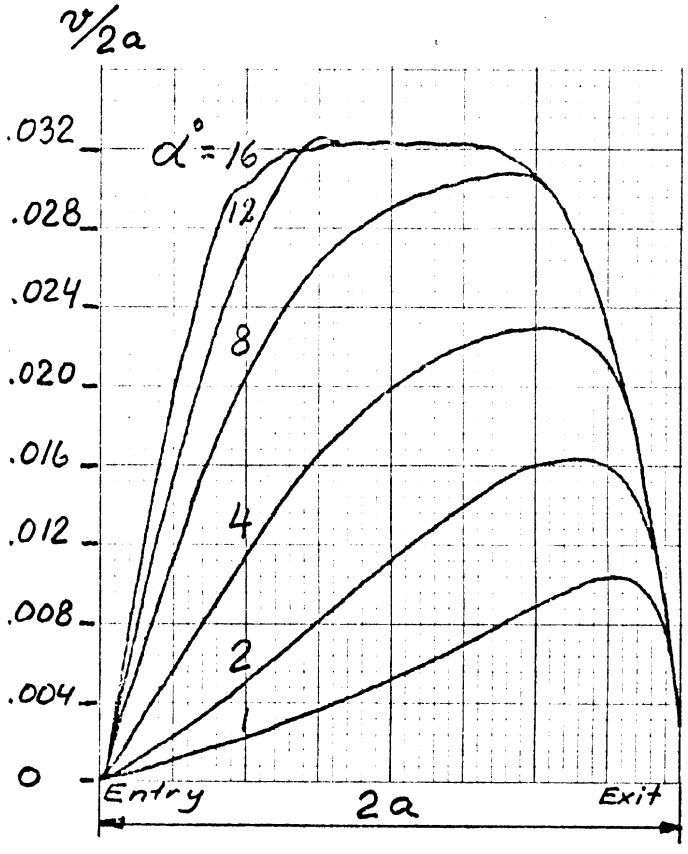

Figure 6.9 Distribution of Element Lateral Sliding Velocity V_{sy} (top) and Lateral Element Deflection Ratio v/2a (bottom) for α° = 1 - 16 at S_x = 0.

which has to overcome the friction force, is built up more rapidly the greater the slip angle.

Since the sliding velocity at a traveling velocity of 20 mph and $\alpha° < 16$ hardly goes beyond ~11 mph, which is where the negative slope of the $\mu(V_s)$ curve starts, no noticeable oscillations of the element occur at nominal element damping.

If, however, the element damping is reduced to zero, oscillations do occur, as is evident from Figure 6.2. It should be noted that the frequency of oscillation is found to be ~770 Hz (natural frequency 745 Hz) which is well within the range of observed squeal frequencies of tires. As has been indicated before, the amplitude of the oscillation is governed by the combined effect of the damping coefficient of the element and the negative slope of the $\mu(V_s)$ curve.

Figure 6.10 shows the deflection curves for the beam inside the contact patch at slip angles $\alpha° = 1, 2, 4, 8, 12, 16$. Likewise, the beam slope is shown in Figure 6.11. Besides what has been pointed out already regarding the deflection functions, attention is directed to their shape at the highest angles. This shape approaches that of the vertical pressure distribution (Fig. 6.3).

In Figure 6.12 are shown the distribution of element sliding velocity and deflection in the longitudinal sense for the slip numbers $S_x = .01 - .8$ at $\alpha° = 0$. The main

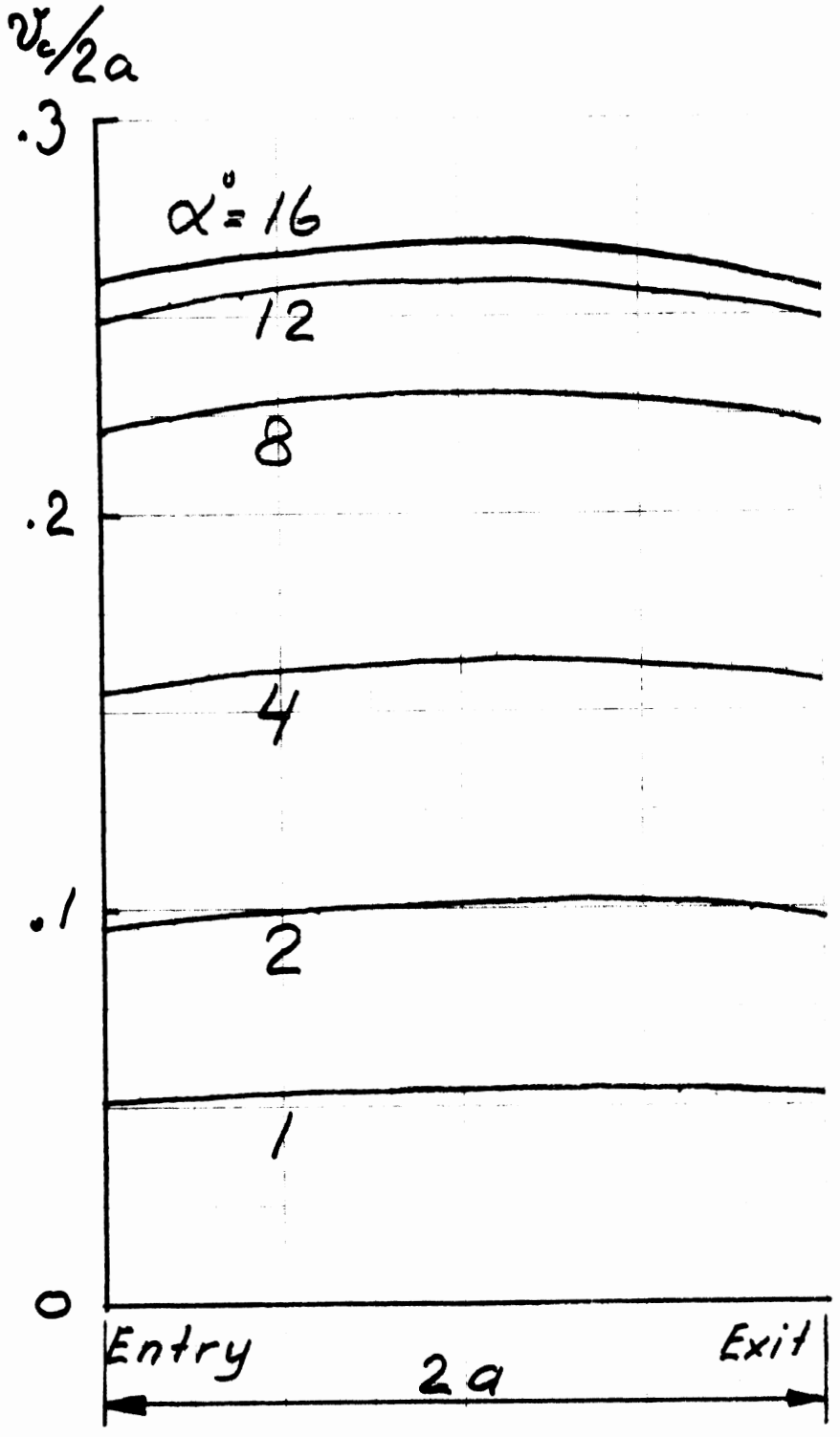

Figure 6.10 Deflection Ratio $v_c/2a$ of Beam Inside Contact Patch at Slip Angles α° = 1 - 16.

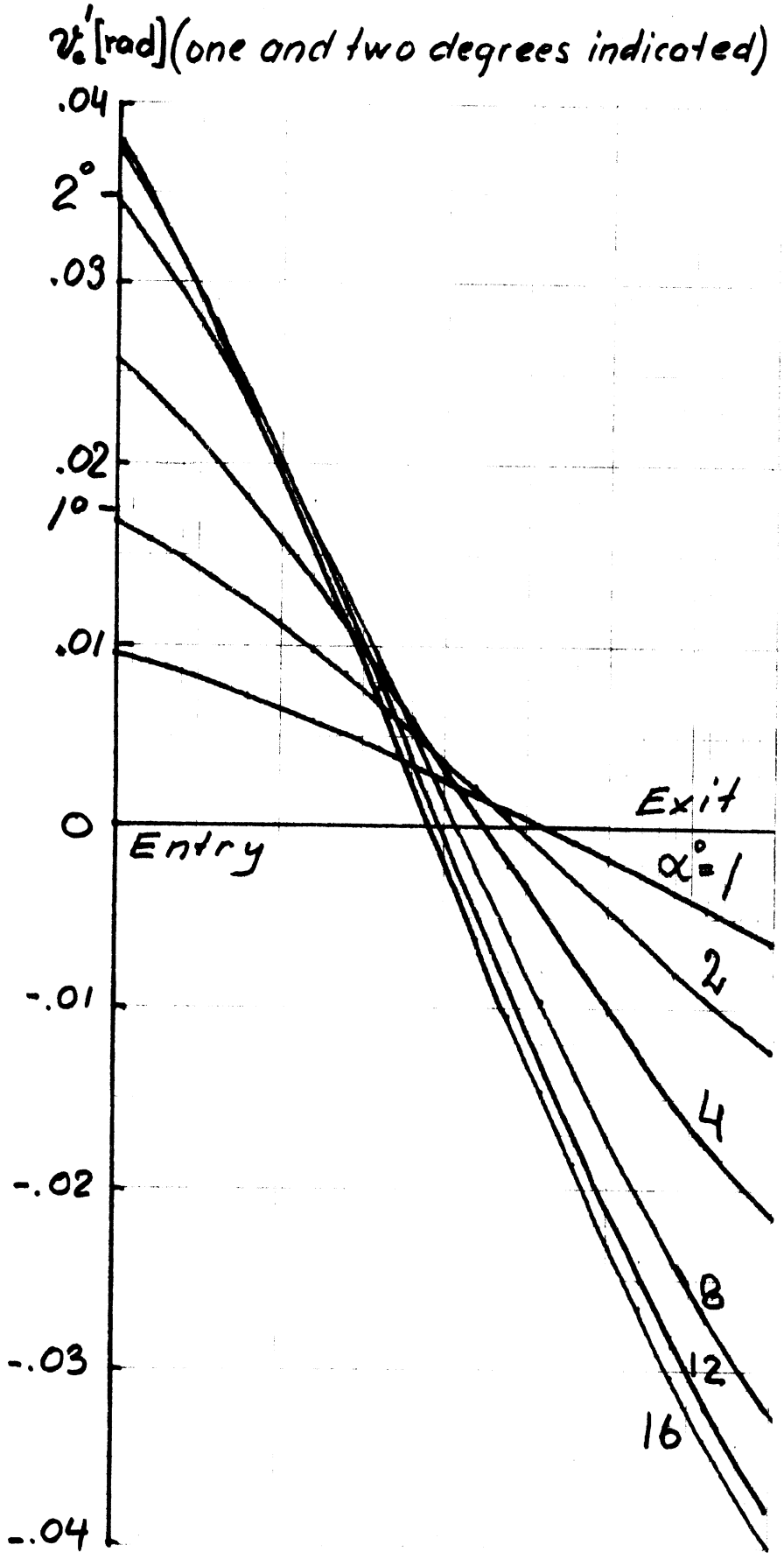

Figure 6.11. Beam Centerline Slop v_c' at Slip Angles $\alpha° = 1 - 16$.

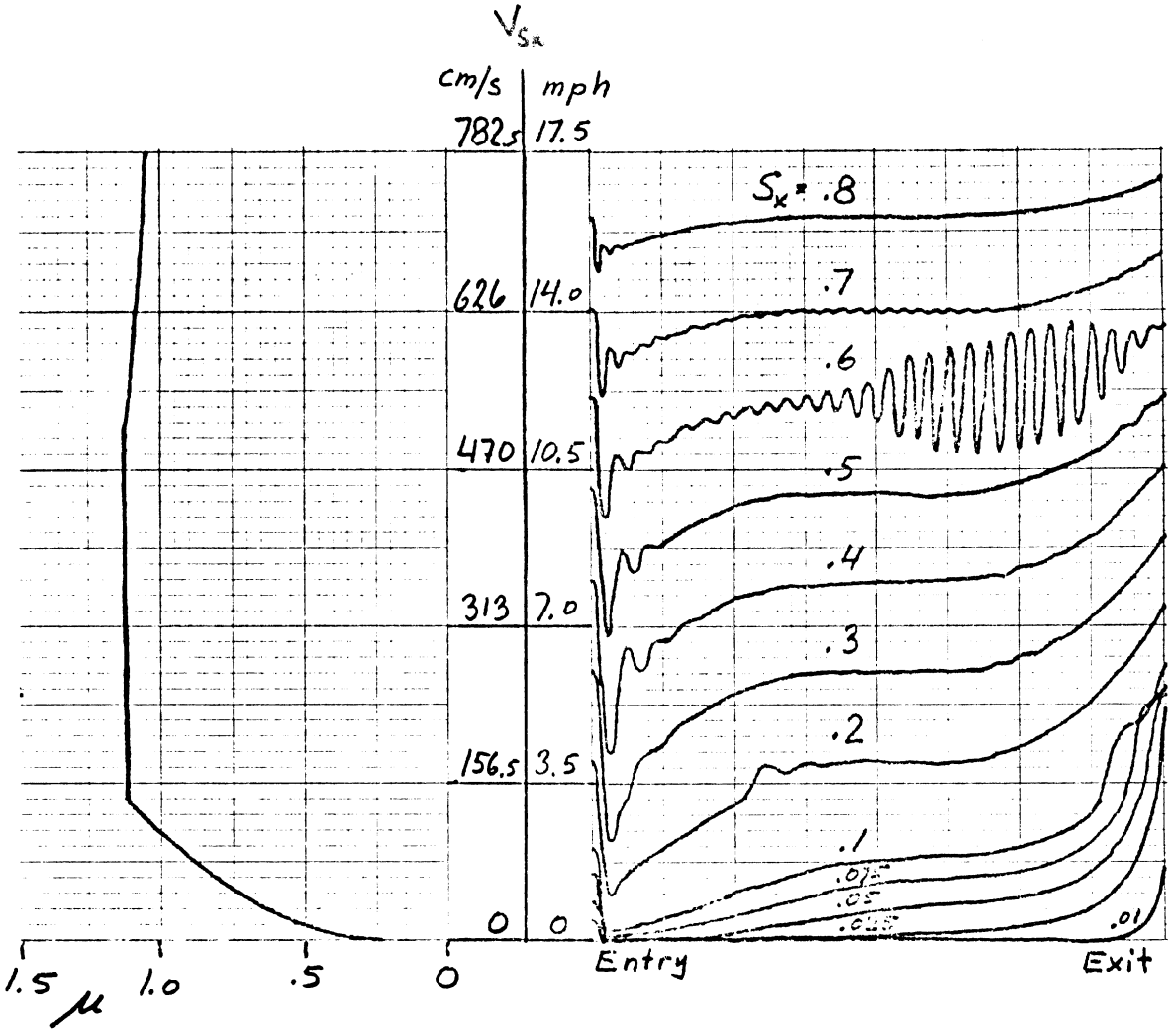

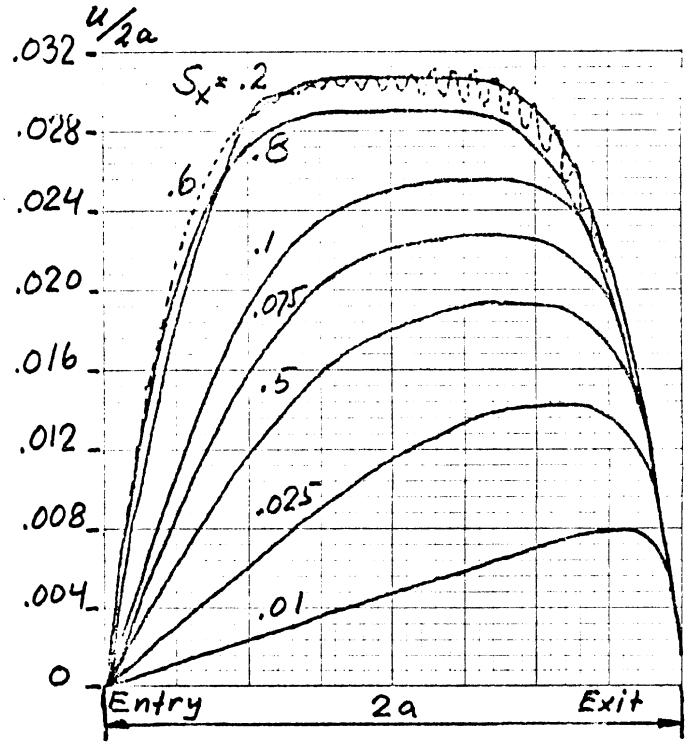

Figure 6.12 Distribution of Element Longitudinal Sliding Velocity (top) and Longitudinal Element Deflection Ratio u/2a (bottom) for S_x = 0.01 - .8 at $\alpha° = 0$.

differences between these results and those for lateral slip are due to the fact that the beam has a lateral elasticity but is longitudinally inextensible.

Because here the sliding velocity reaches well into the range of negative slope of the $\mu(V_s)$ function for $S_x \gtrsim .5$, a pronounced oscillation of the elements occurs for $S_x \approx .6$. In actual experimental conditions the squeal seems already to have started when S_x is approaching a lower value at which maximum F_x occurs. This can be taken as an indication that the plateau of the $\mu(V_s)$ curve should be replaced by a shallow arc, thus allowing the negative slope of the $\mu(V_s)$ curve to commence earlier.

6.5 LONGITUDINAL AND LATERAL FORCE AND ALIGNING MOMENT AT COMBINED SLIP

Figures 6.13 and 6.14 contain the functions $F_x(S_x)$ and $F_y(S_x)$, respectively, with slip angle α as the parameter. For comparison, experimental data obtained on concrete for the R70B tire [2] are shown, together with those computed.

A general trend is for the computed F_x values to be higher than the experimental, the higher the longitudinal and lateral slip. For the F_y values, it is the opposite.

There are several approximations in the model that can conceivably be the cause of these discrepancies.

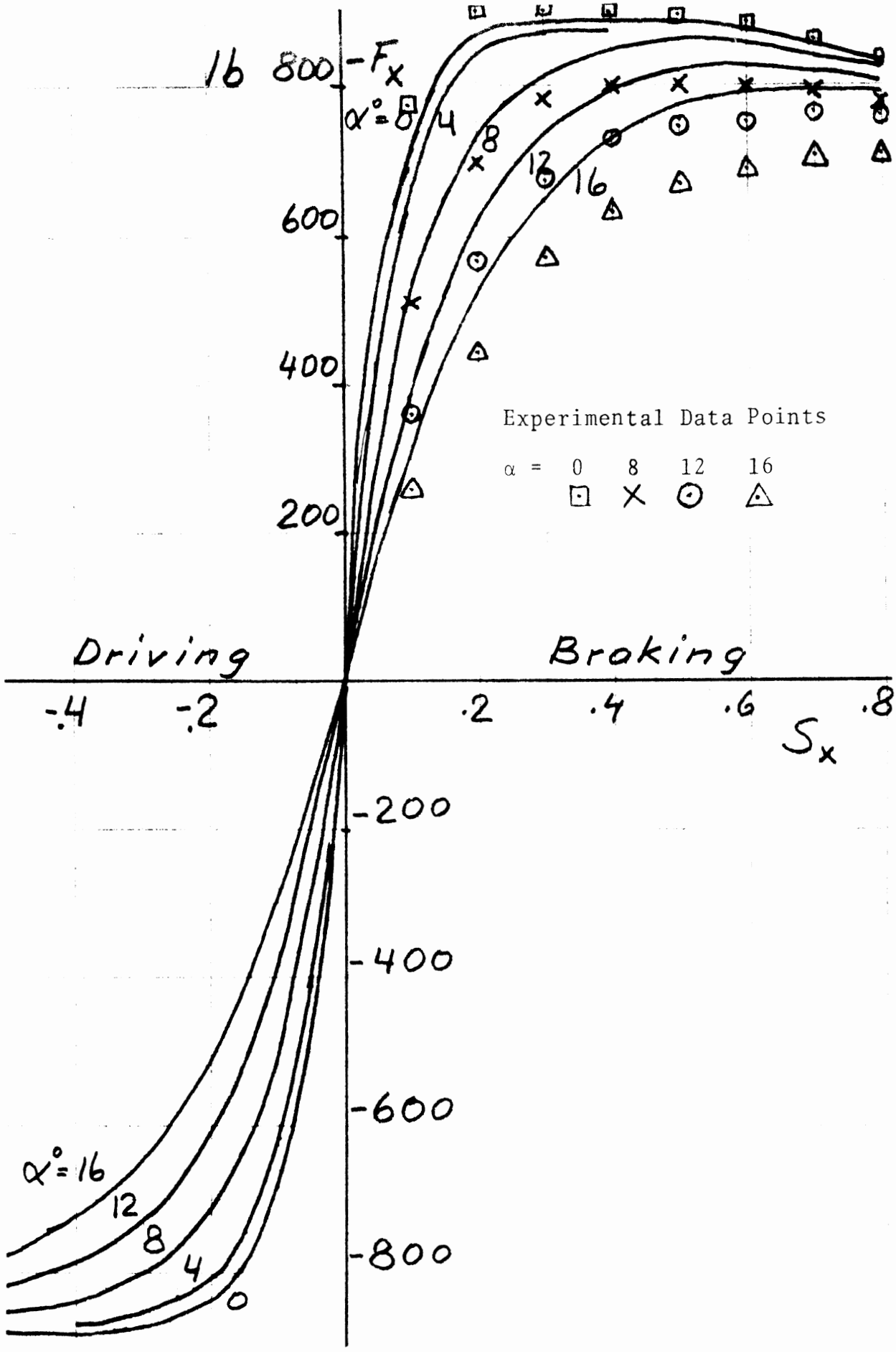

Figure 6.13 Longitudinal Force F_x vs. Longitudinal Slip S_x at Slip Angle $\alpha° = 0 - 16$.

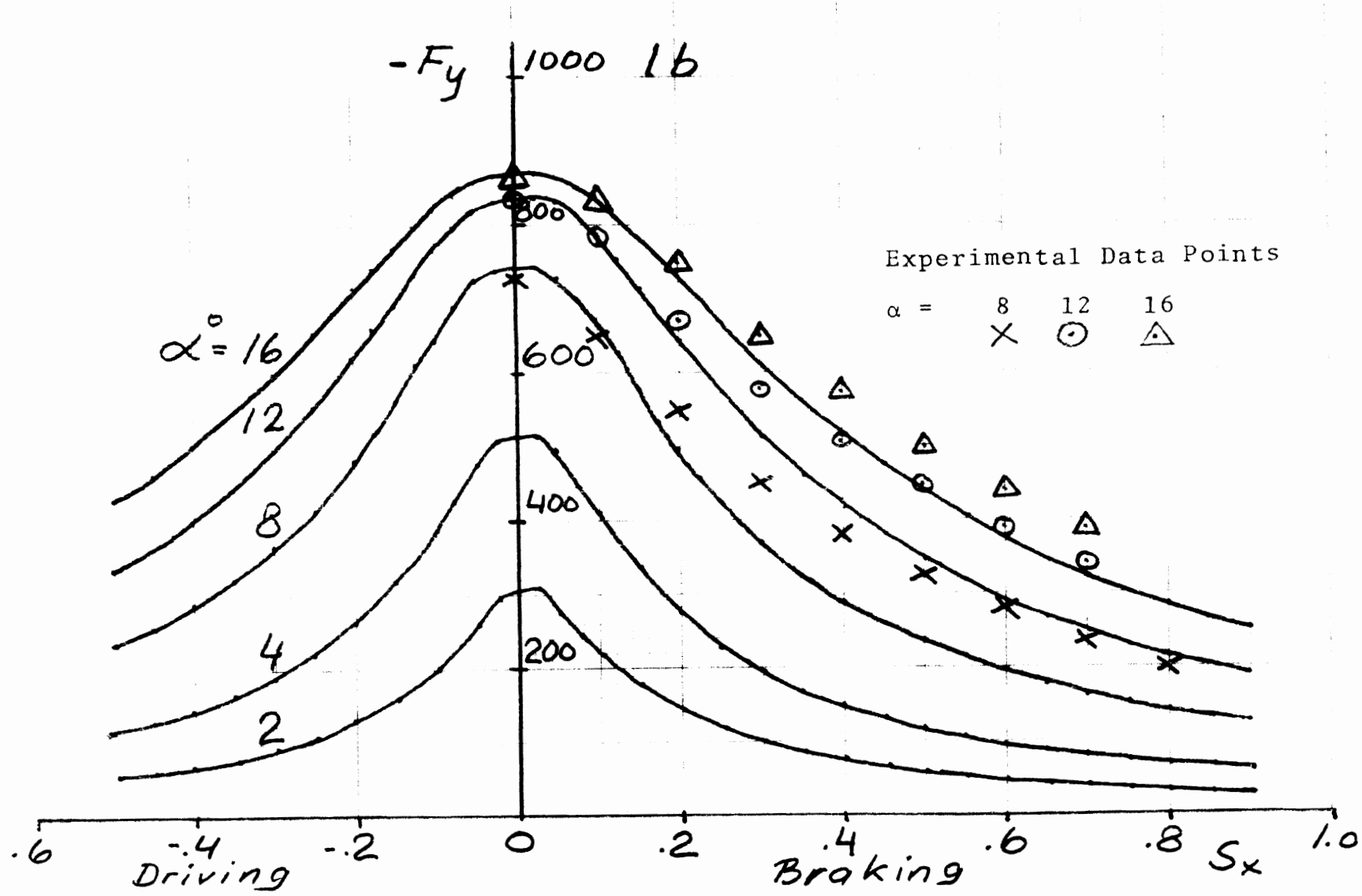

Figure 6.14 Lateral Force F_y vs. Longitudinal Slip S_x at Slip Angle α° = 2 - 16.

1. The model assumes isotropic friction. There are, however, experimental indications of anisotropic friction between road surface and the tread pattern. An explanation of this lies in the orthotopology of the tread pattern. When the rubber blocks in the contact patch tend to tilt due to a friction force, the distribution of normal contact pressure within the boundaries of the block will be affected. This in turn can change the friction coefficient. Because of the orthotopology an orthotropic friction property can be expected. The order of this effect is, however, unknown.

2. Still another effect of orthotopology of the tread pattern is to couple the longitudinal and lateral deflections of the tread elements. Specifically, at large deflections in one direction, the effect in the other direction may be appreciable.

3. Another approximation relates to the element spring force. A constant spring rate has been assumed in the model. From data given in Appendix E this seems to be a too crude approximation with regard to the large deflections encountered by the elements. A more realistic nonlinear force deflection relation of the elements will shift

the computed results in the direction of the experimental. The complexity of the dynamics of the element makes it, however, difficult to make a quantitative estimate of this effect.

4. Still another factor that affects the issue is the representation of the lateral belt deflection. Since there is a strong interaction of distribution of side force in the contact patch and the distribution of the slope of belt centerline, it seems clear that a true representation of the beam deflection is essential.

Figure 6.15 is a $F_y(F_x)$ representation of the data with slip angle α as parameter. A few parametric S_x values are indicated.

The aligning moment, $M_z(S_x)$, is shown in Figure 6.16 with slip angle α as parameter. No experimental data for the R70B tire are available. Theoretical and experimental results of aligning moment given in [13] for a 6.45-14 tire at a vertical load of ~3500 N are presented in Figure 6.17. As can be seen by a comparison, the general trend of the curves of Figure 6.16 seems to be very much in agreement with those of Figure 6.17.

In Figures 6.18 and 6.19 are given $F_y(\alpha)$ and $M_z(\alpha)$ with longitudinal slip S_x as parameter.

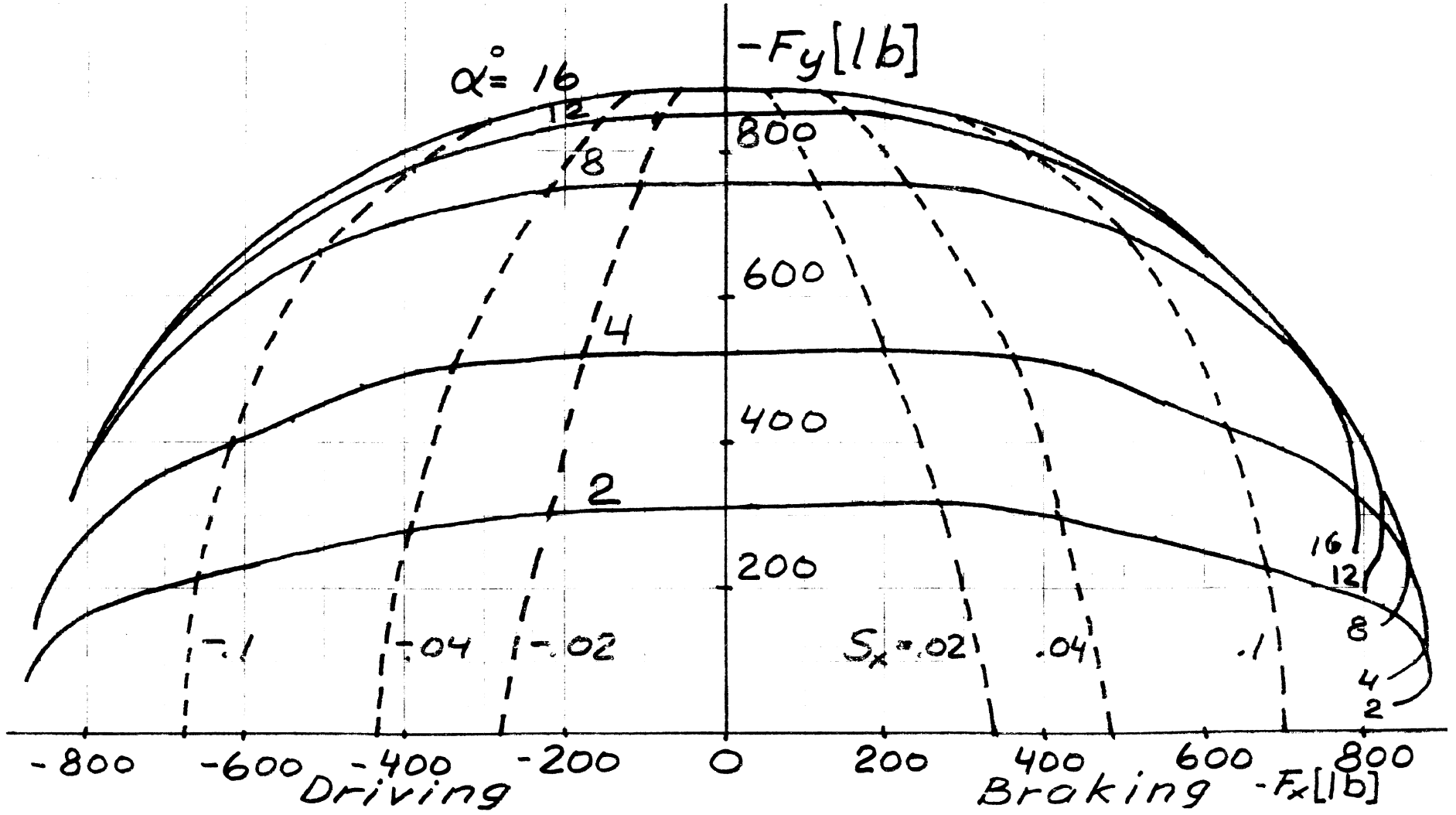

Figure 6.15 Lateral Force F_y vs. Longitudinal Force F_x at Slip Angle $\alpha° = 2 - 16$.

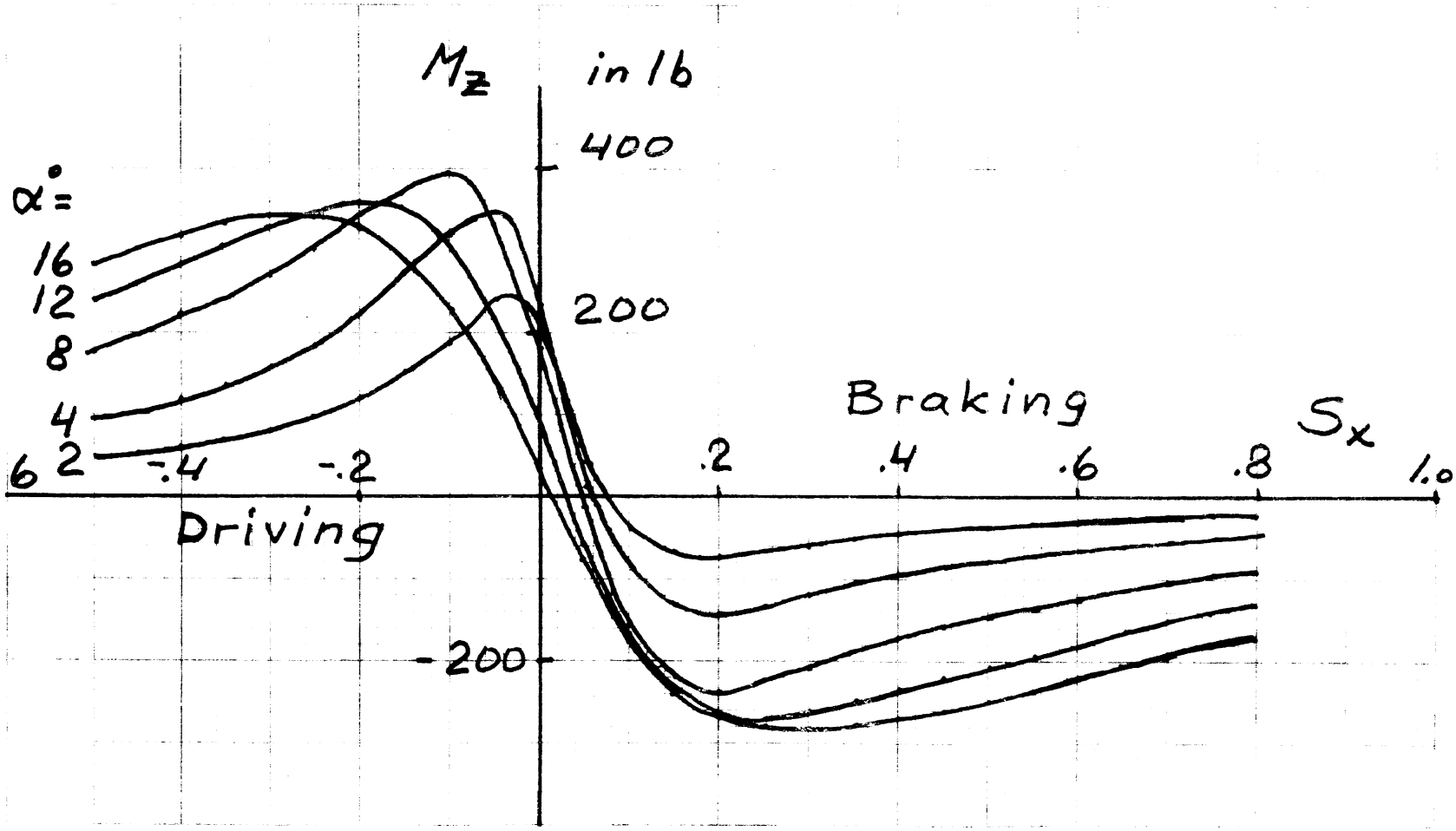

Figure 6.16 Aligning Moment M_z vs. Longitudinal Slip S_x at Slip Angle $\alpha° = 2 - 16$.

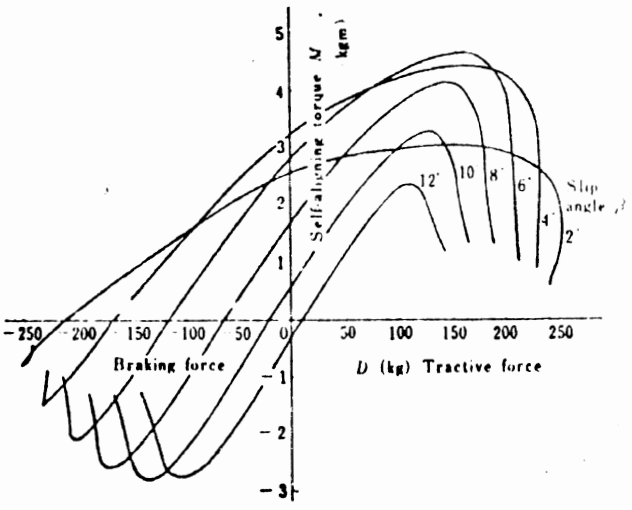

Fig. 9. Self-aligning torque versus tractive and braking forces at various slip angles (Calculated values are shown.)

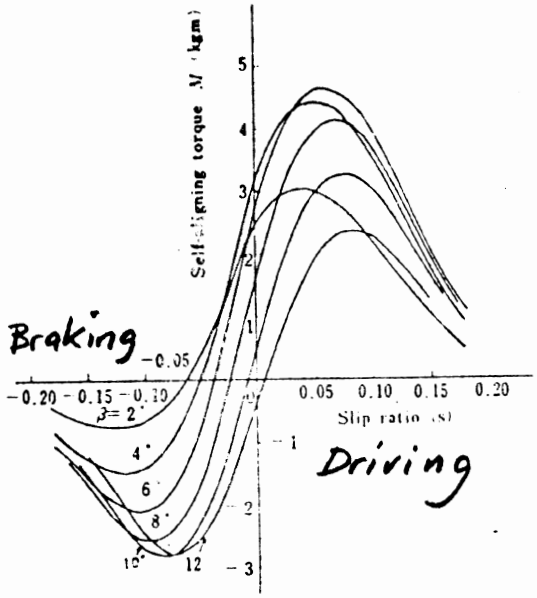

Fig. 7. Self-aligning torque versus slip ratio at various slip angles (Calculated values are shown.)

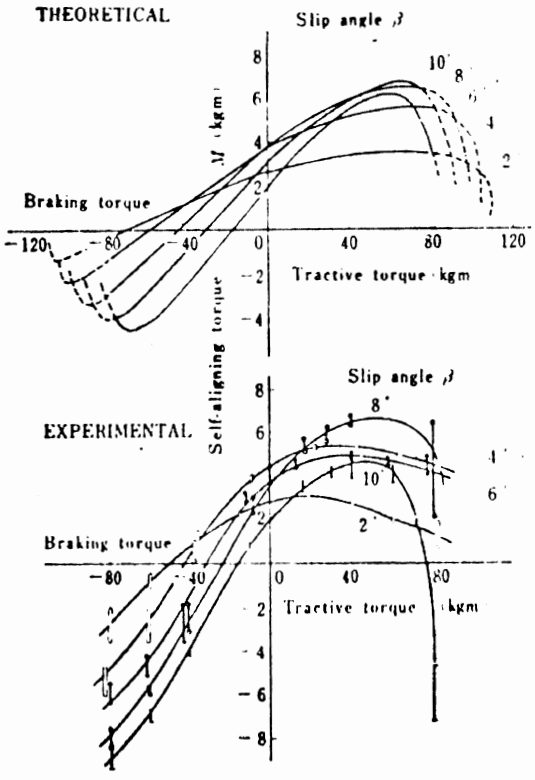

Fig. 14. Self-sligning torque versus tractive or braking torque at various slip angles (Okada's test values and calculated values are shown.)

Figure 6.17. Theoretical and Experimental Aligning Moment Curves Reproduced From Reference [13].

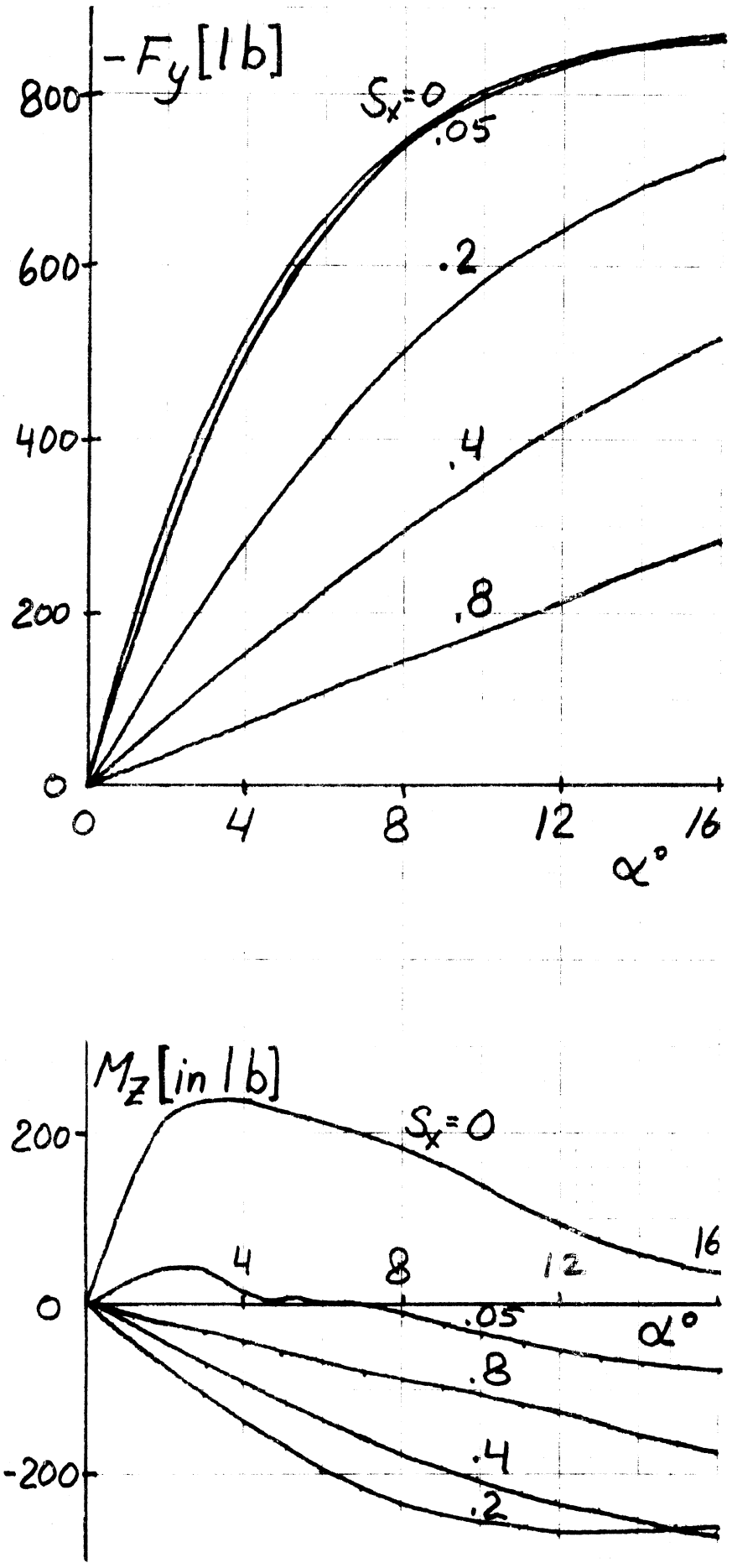

Figure 6.18 Lateral Force F_y and Aligning Moment M_z vs. Slip Angle α at Longitudinal Braking Slip $S_x = 0 - .8$.

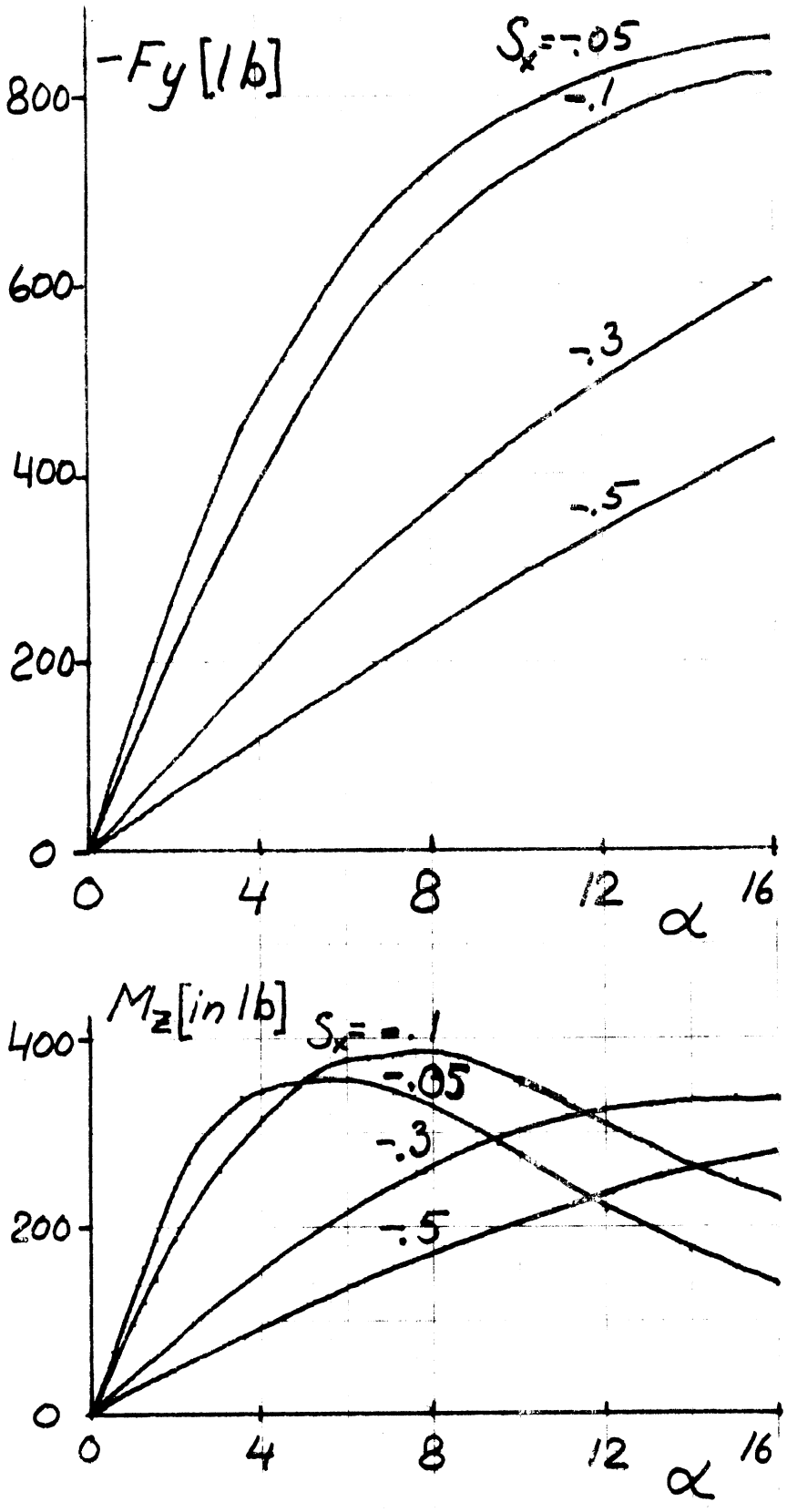

Figure 6.19 Lateral Force F_y and Aligning Moment M_z vs. Slip Angle α at Longitudinal Driving Slip S_x = -.05 - -.5.

6.6 TRANSIENT RESULTS

To obtain the transient results for lateral forces the beam deflection velocity, $\partial v_c/\partial t$, has to be retained. For the solutions to exhibit dynamic equilibrium, a beam deflection damping has to be introduced. This is outlined in Appendix C. The ad hoc value of the damping coefficient, C_B, used is $C_B = .06$. It turns out that this value gives a smooth build-up of lateral force distribution for the dynamic equilibrium solution and also keeps the transient solutions stable. If this damping value is increased to $C_B > .08$, the solutions become unstable and diverge. If it is lower than $C_B = .05$, the response gets too sluggish.

A basic check on the transient program is the gradual build-up of the lateral force, F_y, for a certain constant slip angle from the undeflected starting situation. This has been plotted in Figure 6.20 for $\alpha° = 4$. Comparison is shown with data from a flat-bed test at 1.44 mph. At the small angle tested, the difference in velocity (20 vs. 1.44 mph) should have no effect. The model results correlate well with the experimental data shown in Figure 6.20.

A central application of the transient capability of the model is to the analysis of shimmy behavior.

The tire has been subject to yaw oscillations at various frequencies in the range $1.5 < f < 30$ Hz (at 20 mph free-rolling speed) at a mean slip angle $\alpha°_M = 0$ and an angle amplitude (half peak-to-peak) of $\alpha°_A = 1$.

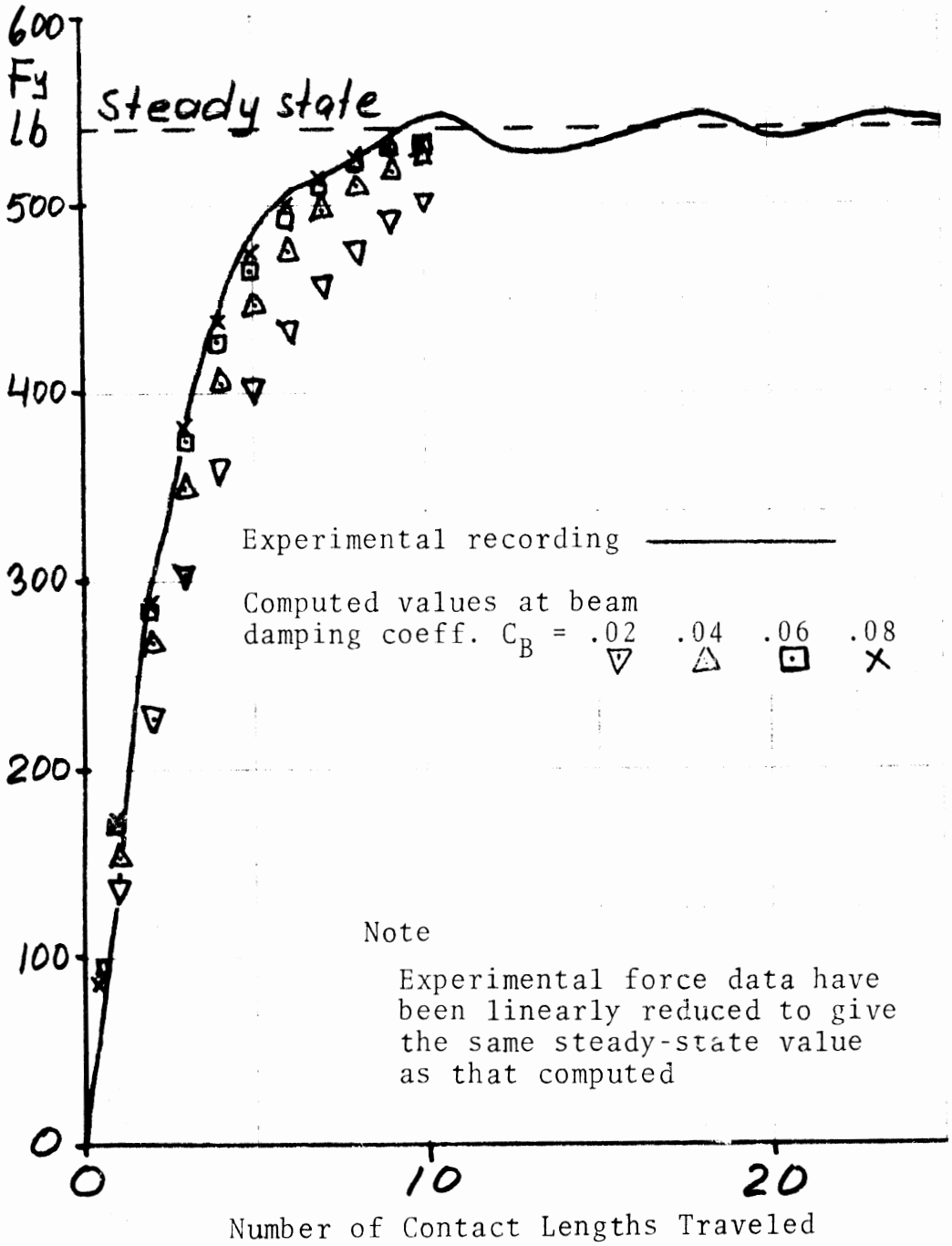

Figure 6.20 Gradual Build-up of Lateral Force F_y from an Initially Undeflected Tire at $\alpha° = 4$. Comparison with Flat Bed Run.

The ratio of transient to steady-state amplitude value of lateral force, $\bar{F}_y$, and the contribution, $\bar{M}_{zy}$, of the lateral force distribution to the aligning torque, $\bar{M}_z$, have been plotted on double logarithmic scales and the phase angle on semi-logarithmic scale as functions of the non-dimensional frequency $\bar{\omega}_a = 2\pi f \cdot a/W$ where a is half the contact length and W is the free-rolling speed.

Since the contribution, $\bar{M}_{zx}$, to the aligning torque from a distribution of longitudinal forces has been computed in a simplified way, only the part contributed by the lateral force distribution, $\bar{M}_{zy}$, has been presented in the graphs. The contribution, $\bar{M}_{zx}$, by the longitudinal forces is given in Figure 6.21. To obtain the total aligning moment, $\bar{M}_z$, a vectorial addition of the two components has to be done.

Figure 6.22 shows $\bar{F}_y(\bar{\omega}_a)$ and corresponding phase angle $\phi_F(\bar{\omega}_a)$. Similarly, Figure 6.23 gives $\bar{M}_{zy}(\bar{\omega}_a)$ and corresponding phase angle $\phi_M(\bar{\omega}_a)$. Figure 6.24 gives the polar representation of the $\bar{F}_y(\phi_F)$ relation. The $\bar{M}_{zy}(\phi_M)$ relation is given in Figure 6.25. No experimental shimmy measurements have been done with this tire. We therefore have to resort to comparison with data presented, e.g., by Pacejka [14] and [15], or Philips [16] for an estimate of the reliability of the model output. This comparison turns out favorably, as shown particularly by the $\bar{M}_{zy}(\bar{\omega}_a)$ and $\phi_M(\bar{\omega}_a)$ functions. The most noticeable feature of the results is

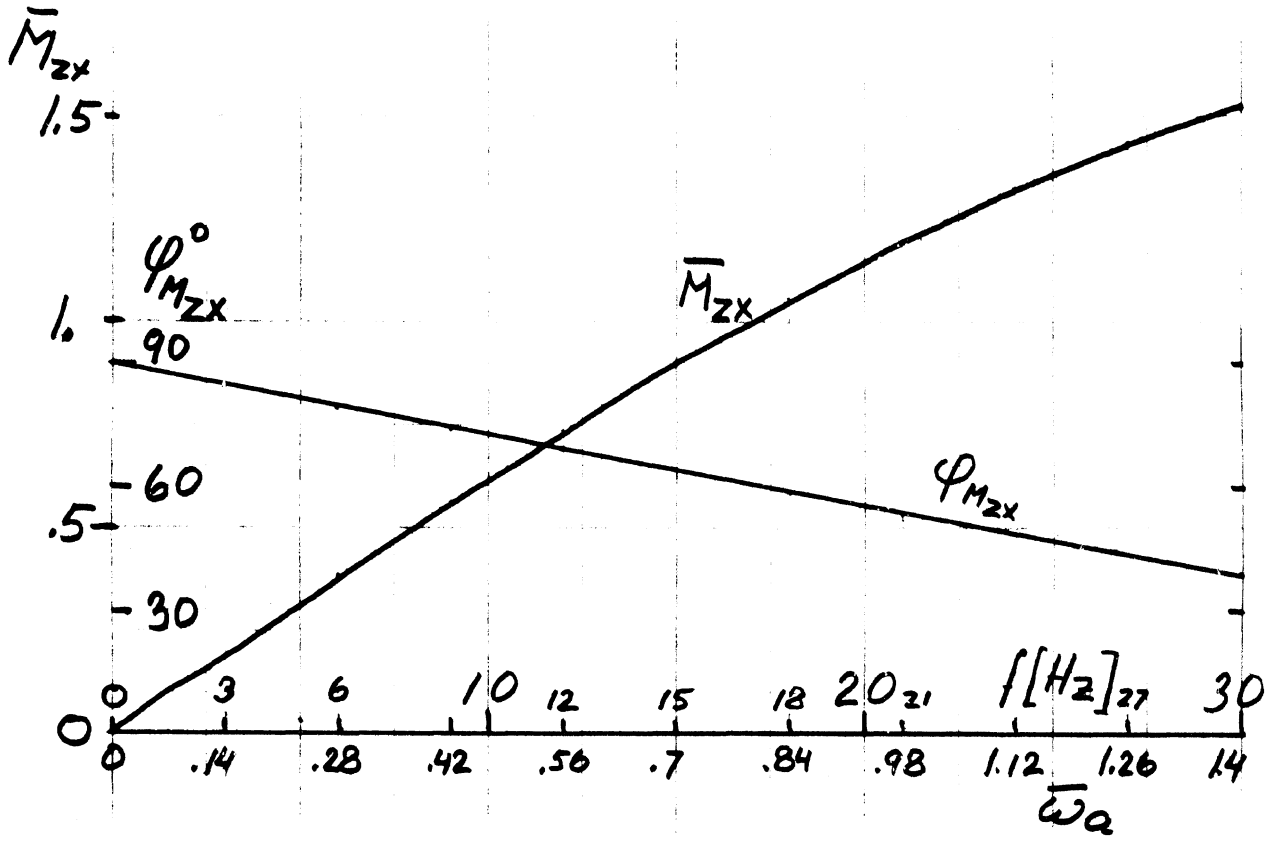

Figure 6.21 Aligning Moment Amplitude Ratio $\bar{M}_{zx}$ and Phase Angle $\phi_{M_{zx}}$ Due to Finite Wheel Width vs. $\bar{\omega}_a$ at W = 20 mph.

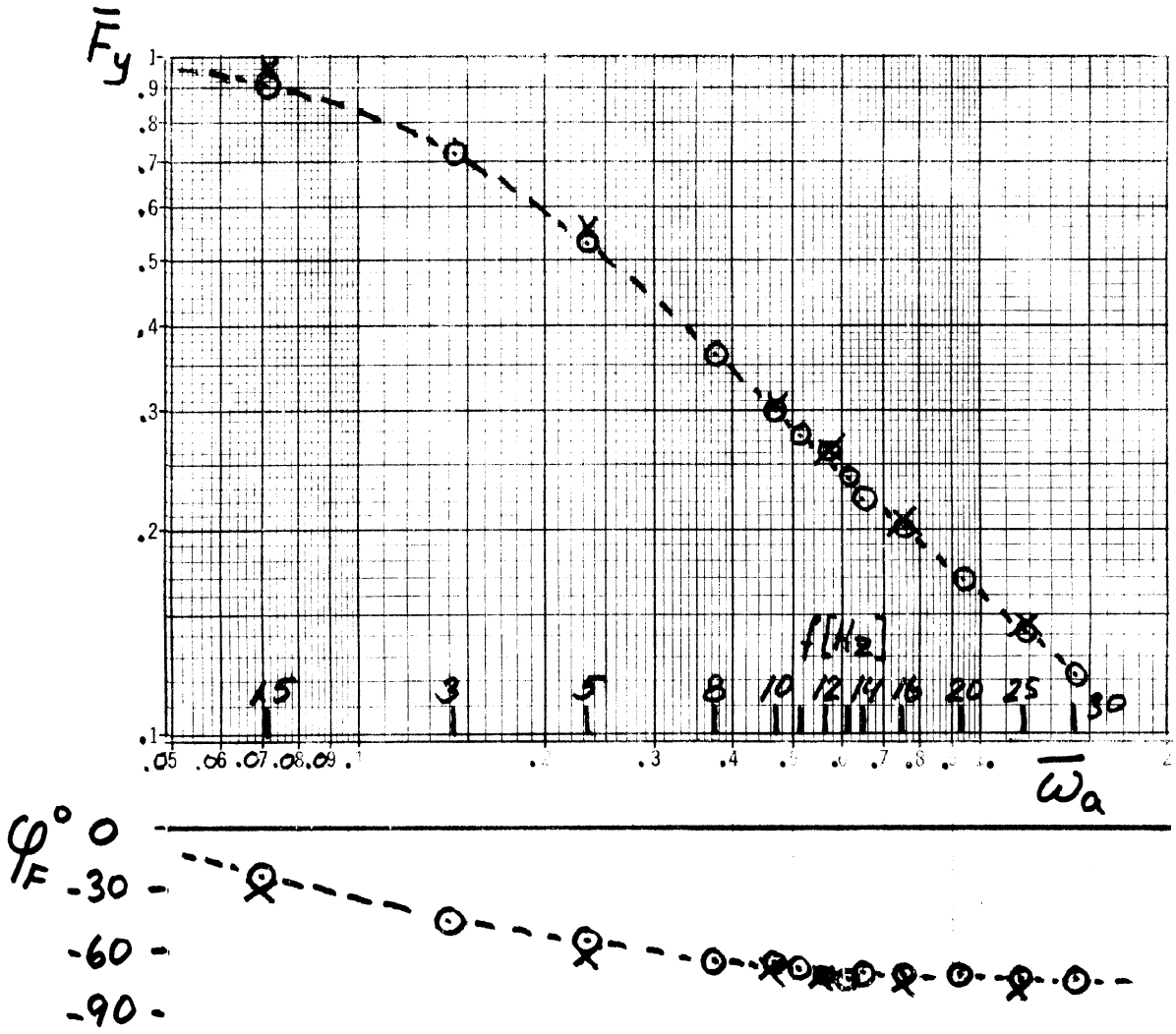

Computed Data: Sliding ⊙ , Stiction X
Assumed Course of Computed Curve -------

Figure 6.22 Lateral Force Amplitude Ratio $\bar{F}_y$ (top) and Phase Angle ϕ_F (bottom) vs. Non-Dimensional Reduced Frequency $\bar{\omega}_a$ at W = 20 mph. Mean Angle α_M° = 0 and Angular Amplitude α_A° = 1.

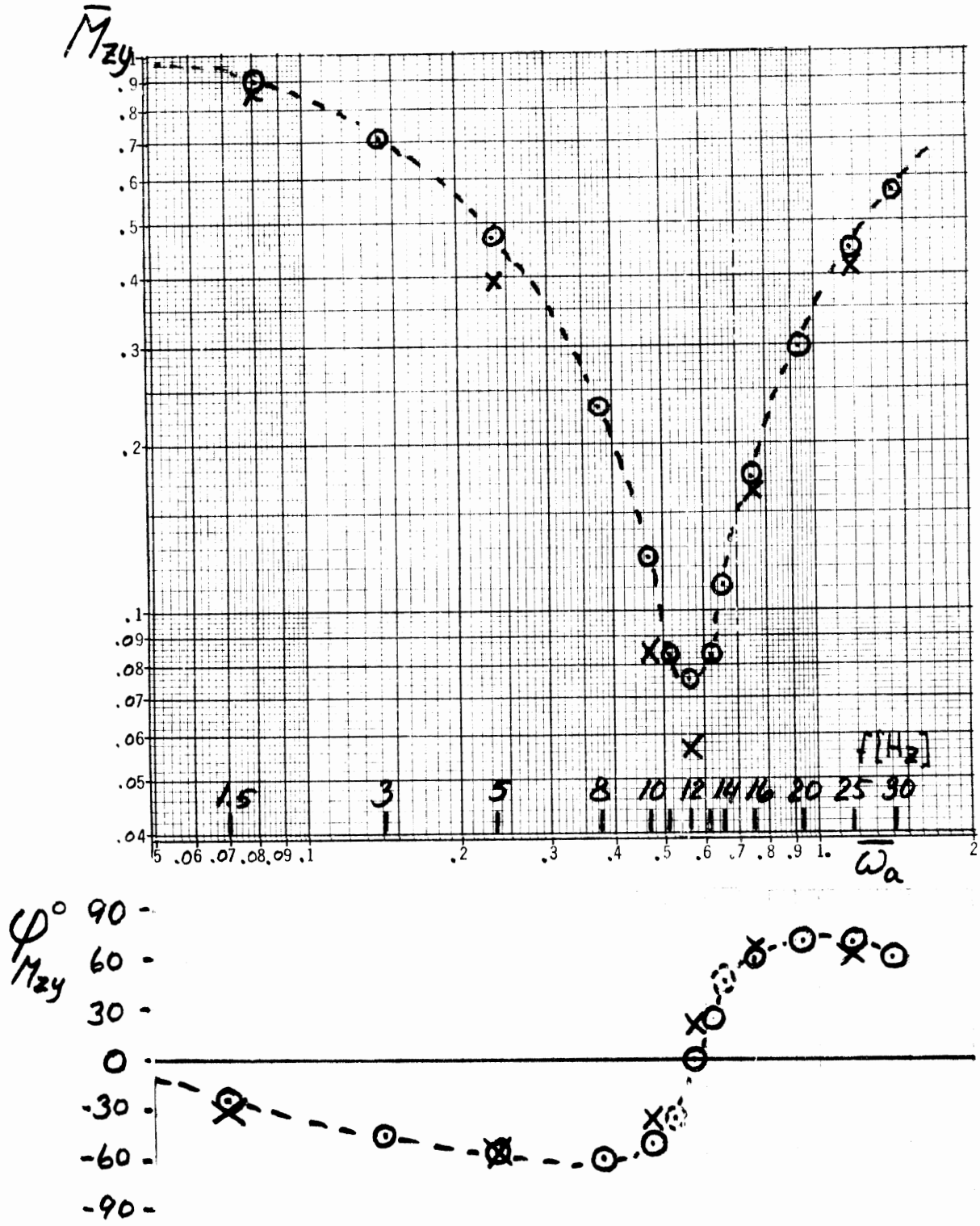

Computed Data: Sliding Θ , Stiction X

Assumed Course of Computed Curve -------

Figure 6.23 Aligning Moment Amplitude Ratio $\bar{M}_{zy}$ (top) and Phase Angle $\phi_{M_{zy}}$ (bottom) vs. Non-Dimensional Reduced Frequency $\bar{\omega}_a$ at W = 20 mph, Mean Angle α°_M = 0 and Angular Amplitude α°_A = 1.

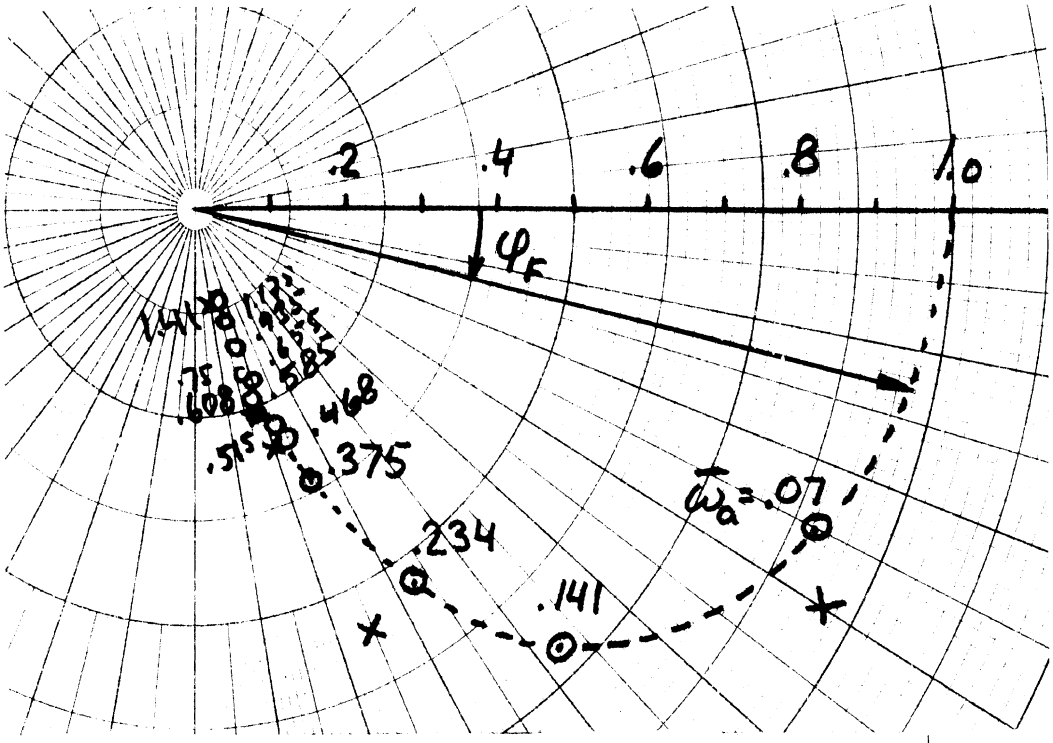

Figure 6.24 Polar Plot $\bar{F}_y(\phi_F)$ with the Non-Dimensional Frequency $\bar{\omega}_a$ Indicated. Computed Values for Element Sliding and Stiction.

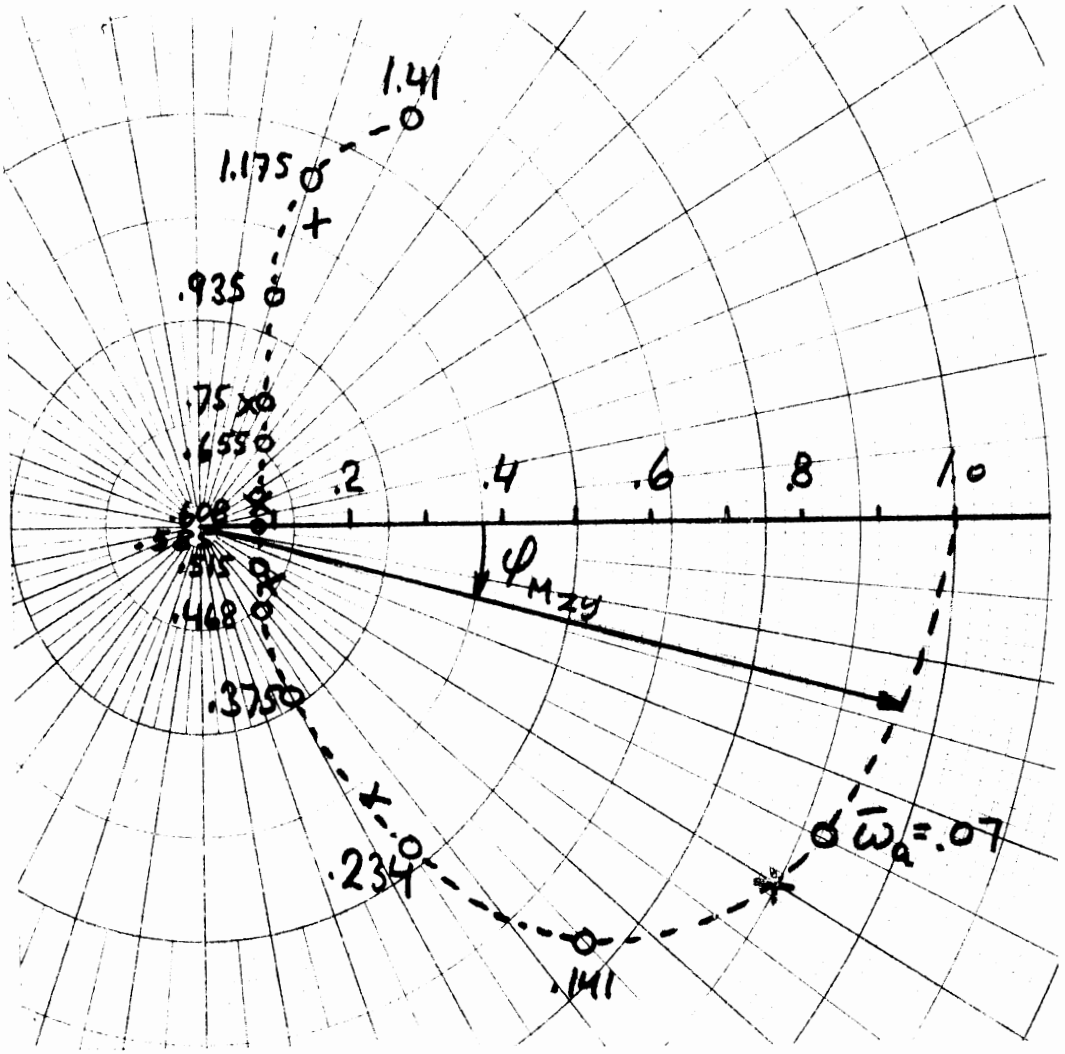

Computed Data: Sliding ⊙, Stiction X
Assumed Course of Computed Curve-----

Figure 6.25 Polar Plot $\bar{M}_{zy}(\phi_{M_{zy}})$ with Non-Dimensional Frequency $\bar{\omega}_a$ Indicated. Computed Values for Element Sliding and Stiction.

to shift the functions in the plot diagrams to the right in the neighborhood of the origin. No doubt this effect can be attributed to the introduced beam ad hoc damping.

The computations have been made both for sliding ability of the tread elements and for no sliding anywhere along the contact patch ($\mu = \infty$). As can be seen from the presented results, no appreciable difference between the two conditions is apparent. This finding is explained by a study of the steady-state sliding situation at $\alpha° = 1$. The two sliding ranges are confined to the extreme end points of the contact patch, and therefore they affect only to a lesser degree the distribution of lateral force.

At larger mean angles the situation is different, since here the sliding velocity is zero for only a small portion of the contact patch. This report, however, does not present the calculation of shimmy data at mean angles other than zero. Due to the non-linearity of $M_z(\alpha)$ and $F_y(\alpha)$ at $\alpha° > 3$ such data would have to be obtained by applying the model to a complete, albeit simple, system comprising a castered wheel, with inertia, subject to a compliance moment.

The deflection curves, relative to the beam produced by each new element that enters the contact patch, as the yaw angle at different frequencies gradually varies, have been obtained on a plotter. This variation of element deflection distribution is presented in Figure 6.26 (bottom) for the

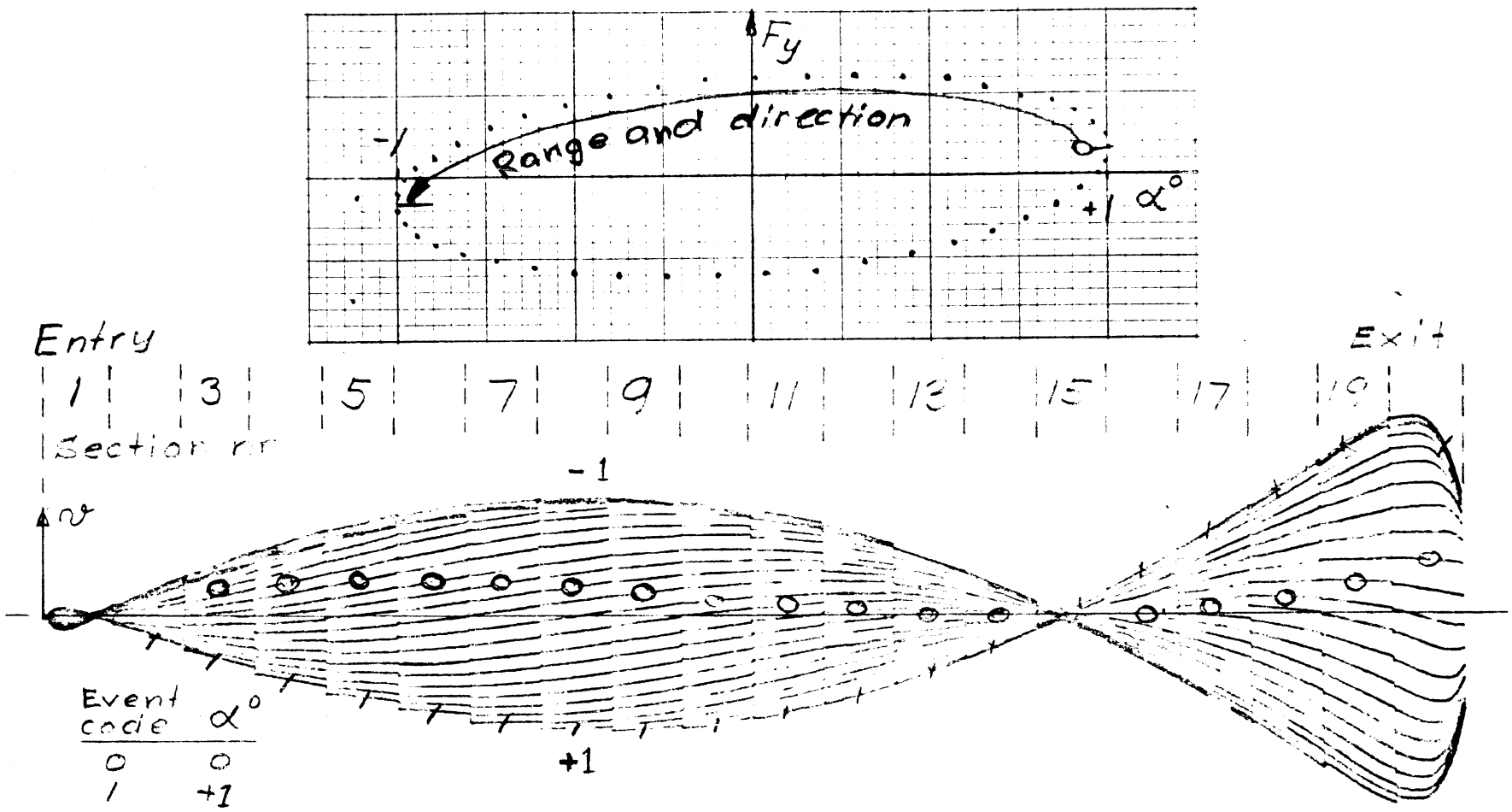

Figure 6.26 $F_y(\alpha)$ Function (top) and Element Lateral Deflection v Relative to Beam Centerline for $\alpha° = +1 \rightarrow 0 - 1$ (bottom) at $\bar{\omega}_a = 1.4$.

non-dimensional frequency $\bar{\omega}_a \approx 1.4$. The top part of Figure 6.26 shows the $F_y(\alpha)$ function related to this deflection distribution. The lateral force distribution is, but for the small element damping, proportional to this deflection.

The yaw angle range covered in the lower part of Figure 6.26 is $\alpha° = +1 \rightarrow 0 \rightarrow -1$. This range and the direction the function is traversed is indicated in the top figure.

The dots in this figure indicate successive coordinates as α gets incremented according to the relation

$$\alpha_n = \alpha_A \cos(\omega t_n)$$

$$t_n = t_{n-1} + \Delta t$$

where Δt is the time taken for the elements to travel the length of a contact patch section.

The continuous lines, slightly broken at the section boundaries, show the path, relative to the beam, that each element follows on its way through the contact patch from entry to exit.

The "zero" in each section indicates the path of the element within a section when the yaw angle of the wheel plane passes the value of zero. The figure reveals how the elements replace each other in the sections being slightly differently deflected due to the change in yaw angle during

the section passage time. The slashes on the elements in the one extreme position indicate their deflections when the yaw angle is $\alpha° = +1$. The other extreme position is in the neighborhood of $\alpha° = -1$.

Perhaps the most striking feature of the distribution of element deflection is the nodal point. This node is coming in from the exit end as the frequency increases. It lies at the exit for $\bar{\omega}_a \simeq .56$.

Figure 6.27 (bottom) shows the distribution of element deflection at $\bar{\omega}_a = .56$ where $\bar{M}_{zy}$ has its minimum. The top of the figure gives the $F_y(\alpha)$ function related to the deflection part. The yaw angle range is $\alpha° = 0 \rightarrow -1 \rightarrow 0$. This is indicated in the top figure. Due to poor accuracy of a computer component when this plot was made, the continuity of the lines is broken at some instances. From the symmetry of the distribution of deflection at $\alpha° = 0$ it can be inferred that the resulting alignment moment at this angle must be small, as is also shown in Figure 6.23.

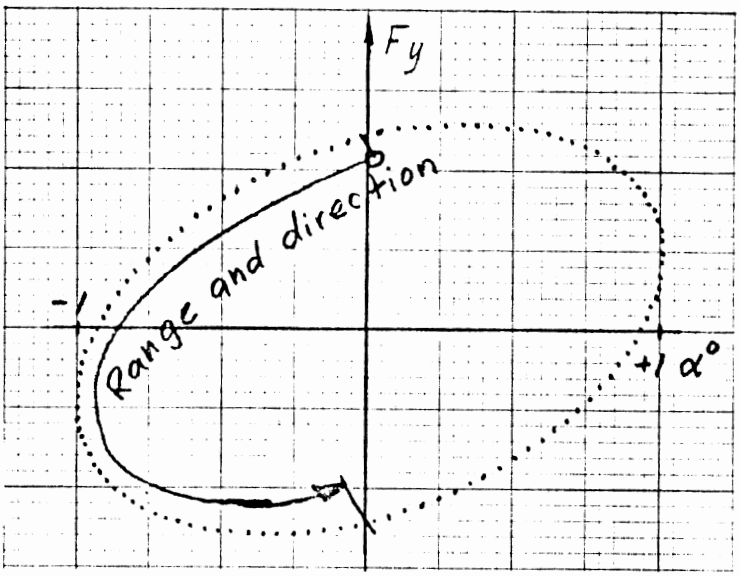

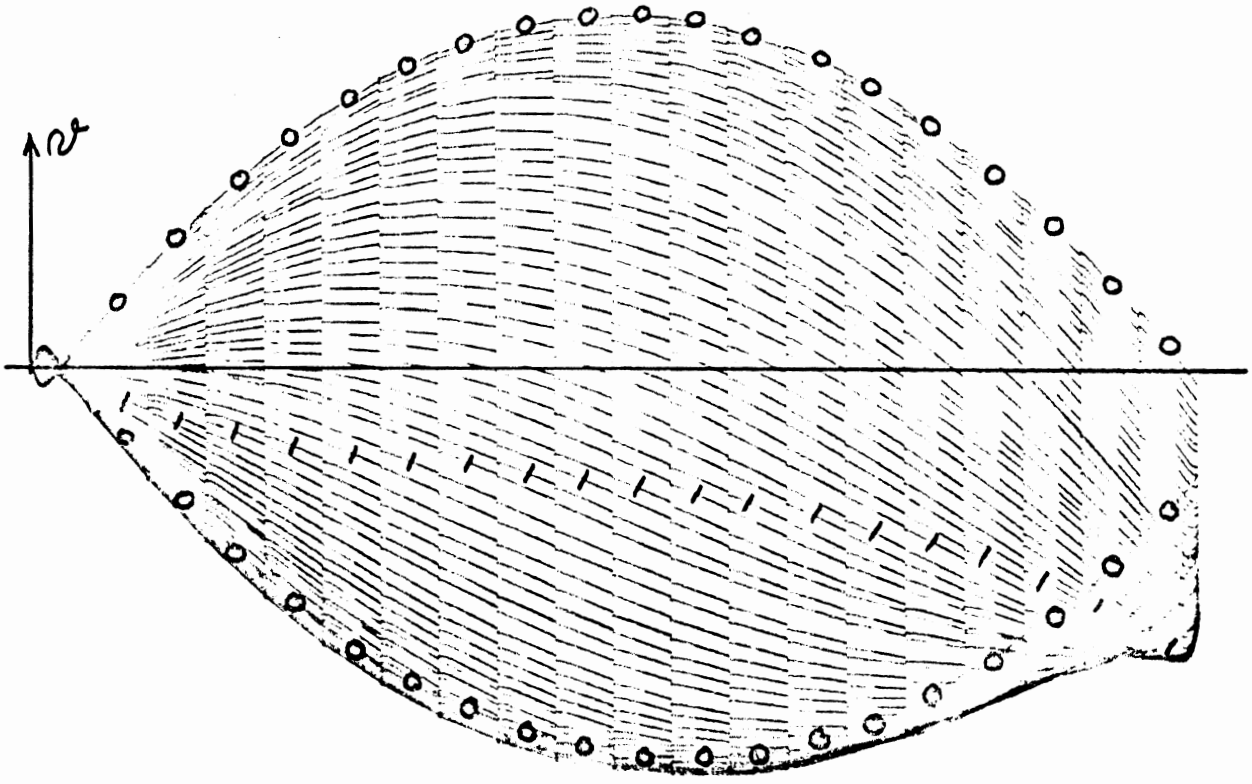

Figure 6.27 $F_y(\alpha)$ Function (top) and Element Lateral Deflection v Relative to Beam Centerline for $\alpha^\circ = 0 \rightarrow -1 \rightarrow 0$ (bottom) at $\bar{\omega}_a = .56$.

7. CONCLUSIONS

The tread-element-following model gives a very good insight into the distribution of element sliding speed and also the deflection pattern of tread and carcass and hence the distribution of traction forces in the contact area due to certain shape of the friction function $\mu(V_s)$. It is also possible to work backwards from experimentally obtained force-slip relations to obtain a reasonable representation of the friction function which was prevailing when the force measurements on the tire were made on the road. An optimization fitting of experimentally obtained results including particularly the aligning moment will have the capability of yielding a detailed representation of the actual $\mu(V_s)$ function. However, reasonable force distributions and sliding-stiction conditions of the tread elements in the contact patch in good accord with experimentally obtained data have been the result of the model.

It has been noted with satisfaction that the dynamic representation of the tread elements can give rise to a squeal oscillation of experimentally observed frequency. The oscillations occur, as observed on the real tire, when the slip variable has brought the elements to operate on the declining part of the $\mu(V_s)$ curve.

The lateral deflection of the tread base has been given a relatively simple representation: a beam on a foundation

with a lateral spring constant unaffected by the radial flattening in the contact area. It has become evident from the performed study that the slope of the beam at the entry point of the contact patch determines to a great extent the deflections of the elements in the contact patch; for obtaining the distribution of the lateral force, it is conceivable that this tread base representation is somewhat crude.

A one-element model, i.e., a model with only one tread element traveling through the contact patch at a time, is sufficient for a steady-state situation when the conditions in the contact patch are functions of location only. For transient phenomena, however, the conditions in the contact patch vary not only with location but also with time at each location. This makes it necessary to introduce a multitude of elements in order to give a realistic representation of the transient behavior of the tire. We have used 20 elements which seems to be sufficient for the lower portion of the frequency range, say, below a value of $\bar{\omega}_a \tilde{\sim} .4$ (non-dimensional circular frequency). For higher values the variation at a location becomes too large to be covered by a time increment which is a 20th of the patch passage time. A larger number of elements must be considered. The model provides for a successive increase of elements as required.

The transient yawing results for side force and aligning moment compare well with those given in published papers for

non-sliding elements at a mean slip angle of zero degrees. There is, however, a suspicion that the beam damping introduced for stability purposes, is not optimal. This ad hoc damping seems to influence the data unduly at higher frequencies.

The capability of the model to allow oscillations about a mean slip angle different from zero, when extended sliding may occur, has not been fully explored. Storage oscilloscope observations of sliding and deflections have, however, revealed the expected approximate superpositions of the oscillatory behavior on the steady-state situation. It would be interesting, and definitely of some value, to use the model for the study of a pivoting wheel (one with mass) that can be given a bias pivoting moment that brings the mean slip angle within the range where the maximum of the aligning moment occurs ($\alpha° \simeq 3$). The non-linearities of this arrangement would most certainly give rise to interesting effects.

The tread-element-following model is complex and requires quite a lot of computation time, particularly for the beam deflection due to the distributed point loads. It is, therefore, a great advantage, in view of time reduction, to have access to a hybrid computation facility. A ratio of ~ 17.5 has been obtained for the time required for pure digital solutions on the PDP 11/45 to the time of hybrid

computations, using the combination of this computer with the AD-4 analog computer. The hybrid program can probably be improved to make even more use of the analog, reducing further the hybrid running time and it is not inconceivable that this time ratio can be raised to a value of ~ 50.

8. SUGGESTIONS FOR FUTURE DEVELOPMENTS

1. Refined representation of the friction function, $\mu(V_s)$.

2. Optimization fitting of the $\mu(V_s)$ function to a combination of lateral force, aligning moment, and longitudinal force.

3. A more accurate representation of lateral carcass deflection through refined beam equation or experimentally obtained Green function. Emphasis on slope distribution.

4. Introduction of nonlinear tread element force-deflection functions.

5. Consideration of coupled lateral and longitudinal element deflections.

6. Finite tire width with a multitude of circumferential element rows to account for nonlinear contribution to aligning moment from longitudinal forces at non-zero shimmy mean angles.

7. As a consequence of (6), an introduction of an area distribution of vertical pressure in the contact patch will be appropriate.

8. Improve the beam damping scheme for transient motions.

9. Run the model on a castered wheel with inertia and steering compliance at mean angles in the nonlinear range of the aligning moment.

10. Introduce tire inertia forces.

11. Account for tire inclination (camber).

9. ACKNOWLEDGEMENT

The author's thanks are due to Joe Dunne, whose excellent knowledge of the application to the PDP 11/45 of FORTRAN programming made the transfer of the original PDP 15 FORMIC version easy and whose keen eye for programming bugs has been highly appreciated; to Sid Peat whose never ceasing vigilance on the analog computer kept the hybrid program going; to Doug Brown and Tom Post for the valuable assistance in performing the measurements on tire properties made for this investigation; to Tom Tielking for valuable and inspiring discussions on tire dynamics and for transposing the author's Swedish-influenced English into current American, and to Jeannette Nafe for her rapid and impeccable typing of this report.

10. REFERENCES

1. Pacejka, H.B. and Fancher, P.S., "Hybrid Simulations of Shear Force Development of a Tire Experiencing Longitudinal and Lateral Slip." Proceedings of the XIV FISITA Congress, 1972.

   Also

   Pacejka, H.B. and Mital, N.K., A Hybrid Model of Tire Shear Force Generation. Interim Document 3 of Project 329180, Highway Safety Research Inst., Univ. of Michigan, Sponsored by Motor Vehicle Manufacturers Association, August 1972.

2. Tielking, J.T., Tire Traction Data Measured by the HSRI Mobile Tire Tester. Interim Document 5, HSRI Project 329180, March 1973.

3. Fromm, H., "Schwingungsvorgänge an der Lenkung von Kraftfahrzeugen." Verh. des 3. intern. Kongr. für Technische Mechanik, Stockholm, 1930, Tiel III, p. 278.

4. Fiala, E., "Seitenkräfte am rollenden Luftreifen." V.D.I. Zeitschrift, Vol. 96 (1954) Nr. 29.

5. Wylie, J., "Dynamic Problems of the Tricycle Alighting Gear." Journ. Aeron. Sci., 7(1939)2, p. 56.

6. Kantrowitz, A., Stability of Castering Wheels for Aircraft Landing Gears. NACA Report 686, 1940.

7. v.Schlippe, B. and Dietrich, R., Das Flattern eines bepneuten Rades. Bericht 140 der Lilienthal Gesellschaft, 1941; also, NACA TM 1365 (1954).

8. Saito, Y., "A Study of Dynamic Steering Properties of Pneumatic Tyres." Proceedings of the FISITA Congress, 1962.

9. Segel, L., "Force and Moment Response of Pneumatic Tires to Lateral Motion Input." Jour. of Engr. for Industry, Vol. 88, No. 1, February 1966

10. Pacejka, H.B., The Wheel Shimmy Phenomenon, a Theoretical and Experimental Investigation. Veh. Res. Lab., Tech. Univ. of Delft, Report 170, 1966; also, "Analysis of the Shimmy Phenomenon." Proc. Inst. Mech. Engrs., Vol. 180, pt. 2A, No. 10, 1965-66.

11. Savkoor, A., Green's Function Approach to Tyre Flexibility. Veh. Res. Lab., Tech. Univ. of Delft, Report 170, 1966; also, "The Lateral Flexibility of Pneumatic Tires and Its Application to the Lateral Rolling Contact Problem." FISITA/SAE Congress, Paper 700378, 1970.

12. Borgmann, W., "Theoretische und experimentelle Untersuchungen an Luftreifen bei Schräglauf." Dissertation, Technische Hochschule, Braunschweig, 1962.

13. Sakai, H., "Theoretical Study of the Effect of Tractive and Braking Forces on Cornering Characteristics of Tires." Bulletin of J. SAE, No. 3, 1971, p. 64.

14. Pacejka, H.B., "The Wheel Shimmy Phenomenon." Doctoral Thesis, from Delft Univ. of Technology, 1966; also as Report WTHD48(1973), Delft Univ. Tech.

15. Pacejka, H.B., "Approximate Dynamic Shimmy Response of Pneumatic Tires." Vehicle Systems Dynamics, 2(1973), pp. 49-60.

16. Philips, B., "The Static Steady-State and Dynamic Characteristics of Pneumatic Tyres." Doctoral Thesis from Lanchester Polytechnic, Coventry, 1973.

17. Grosch, K.A., "The Relation between the Friction and Visco-Elastic Properties of Rubber." Proceedings, Royal Society of London, Vol. A274(1963), p. 21.

18. Grosch, K.A., "The Speed and Temperature Dependence of Rubber Friction and Its Bearing on the Skid Resistance of Tires." The Physics of Tire Traction, G.M. Symposium, (D.F. Hays & A.L. Browne, Eds.), 1973.

19. Frank, F., "Teorie des Reifenschräglaufs." Dissertation from Inst. of Tech., Darmstadt, 1965.

20. Hinton, B.J., "An Investigation of Tire Tread and Deformation Under Lateral Point Load." Diploma Thesis, No. 61/2, Advanced School of Automobile Engineering, Cranfield (England), 1961.

21. Winsor, F., "Relaxation Length of Bias Tires." Doctoral Thesis, Princeton Univ., November 1972.

22. Tielking, J.T. and Mital, N.J., A Comparative Evaluation of Five Tire Traction Models. Interim Document 6, HSRI Project 329180, January 1974.

23. Trivisonno, N.M., Beatty, J.R., Miller, R.F., "The Origin of Tire Squeal." Kautschuk und Gummi, Kunststoffe 20(1967) Heft 5.

24. Schubert, K., Seitenkräfte an rollenden Luftreifen bei periodischen Felgenquerbewegungen. Deutsche Kraftfahrtforschung und Strassenverkehrstechnik, Heft 230, 1973.

11. SYMBOLS AND TERMINOLOGY

A,B	constants in the equation for unit load beam deflection
a	contact patch half length
b	contact patch half width
b_B	belt half width
C_B	beam damping coefficient
c_x,c_y	tread element damping constants
$E \cdot I$	beam stiffness
F_x,F_y,F_z	resulting forces on the wheel
f	oscillation cycle frequency
f_n	natural tread element cycle frequency
K	beam foundation spring constant
K_c	circumferential carcass spring constant
K_{CT}	combined longitudinal carcass and tread spring constant
K_L	longitudinal carcass spring constant
k_x,k_y	tread element spring constants
L	tire circumference half length
M_z,M_{zx},M_{zy}	aligning moment and components due to longitudinal and lateral force distributions
m_n	nominal longitudinal distribution of tread element mass

m	reduced longitudinal distribution of tread element mass
N	beam tension
P	inflation pressure
$PL = 2 \cdot a$	
$PW = 2 \cdot b$	
Q	beam point load
q	resulting friction force intensity
q_x, q_y	components of friction force intensity
q_z	vertical pressure intensity
q'_x, q'_y	components of the sum of tread element spring and damping intensities
S_x	longitudinal slip
s_n	roots of the beam equation
t	independent variable time; also tread thickness
t_o	time at section entry
t_s	time from section entry
Δt	section passage time
U_c	longitudinal displacement of contact patch center due to the longitudinal tire force F_x
u	longitudinal deflection of a tread element relative to its base point on the tread base
V_{AS}	constant in the analytical representation of $\mu(V_s)$

V_{cx}	longitudinal slip of the belt
V_{cy}	lateral slip of the wheel plane
V_x	longitudinal speed of the wheel center
$V_y = V_{cy}$	
V_r	rolling speed of the wheel
V_s	resultant sliding speed of a tread element
V_{sx}, V_{sy}	coordinates of the tread element sliding speed
v	lateral deflection of a tread element relative to its base point on the tread base
v_B	lateral displacement of the tread base relative to the wheel plane at steady state
v_c	lateral beam deflection relative to wheel plane
v_y	lateral displacement of a point on the wheel plane, due to yawing, relative to steady-state wheel plane
W	traveling velocity of the wheel center
W_{Ref}	reference traveling velocity
w_e	effective width of tread pattern
x	base point coordinate in the wheel plane from the x_t origin
x_i	coordinate for beam deflection y_i due to point load at ξ_j
x_r, y_r	steady-state coordinate system for the contact area

x_s	distance from section entry
x_t, y_t	transient coordinate system for the contact area
x_w, y_w, z_w	steady-state coordinate system referred to the wheel contact center
y_i	beam deflection due to unit point load at ξ_i (Green's function)
y_{AL}	amplitude of lateral displacement of the wheel plane
y_L	lateral transient displacement of the wheel plane
α	slip angle (steady state)
$\alpha_M = \alpha$	mean angle at transient yawing
α_y	increment of mean slip angle due to transient yawing
α_{yA}	amplitude of transient yawing
γ	specific mass of the tread rubber
μ	friction coefficient
μ_{po}, μ_{pl} $\mu_{pt}, \mu_H, \mu_{AS}$	constants in the analytical representation of $\mu(V_s)$
ξ_j	coordinate of beam point load
ϕ_F	phase angle for $\overline{F}_y$
$\phi_{M_{zx}}, \phi_{M_{zy}}$	phase angles for $\overline{M}_{zx}$ and $\overline{M}_{zy}$

ω	oscillation angular frequency
$\bar{\omega}_a$	non-dimensional angular frequency; reference length a
$(\cdot)=d(\ )/dt$	time derivative
$(')=d(\ )/dx$	function slope
$(\partial/\partial t)_x$	partial derivative with respect to t with x constant
$(\partial/\partial x)_t$	partial derivative with respect to x with t constant
—	bar over variable indicates non-dimensional quantity

Subscripts

FC	final condition for a contact patch section
IC	initial condition for a contact patch section
n	section number in the contact patch or time step number

APPENDIX A

FRICTION COEFFICIENT

The friction force, q, acting on each tread element is obtained from the relation

$$q = \mu \cdot q_z(x)$$

Here $q_z(x)$ is the longitudinal intensity of the vertical load distribution in the contact patch.

Since the elements can respond to the forces applied on them by sliding over the road surface, a knowledge of the effect of sliding velocity on the friction coefficient, μ, is needed.

Results of testing of tread elements in sliding over an actual road surface seems to be scarce and incomplete. Unfortunately, they are entirely non-existent for the test conditions of the R70B tire used in this work.

The sliding testing of blocks of elastomers of various compounds on idealized rough surfaces under well-defined laboratory conditions can, however, throw informative light on the general relationship between friction and sliding speed. This can serve as a guideline for the choice of a suitable $\mu(V_s)$ function for the special application at hand.

Grosch [17], [18] has presented friction curves for various rubber compounds on dry glass and carborundum surfaces. Figure A1, from [17], shows the effect of surface texture on a styrene-butadiene (SBR) without carbon black. Figures A2 and A3 from [18] show the effect of adding carbon black to the rubber stock. In Figure A4 from [18], Grosch shows some of the effects of lubricating the track.

The striking effect of adding carbon black to the compound is revealed in Figures A2 and A3. A lowering of the friction peak and a considerable extension of the high friction range in a gently curved plateau is the result.

The R70B tire has been tested for lateral force on a dry concrete road surface. It is now assumed that the $\mu(V_s)$ function has a general shape given in the semi-log diagram of Figure A5.

In a linear diagram, this function is assumed to take the shape given in Figure A6. In the computations this is approximated by part of a parabola, a hyperbola, and a plateau as indicated by dotted lines in Figure A6. These functions are specified by six parameters (μ_{Po}, μ_{P1}, μ_{PT}, μ_H, μ_{AS}, V_{AS}) which have been found by trial and error to give a reasonable fit to the experimentally obtained lateral force curve for the test tire at 20 mph. Since the shape of the $\mu(V_s)$ curve strongly influences the distribution of lateral force and hence the aligning moment, it would be of even greater value

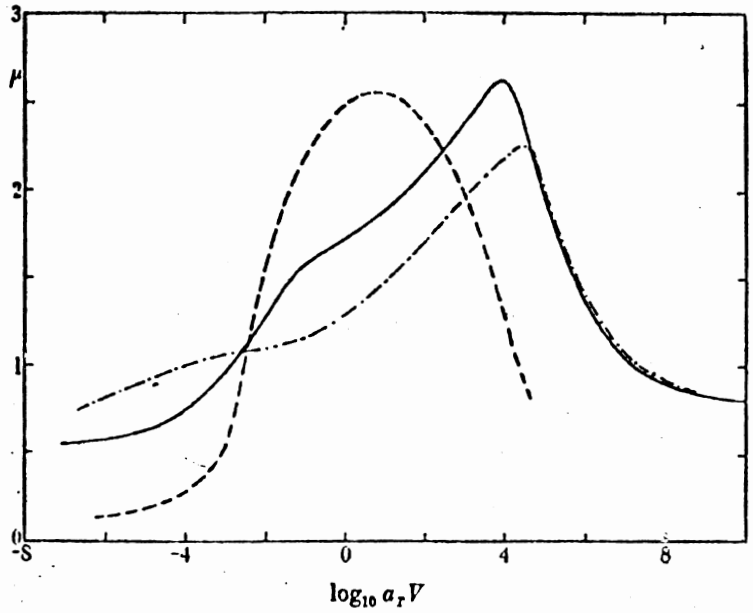

FIGURE 7. Master curves of the coefficient of friction for styrene-butadiene rubber B on the three surfaces: – – – –, wavy glass; ———, clean silicon carbide; –·–·–·–·–, dusted silicon carbide; all curves referred to 20 °C.

Figure A1. From [17].

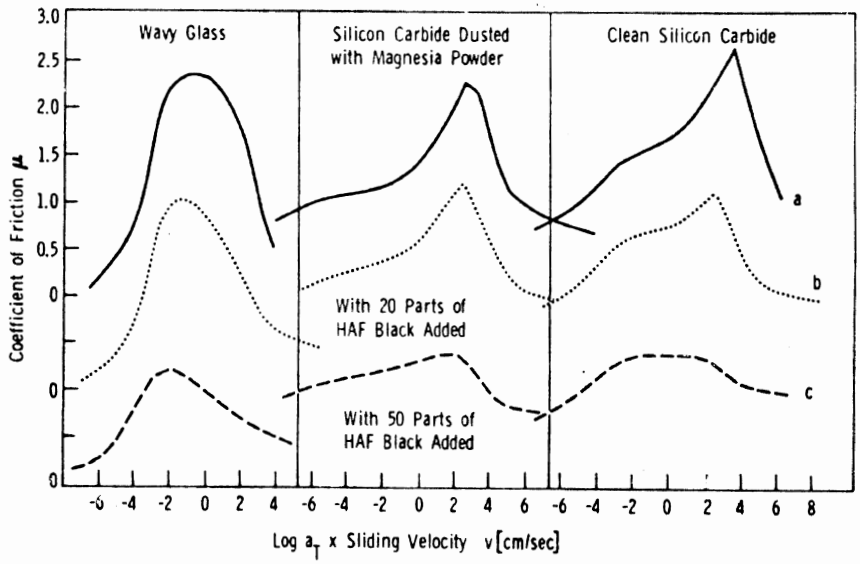

Fig. 5. Master curves of the friction coefficient of an acrylonitrile rubber (a) as gum rubber (b), filled with 20 pphr HAF black and (c) filled with 50 pphr HAF on three different surfaces.

Figure A2. From [18].

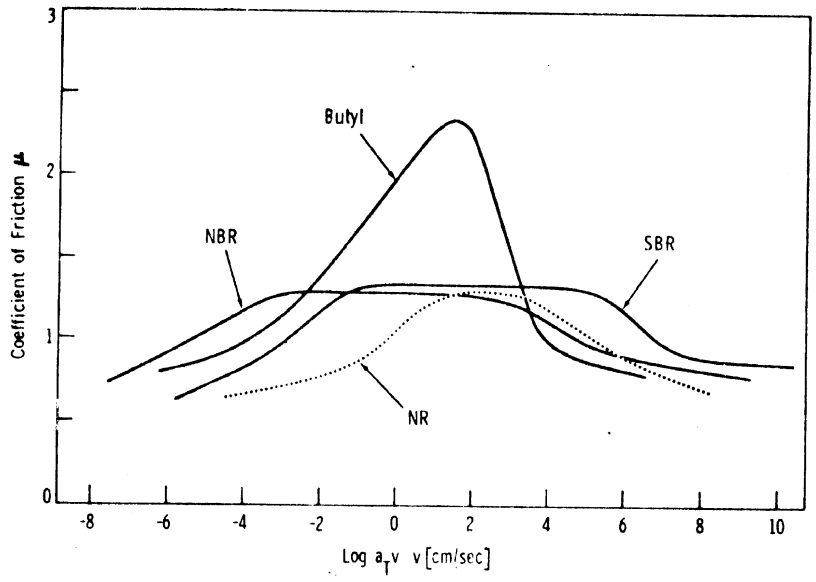

Fig. 6. Master curves of the friction coefficient on carborundum paper for four rubbers of different glass transition temperature, all filled with 50 pphr HAF black (7).

Figure A3. From [18].

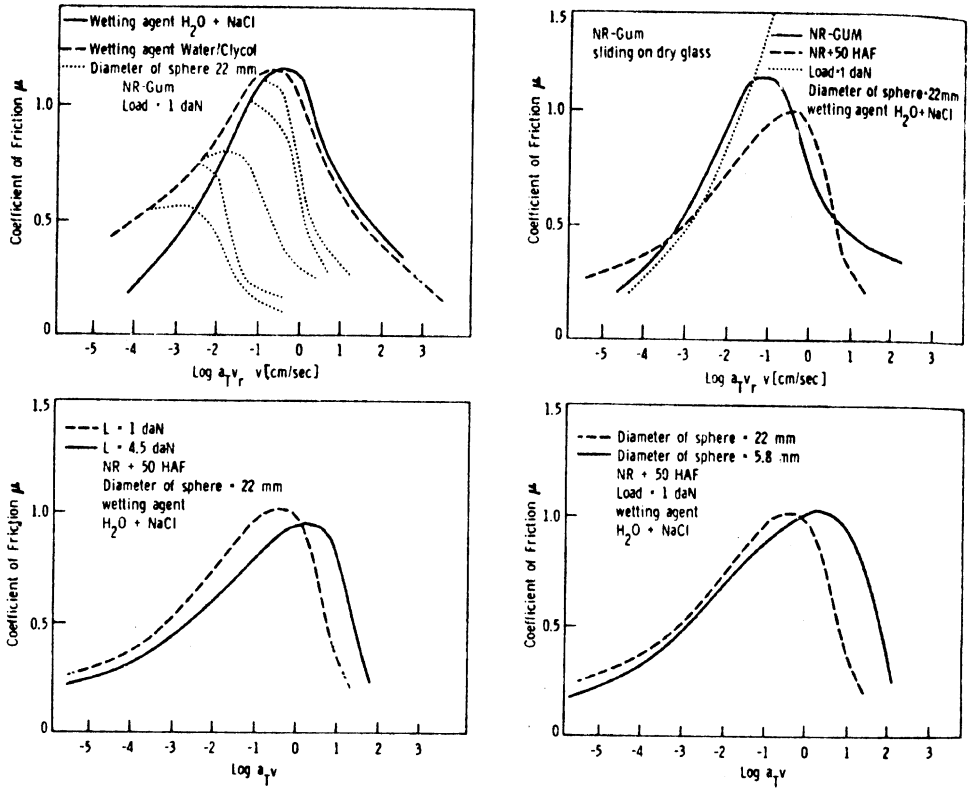

Fig. 9. Friction master curves obtained with a steel slider on a lubricated rubber track, Upper Left: two different lubricants. For the high-viscosity lubricant only the rising part forms a master curve. Upper Right: Comparison of gum NR with black filled NR. Dotted lines shows the master curve of gum NR on dry glass. Lower Left: Two different loads. Lower Right: Two different slider diameters.

Figure A4. From [18].

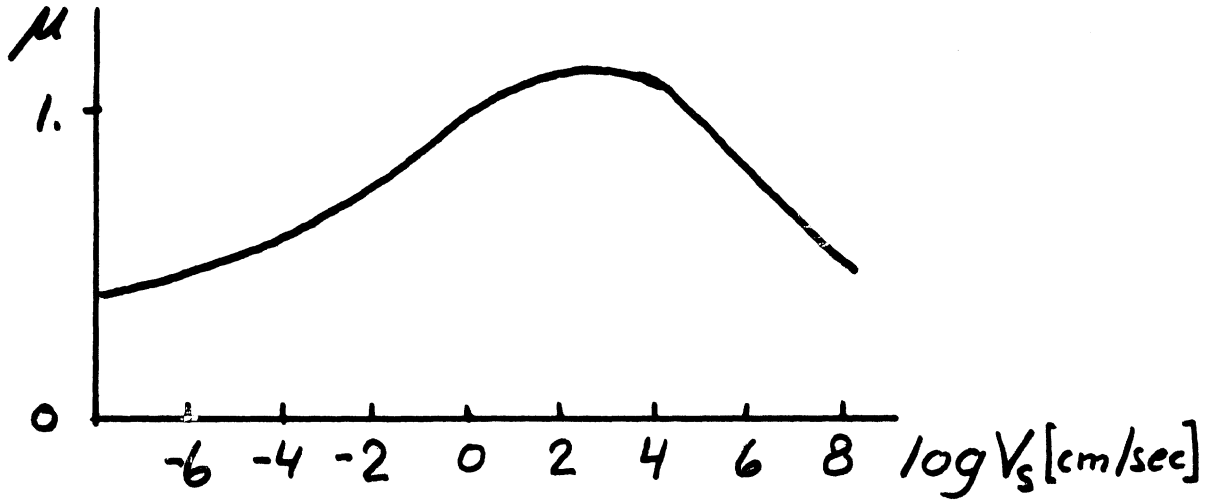

Figure A5. Assumed General Shape of $\mu(V_S)$ Function.

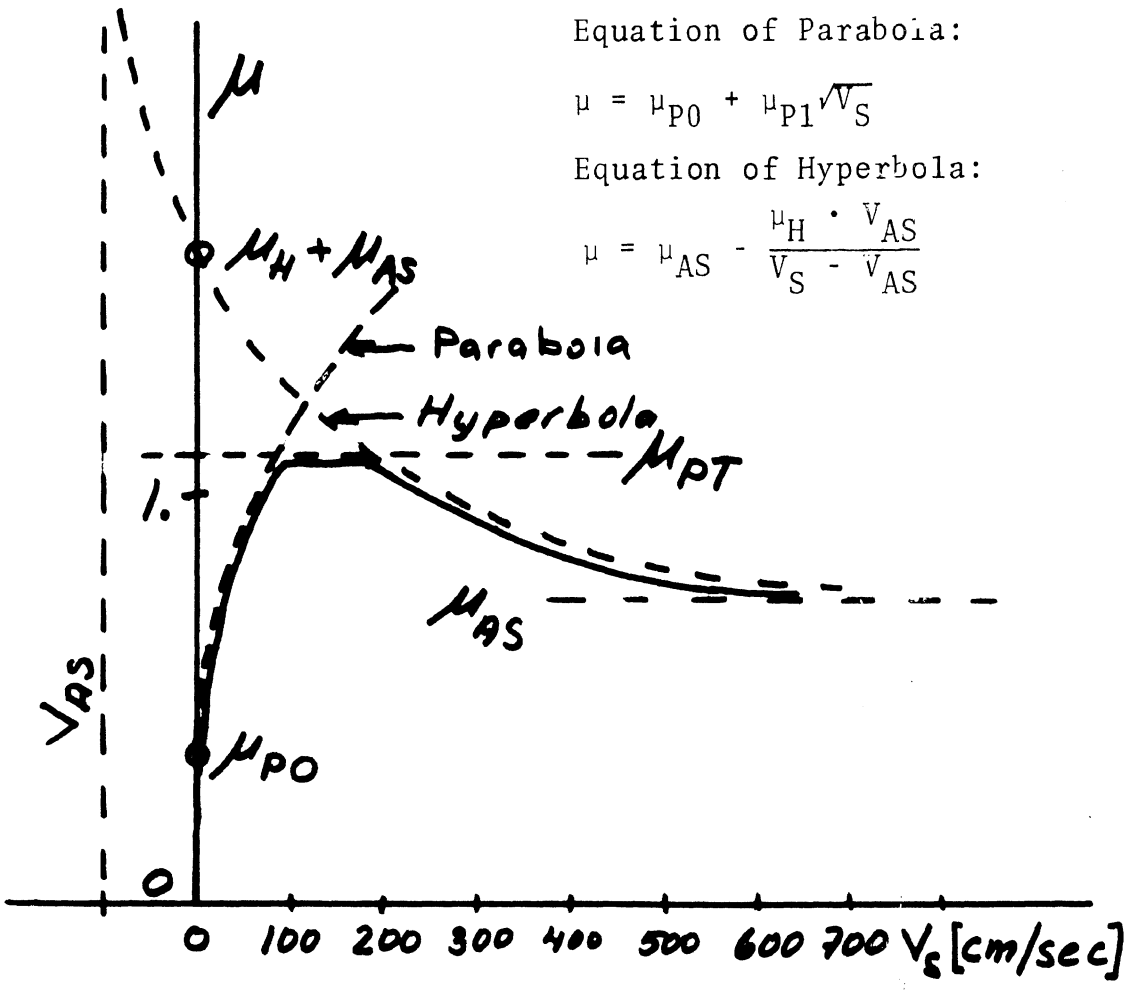

Figure A6. Analytical Approximation of $\mu(V_S)$ Function.

to try to optimize the $\mu(V_s)$ curve, making use of a $M_z(\alpha)$ relationship when available.

It should also be possible to adjust through iteration by an optimization process the detailed shape of the $\mu(V_s)$ curve until an optimal fit is obtained for each one of known F_x, F_y, and M_z functions or even a combination of them. It should be observed that the chosen $\mu(V_s)$ representation has a finite value of $\mu(0)$.

Some considerations will now be given to the time an element spends in the contact patch and the effect this has on the choice of accurate representation of μ at small sliding speeds.

Assuming a traveling speed of 20 mph and a length of the contact patch of .5 feet, the time that an element is in contact with the ground will be $1.68 \cdot 10^{-2}$ sec.

Looking at Figure A7 we see that in the case that the real μ representation (1) would bring μ to an equilibrium position at $0 < V_s < \Delta V_s$ the approximate curve (2) would bring V_s to zero. If we thus lose the accurate representation of μ for velocities below, say, 1. cm/s, then the maximum error in displacement this could give rise to, for an element sliding at this speed through the whole length of the contact patch, would be

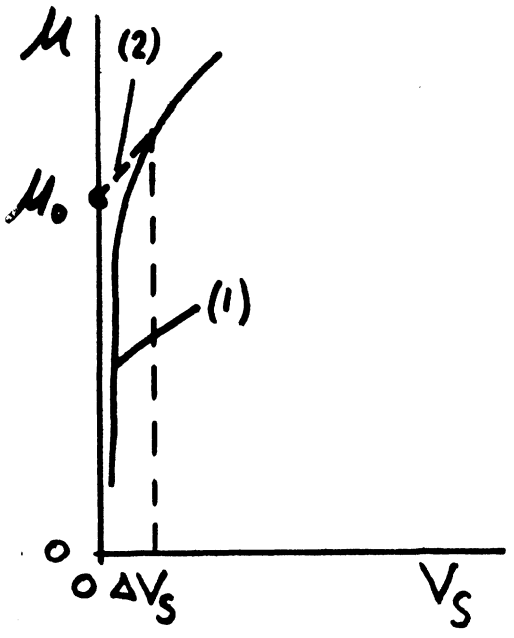

Figure A7. To the Explanation of the Effect of a Simplified $\mu(V_S)$ Function for $V_S \approx 0$.

$$1. * 1.68 \cdot 10^{-2} = 1.68 \cdot 10^{-2} \text{cm}$$

With a contact patch length of 13.3 cm, this represents an angle of ~ .07°.

For practical purposes it is thus permissible to make $\mu(0) = \mu(\Delta V_s)$ for $\Delta V_s \lesssim .5$ cm/s at this traveling speed.

This also has advantages in the mechanization on the computers of the equations of motion for the tread elements.

APPENDIX B

THE BEAM DEFLECTION FUNCTIONS

The lateral deflection, $v_c(x)$, of the beam is the result of the pull of the N lateral point loads, $Q(x_i)$, at the contact patch section midpoints. The deflection of the simultaneous action of the N point loads is the sum of the deflection caused by each individual load (Figure B1, p. 104).

If $y(\xi_i, x_i)$ is the deflection of the beam at x_i due to a <u>unit</u> point load, $Q(\xi_j)$, then the deflection $v_c(x_i)$ by the sum of N point loads is

$$v_c(x_i) = \sum_{j=1}^{N} Q(\xi_j) y(\xi_j, x_i) \tag{B.1}$$

Likewise, the slope function $v_c'(x_i)$ is given by

$$v_c'(x_i) = \sum_{j=1}^{N} Q(\xi_j) \cdot y'(\xi_j, x_i) \tag{B.2}$$

with

$$\left.\begin{aligned} x_i &= a - \frac{2a}{N}(i - 1 + .5) \\ \xi_j &= a - \frac{2a}{N}(j - 1 + .5) \end{aligned}\right\} \tag{B.3}$$

where

$$y' = dy/dx$$

The differential equation for the deflection function, $y(x)$, of a taunt beam on a foundation with transverse loads at the end points is approximately given by

$$-E \cdot I \cdot y^{1v} + N \cdot y'' - K \cdot y = 0 \qquad (B.4)$$

where

$E \cdot I$ is the bending stiffness [Nm^2]

N is the tension in the beam [N]

K is the lateral spring constant of the foundation [N/m^2].

Note that lateral shear in the beam and radial shear in the foundation (sidewalls) is disregarded. Also, the spring constant, K, is not corrected for the radial tire deflection in the contact area. These effects could be included in a more elaborate beam equation or, better still, by obtaining, through proper measurement, the Green-function of the tire at specific inflation pressures and vertical loads. Thus, the variation in K in the range of the contact patch could also be accounted for.

With reference to Figure B2, the range of beam deflection is

$$-L \leq x < L \ *$$

where 2L is the circumference of the belt of the tire.

*Note from Figure B2 the definition of x used for the computation of the deflection y.

A transverse point load, Q/2, is acting on the beam at $x = \pm L$, giving rise to a symmetrical deflection function

$$y(x) = y(-x)$$

The solution of (B.4) is obtained the usual way as the sum

$$y = \Sigma A_n e^{s_n x} \tag{B.5}$$

The s_n's are the roots of the equation

$$-E \cdot I \cdot s^4 + N \cdot s^2 - K = 0 \tag{B.6}$$

The A_n's are due to the conditions at $x = \pm L$. Equation (B.6) is transferred to

$$s^4 - 2a \cdot s^2 + b = 0 \tag{B.7}$$

where

$$a = N/(2E \cdot I)$$

$$b = K/(E \cdot I)$$

From (B.7) we obtain

$$(s^2 - a)^2 = a^2 - b = -c^2 \tag{B.8}$$

Normally, $a^2 < b$ making c^2 positive, in which case we may write

$$(s^2 - a)^2 = c^2 e^{i(\pi + n2\pi)}$$

$$n = 0,1,... \qquad \text{(B.9)}$$

This yields

$$s_{1,2}^2 = a + ce^{i(\pi/2 + n\pi)} \qquad \text{(B.10)}$$

With reference to Figure B.3, Equation (B.9) can be written

$$s_{1,2}^2 = r^2 e^{i(\pm\theta + 2\pi n)}$$

$$n = -,1,... \qquad \text{(B.11)}$$

where

$$r^2 = \sqrt{a^2 + c^2} = \sqrt{a^2 + b - a^2} = \sqrt{b} \qquad \text{(B.12)}$$

and

$$\theta = tg^{-1} \frac{c}{a} \qquad \text{(B.13)}$$

So the four roots of (B.8) can now be written

$$\left.\begin{aligned} s_{1,2} &= r \cdot e^{(\theta/2 + n\pi)} \\ s_{3,4} &= r \cdot e^{(-\theta/2 + n\pi)} \\ n &= 0,1,... \end{aligned}\right\} \qquad \text{(B.14)}$$

$$\left.\begin{aligned} s_{1,2} &= r(\cos(\theta/2 + n\pi) + i \sin(\theta/2 + n\pi)) \\ s_{3,4} &= r(\cos(-\theta/2 + n\pi) + i \sin(-\theta/2 + n\pi)) \end{aligned}\right\} \qquad \text{(B.15)}$$

with

$$\left.\begin{aligned} al &= r \cdot \cos(\theta/2) \\ \text{and} & \\ bl &= r \cdot \sin(\theta/2) \end{aligned}\right\} \qquad \text{(B.16)}$$

This gives

$$\begin{aligned} s_1 &= al + i \cdot bl \qquad s_2 = -s_1 \\ s_3 &= al - i \cdot bl \qquad s_4 = -s_3 \end{aligned} \qquad \text{(B.17)}$$

We can now write

$$\begin{aligned} y_1 &= C_1 e^{al \cdot x} (\cos(bl \cdot x) + i \sin(bl \cdot x)) \\ y_2 &= C_2 e^{-al \cdot x} (\cos(bl \cdot x) - i \sin(blx)) \\ y_3 &= C_3 e^{al \cdot x} (\cos(bl \cdot x) - i \sin(blx)) \\ y_4 &= C_4 e^{-al \cdot x} (\cos(bl \cdot x) + i \sin(bl \cdot x)) \end{aligned} \qquad \text{(B.18)}$$

Because of the symmetry $y(x) = y(-x)$, we have $C_1 = C_2$ and $C_3 = C_4$. The sum $y = \sum_{n=1}^{4} y_n$ can now be written

$$y = A \cdot \cos(bl \cdot x)(e^{al \cdot x} + e^{-al \cdot x}) + B \cdot \sin(bl \cdot x)(e^{al \cdot x} - e^{-al \cdot x}) \qquad \text{(B.19)}$$

or expressed in hyperbolic functions

$$y = 2\ [A\cdot\cos(b1\cdot x)\cdot\cosh(a1\cdot x) + B\cdot\sin(b1\cdot x)\cdot\sinh(a1\cdot x)]$$

Since the slope, y', later will be needed, its derivation is also given here.

$$y = 2[A(a1\cdot\cos(b1\cdot x)\cdot\sinh(a1\cdot x) - b1\cdot\sin(b1\cdot x)\cdot\cosh(a1\cdot x))$$
$$+ B(a1\cdot\sin(b1\cdot x)\cdot\cosh(a1\cdot x) + b1\cdot\cos(b1\cdot x)\cdot\sinh(a1\cdot x))] \qquad (B.20)$$

In case $a^2 \geq b$, we have

$$s_{1,2}^2 = a \pm \sqrt{a^2 - b} = a\left[1 \pm \sqrt{1 - \frac{b}{a^2}}\right] \qquad (B.21)$$

which gives the four real roots

$$\left.\begin{aligned} s_1 &= \sqrt{a(1 + \sqrt{1 - b/a^2})} & s_2 &= -s_1 \\ s_3 &= \sqrt{a(1 - \sqrt{1 - b/a^2})} & s_4 &= -s_3 \end{aligned}\right\} \qquad (B.22)$$

As before, the four contributions to the deflection function are

$$y = C_1 e^{s_1\cdot x} + C_2 e^{-s_1\cdot x} + C_3 e^{s_3\cdot x} + C_4 e^{-s_3\cdot x} \qquad (B.23)$$

which, because of the symmetry, can be written

$$y = A\left(e^{s_1 x} + e^{-s_1 x}\right) + B\left(e^{s_3 x} + e^{-s_3 x}\right) \qquad (B.24)$$

Its derivative, y', is

$$y' = A\left(s_1 e^{s_1 x} - s_1 e^{-s_1 x}\right) + B\left(s_3 e^{s_3 x} - s_3 e^{-s_3 x}\right) \qquad (B.25)$$

The value of the constants A and B has now to be determined. For this we need two conditioning equations. The first one is obtained from the integral of the spring forces in the foundation which, due to the beam deflection, must equal the point load.

Hence

$$Q = 2K\int_0^L y\,dx \qquad (B.26)$$

The other condition is given by the fact that the slope at x = L (or x = -L) must be zero.

$$y' = 0 \text{ for } x = L \qquad (B.27)$$

For $a^2 < b$ and a unit load Q = 1 condition, (B.26) gives

$$1 = A \cdot C_1 + B \cdot C_2 \qquad (B.28)$$

where

$$C_1 = \frac{2K}{a1^2 + b1^2} \left[b1 \cdot \sin(b1 \cdot L)(e^{a1 \cdot L} + e^{-a1 \cdot L}) \right.$$

$$\left. + a1 \cdot \cos(b1 \cdot L)(e^{a1 \cdot L} - e^{-a1 \cdot L}) \right] \qquad (B.29)$$

$$C_2 = \frac{2K}{a1^2 + b1^2} \left[a1 \cdot \sin(b1 \cdot L)(e^{a1 \cdot L} + e^{-a1 \cdot L}) \right.$$

$$\left. - b1 \cdot \cos(b1 \cdot L)(e^{a1 \cdot L} - e^{-a1 \cdot L}) \right]$$

Condition (B.27) gives

$$0 = A \cdot D_1 + B \cdot D_2 \qquad (B.30)$$

with

$$D_1 = a1 \cdot \cos(b1 \cdot L)(e^{a1 \cdot L} - e^{-a1 \cdot L}) - b1 \cdot \sin(b1 \cdot L)(e^{a1 \cdot L} + e^{-a1 \cdot L})$$

$$D_2 = a1 \cdot \sin(b1 \cdot L)(e^{a1 \cdot L} + e^{-a1 \cdot L}) + b1 \cdot \cos(b1 \cdot L)(e^{a1 \cdot L} - e^{-a1 \cdot L})$$

(B.31)

The constants A and B can now be obtained from (B.28) and (B.30)

$$A = \frac{D_2}{C_1 D_2 - D_1 C_2}$$

$$B = -\frac{D_1}{C_1 D_2 - D_1 C_2} \qquad (B.32)$$

Likewise, for $a^2 \geq b$, we obtain for the constants C_1, C_2, and D_1, D_2, the following expressions:

$$
\begin{aligned}
C_1 &= \frac{2K}{s_1}\left(e^{s_1 \cdot L} - e^{-s_1 \cdot L}\right) \\
C_2 &= \frac{2K}{s_3}\left(e^{s_3 \cdot L} - e^{-s_3 \cdot L}\right) \\
D_1 &= s_1\left(e^{s_1 \cdot L} - e^{s_1 \cdot L}\right) \\
D_2 &= s_3\left(e^{s_3 \cdot L} - e^{s_3 \cdot L}\right)
\end{aligned}
\qquad \text{(B.33)}
$$

The functions $y(\xi_j, x_i)$ and $y'(\xi_j, x_i)$ are now obtained from (B.19) and (B.20) or (B.24) and (B.25).

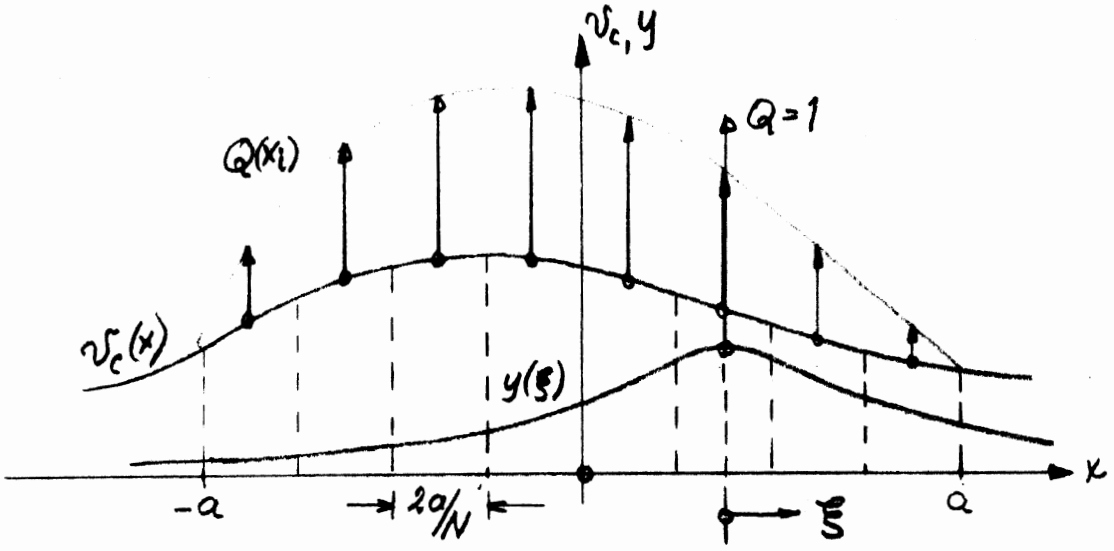

Figure B1. Unit Load Deflection $y(\xi)$ and Beam Deflection $v_c(x)$ Due to Distributed Point Loads $Q(x_i)$.

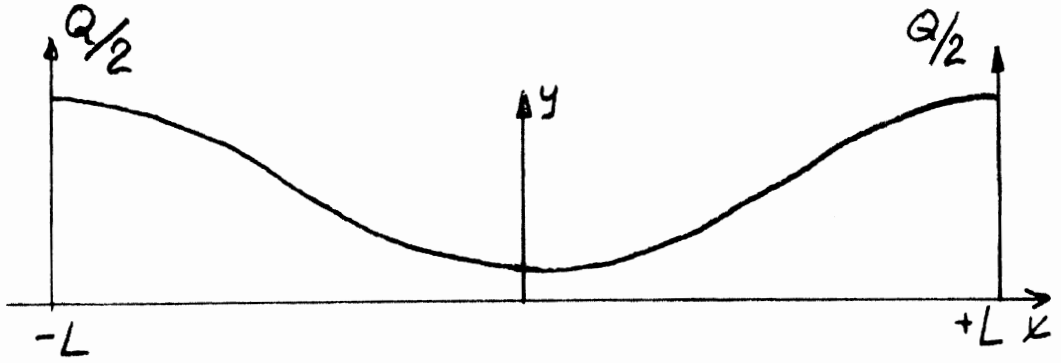

Figure B2. Coordinate System and Point Load for the Beam Equation.

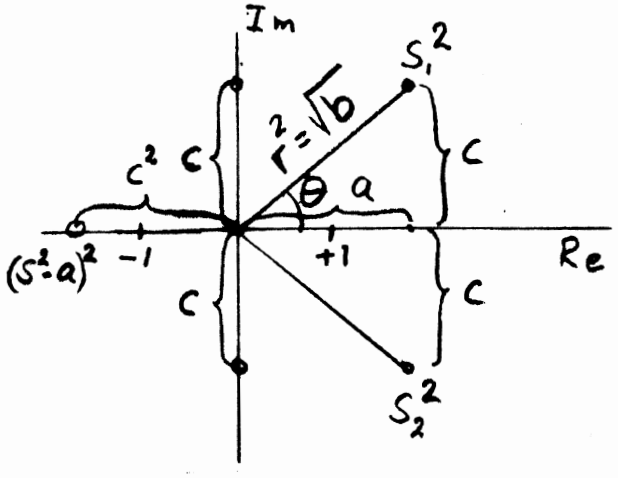

Figure B3. To the Solving of the Roots of s when $a^2 < b$.

APPENDIX C

LINEAR APPROXIMATIONS WITHIN THE CONTACT PATCH SECTION AND DAMPING OF BEAM DEFLECTIONS

1. GENERAL

The element base point deflection functions, v_B and $\dot{v}_B$, are defined by the following sums (see Figure 4.2):

$$v_B = v_c + v_y + y_L$$

and

$$\dot{v}_B = \dot{v}_c + \dot{v}_y + \dot{y}_L$$

Within a section of the contact patch the separate functions and their sums are given linear approximations exemplified by

$$v_B = v_{B,IC} + \dot{v}_B \cdot t_s$$

Here, $v_{B,IC}$ is the value of v_B as it enters the section at time $t_s = 0$. The time derivative, $\dot{v}_B$, is taken at section midpoint.

In the computer programs, the distance traveled in the section, x_s, will be used in lieu of t_s.

Making use of the relation

$$x_s = -V_r \cdot t_s$$

v_B is now expressed by its section initial value and the product of function midpoint slope, v_B' and the distance x_s traveled thus:

$$v_B = v_{B,IC} - \dot{v}_B/V_r \cdot x_s = v_{B,IC} - v_B' \cdot x_s$$

Likewise

$$\dot{v}_B = \dot{v}_{B,IC} - \dot{v}_B' \cdot x_s$$

2. BEAM DEFLECTION FUNCTIONS

The beam deflection linearization is given by

$$v_c = v_{c,IC} + \dot{v}_c \cdot t_s$$

The total derivative, $\dot{v}_c$, is given by

$$\dot{v}_c = \frac{dv_c}{dt} = \frac{\partial v_c}{\partial t} + \frac{\partial v_c}{\partial x}\frac{dx}{dt} = (\dot{v}_c)_x + (v_c')_t \cdot \frac{dx}{dt}$$

Since

$$\frac{dx}{dt} = \frac{dx_s}{dt_s} = -V_r$$

this can be written

$$\dot{v}_c = (\dot{v}_c)_x - V_r(v_c')_t$$

This gives

$$v_c = v_{c,IC} + [(\dot{v}_c)_x - V_r \cdot (v_c')_t] \cdot t_s$$

or

$$v_c = v_{c,IC} + [(v_c')_t - (\dot{v}_c)_x / V_r] \cdot x_s$$

For $(v_c')_t$, the mid-section values are obtained according to calculations in Appendix B.

The partial time derivative, $(\dot{v}_c)_x$, for a section is also taken at the section midpoint. Basically, it should be calculated from the difference of consecutive midpoint values of v_c in the following way:

$$(\dot{v}_c)_x = [(v_c)_t - (v_c)_{t-\Delta t}]/\Delta t$$

The time increase, Δt, is the section passage time given by

$$\Delta t = \frac{2a}{N \cdot V_r}$$

where 2a is the length of the contact patch and N is the number of sections.

This direct way of obtaining $(\dot{v}_c)_x$ results, however, in computational instability. A damping scheme outlined in the following section has therefore to be applied.

3. DAMPING OF BEAM DEFLECTION

The retaining of the beam velocity term $(\dot{v}_c)_x$ in the computations for the transient motions requires the introduction of a beam damping to avoid instability. This damping effect is obtained by moderating the change of consecutive values of $(\dot{v}_c)_x$ for a section. This is brought about by the following scheme for the computation in the next time step, $t + \Delta t$, step (n+1), of $(\dot{v}_c)_{x,n+1}$ and an estimated beam deflection $(v_{ce})_{n+1}$ for each section from known values of $(\dot{v}_c)_{x,n}$ at the present time t, step (n). Δt is the section passage time.

$$(\dot{v}_c)_{x,n+1} = (\dot{v}_c)_{x,n} + C_B \cdot [(v_c)_n - (v_{ce})_n]/\Delta t$$

$$(v_{ce})_{n+1} = (v_c)_n + (\dot{v}_c)_{x,n+1} \cdot \Delta t$$

C_B is the beam damping coefficient. The computation of $(\dot{v}_c)_{x,n+1}$ and $(v_{ce})_{n+1}$ is illustrated in Figure C1.

The initial values $(\dot{v}_c)_{x,IC}$ and $(v_{ce})_{IC}$ in all sections at t = 0 are obtained from

$$(\dot{v}_c)_{x,IC} = - K_{IC} W \cdot \sin \alpha$$

$$(v_{ce})_{IC} = (\dot{v}_c)_{x,IC} \cdot \Delta t$$

K_{IC} is < 1 and depends on the ratio of the stiffness of the beam foundation to that of the tread elements. It should

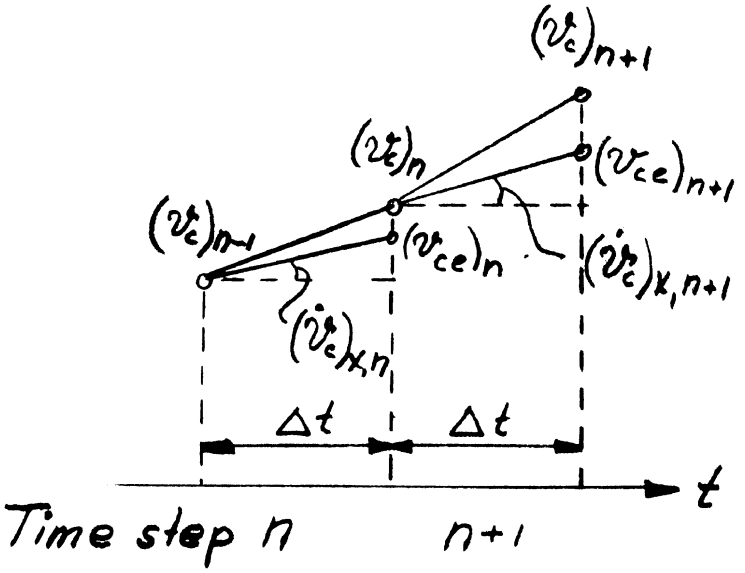

Figure C1. To the Computation of $(\dot{v}_c)_{x,n+1}$ and $(v_{ce})_{n+1}$.

be pointed out that the damping is applied only within that range of the beam which currently is above the contact patch.

4. YAWING MOTION (STEERING)

The yawing motion is defined by the addition of α_y to the steady-state slip angle, α, with

$$\alpha_y = \alpha_{Ay} \cdot \sin(\omega t)$$

The angular speed, $\dot{\alpha}_y$, will be given by

$$\dot{\alpha}_y = \alpha_{Ay} \cdot \omega \cdot \cos(\omega t)$$

and acceleration, $\ddot{\alpha}_y$, by

$$\ddot{\alpha}_y = - \alpha_{Ay} \cdot \omega^2 \cdot \sin(\omega t)$$

At a certain coordinate, x, y_t is displaced the distance, v_y, from the x_r-axis (see Figure 4.2).

$$v_y = - \alpha_y \cdot x$$

When the element moves through a section, α_y and x are assumed to vary linearly according to

$$\alpha_y = \alpha_{y,IC} + \dot{\alpha}_y \cdot t_s$$

and

$$x = x_{IC} + \dot{x} \cdot t_s$$

The $\dot{\alpha}_y$ is to be evaluated at the section midpoint. As before, $\dot{x} = -V_r$. By the relation

$$x_s = -V_r \cdot t_s$$

α_y and x become

$$\alpha_y = \alpha_{y,IC} - \dot{\alpha}_y/V_r \cdot x_s$$

$$x = x_{IC} + x_s$$

Neglecting x_s^2, we now obtain for v_y

$$v_y = -\alpha_{y,IC} \cdot x_{IC} - (\alpha_{y,IC} - x_{IC}\dot{\alpha}_y/V_r) \cdot x_s$$

The function $\dot{v}_y$ is obtained by differentiation of $v_y = -\alpha_y \cdot x$.

$$\dot{v}_y = -\dot{\alpha}_y \cdot x - \alpha_y \cdot \dot{x} = -\dot{\alpha}_y \cdot x + \alpha_y \cdot V_r$$

Setting

$$\dot{\alpha}_y = \dot{\alpha}_{y,IC} + \ddot{\alpha}_y \cdot t_s = \dot{\alpha}_{y,IC} + \ddot{\alpha}_y/V_r \cdot x_s$$

and taking α_y and x as before and again neglecting x_s^2, we obtain for $\dot{v}_y$

$$\dot{v}_y = V_r \cdot \alpha_{y,IC} - \dot{\alpha}_{y,IC} \cdot x_{IC} + (\ddot{\alpha}_y/V_r \cdot x_{IC} - \dot{\alpha}_{y,IC} - \dot{\alpha}_y) \cdot x_s$$

The $\dot{\alpha}_y$ and $\ddot{\alpha}_y$ are to be evaluated at the section midpoint.

5. SIDESLIPPING

A sinusoidal lateral motion, y_L, of the wheel plane is defined by

$$y_L = y_{AL} \cdot \sin(\omega t)$$

and the lateral velocity, $\dot{y}_L$, and acceleration, $\ddot{y}_L$, are given by

$$\dot{y}_L = y_{AL} \cdot \omega \cdot \cos(\omega t)$$

$$\ddot{y}_L = -y_{AL} \cdot \omega^2 \cdot \sin(\omega t)$$

In the same manner as for α_y, we assume the linear variation of y_L within a section to be given by

$$y_L = y_{L,IC} + \dot{y}_L \cdot t_s$$

Introducing x_s for t_s we obtain for y_L

$$y_L = y_{L,IC} - \dot{y}_L/V_r \cdot x_s$$

where $\dot{y}_L$ is to be taken at section midpoint.

Likewise, for the linearization of $\dot{y}_L$ we obtain

$$\dot{y}_L = \dot{y}_{L,IC} - \ddot{y}_L/V_r \cdot x_s$$

where $\ddot{y}_L$ is the mid section value.

APPENDIX D

INITIAL CONDITIONS FOR A SECTION

There is a general desire to keep the size of a program down. On the digital this saves core space and can reduce running time. On the analog this is a necessity because of the limited number of components. In the pure digital program, this has led to the use of the same two sets of algorithms for the two equations of motion of the tread elements in the lateral and longitudinal sense for all sections in the contact patch.

Likewise, on the analog this has led to the use, for all sections, of one common circuit for the lateral displacement and one for the longitudinal. Two separate simultaneously run circuits are used to save time.

This sharing of algorithms and circuits makes it necessary to specify initial conditions and to store end conditions for each section. Considerations for this, based on the approximations of v_B and $\dot{v}_B$ within a section, will be given in the following.

The equation of lateral motion of an element as its base point moves through a section is

$$m\ddot{y}_r + c_y\dot{v} + k_y v = q_y$$

Making use of the linear approximation given in Appendix C, we write

$$\dot{v} = \dot{y}_r - (\dot{v}_c + \dot{v}_y + \dot{y}_L) = \dot{y}_r - \dot{v}_{B,IC} - \dot{v}'_B \cdot x_s$$

$$v = y_r - (v_c + v_y + y_L) = y_r - v_{B,IC} - v'_B \cdot x_s$$

For $\dot{y}_r$, within section n, we now write

$$(\dot{y}_r)_n = (\int \ddot{y}_r dt)_n + (\dot{y}_{r,IC})_n$$

Inserted in $\dot{v}$, this gives for section n

$$(\dot{v})_n = (\int \ddot{y}_r dt)_n + (\dot{y}_{r,IC})_n - \dot{v}_{B,IC} - \dot{v}'_B \cdot x_s$$

The initial conditions $(\dot{y}_{r,IC})_n$ of section n is equal to the final condition $(\dot{y}_{r,FC})_{n-1}$ of the previous section.

For section one (n=1), we have

$$(\dot{y}_{r,IC})_1 = (\dot{v}_{B,IC})_1$$

See Figure D1 for mechanization of $\dot{y}_r$ and $\dot{v}$ on the analog. Likewise, for y_r within section n we write

$$(y_r)_n = (\int \dot{y}_r dt)_n + (y_{r,IC})_n$$

Inserted in (v), this gives, for section n

$$(v)_n = (\int \dot{y}_r dt)_n + (v_{IC})_n - (v'_B)_n \cdot x_s$$

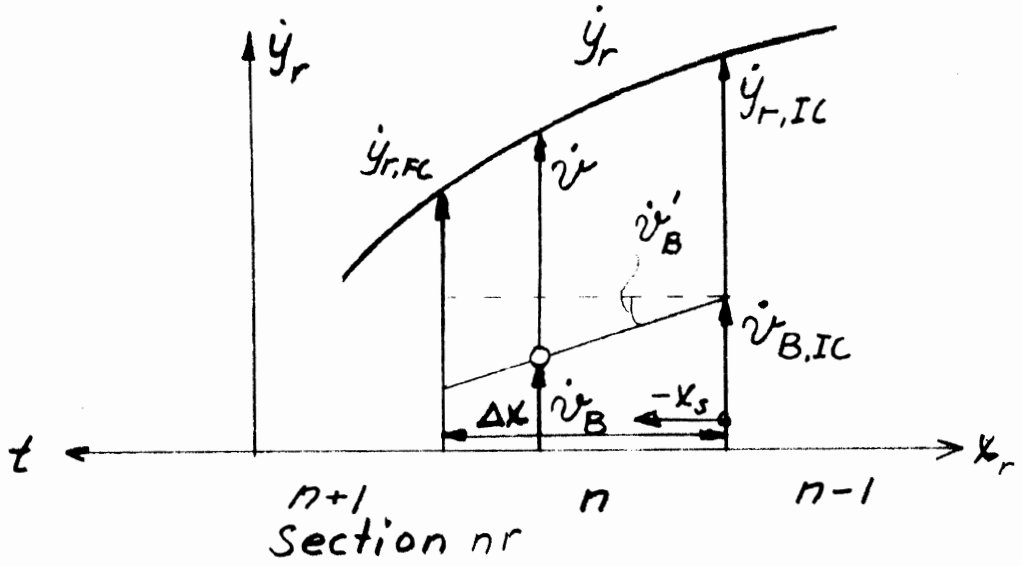

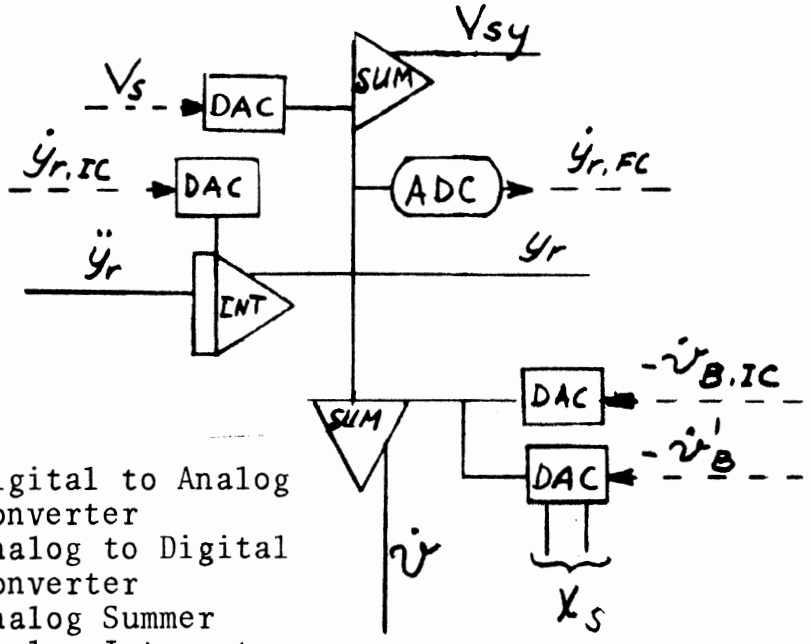

DAC = Digital to Analog Converter
ADC = Analog to Digital Converter
SUM = Analog Summer
INT = Analog Integrator

Figure D1. Lateral Velocity Functions for an Element Moving Through a Section of the Contact Patch (top) and Mechanization on the Analog Computer (bottom).

where

$$(v_{IC})_n = (y_{r,IC})_n - (v_{B,IC})_n$$

With reference to Figure D2, $(v_{IC})_n$ is obtained from final conditions in section n-1 and initial condition in section n.

$$(v_{IC})_n = (y_{r,FC} - v_{B,IC})_{n-1} - v'_{B,n-1} \cdot \Delta x$$

where

$$\Delta x = 2a/N$$

For section n=1 $(v_{IC})_1 = 0$.

The analog mechanization of $(v)_n$ is shown in Figure D2. This scheme saves us from retaining in the output of the integrator also the deflection of the beam, thus enhancing the accuracy.

What has been said here about the lateral functions holds in applicable parts also for the longitudinal functions.

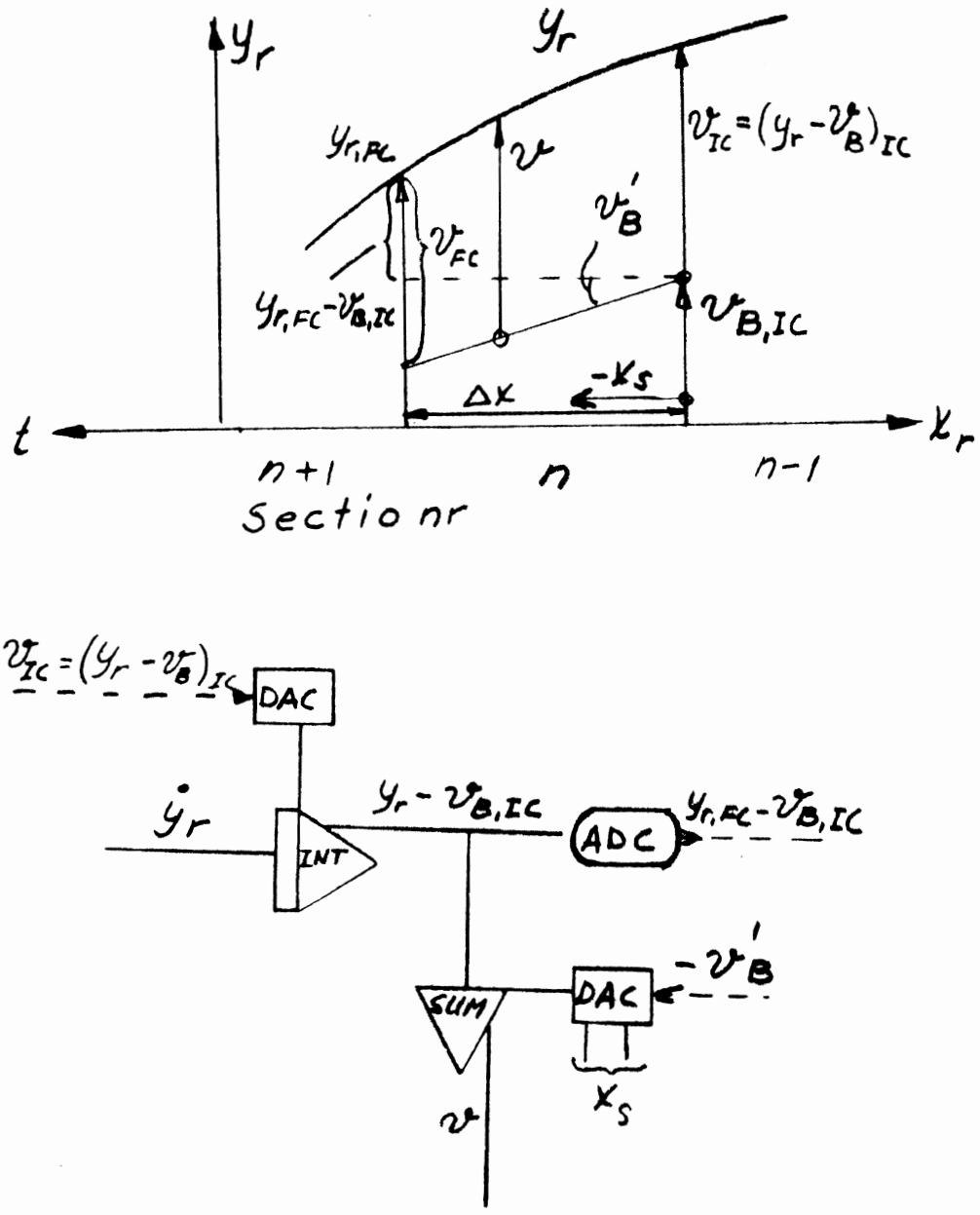

Figure D2. Lateral Deflection Functions for an Element Moving Through a Section of the Contact Patch (top), and Mechanization on the Analog Computer (bottom).

APPENDIX E

DETERMINATION OF TIRE CONSTANTS AND SUMMARY OF ALL DATA USED IN THE COMPUTATIONS

1. BASIC

The results of computations with the model developed in this report have been based on the following constants applicable to a FR70-14 tire on a 6" rim. The tire has the HSRI denotation R70B. The footprint of this tire at 24 psi inflation pressure and a vertical load of 1000 lb. is given in Figure E1.

Inflation pressure	$P = 28$ psi $= 1.93$ bar $= 1.93 \cdot 10^5$Pa
Vertical load	F_z[lb,(N)] = 800,(3560)
Length of contact patch	PL[in,(m)] = 5.25,(.133)

2. BEAM DATA

The cross-section and dimensions of the tire are given in Figure E2. The bending stiffness, $E \cdot I$, of the beam is computed under the assumption that the "effective" dimensions of the belt (width and height) have been identified and that only the belt is carrying the longitudinal stress due to inflation pressure. Then from the circumferential spring constant of the belt, $E \cdot I$ can be computed.

By definition, the elastic modulus is given by

$$E = \frac{\sigma}{\varepsilon} = \frac{\Delta F \cdot L}{A \ \Delta L} = K_c \cdot \frac{2L}{A}$$

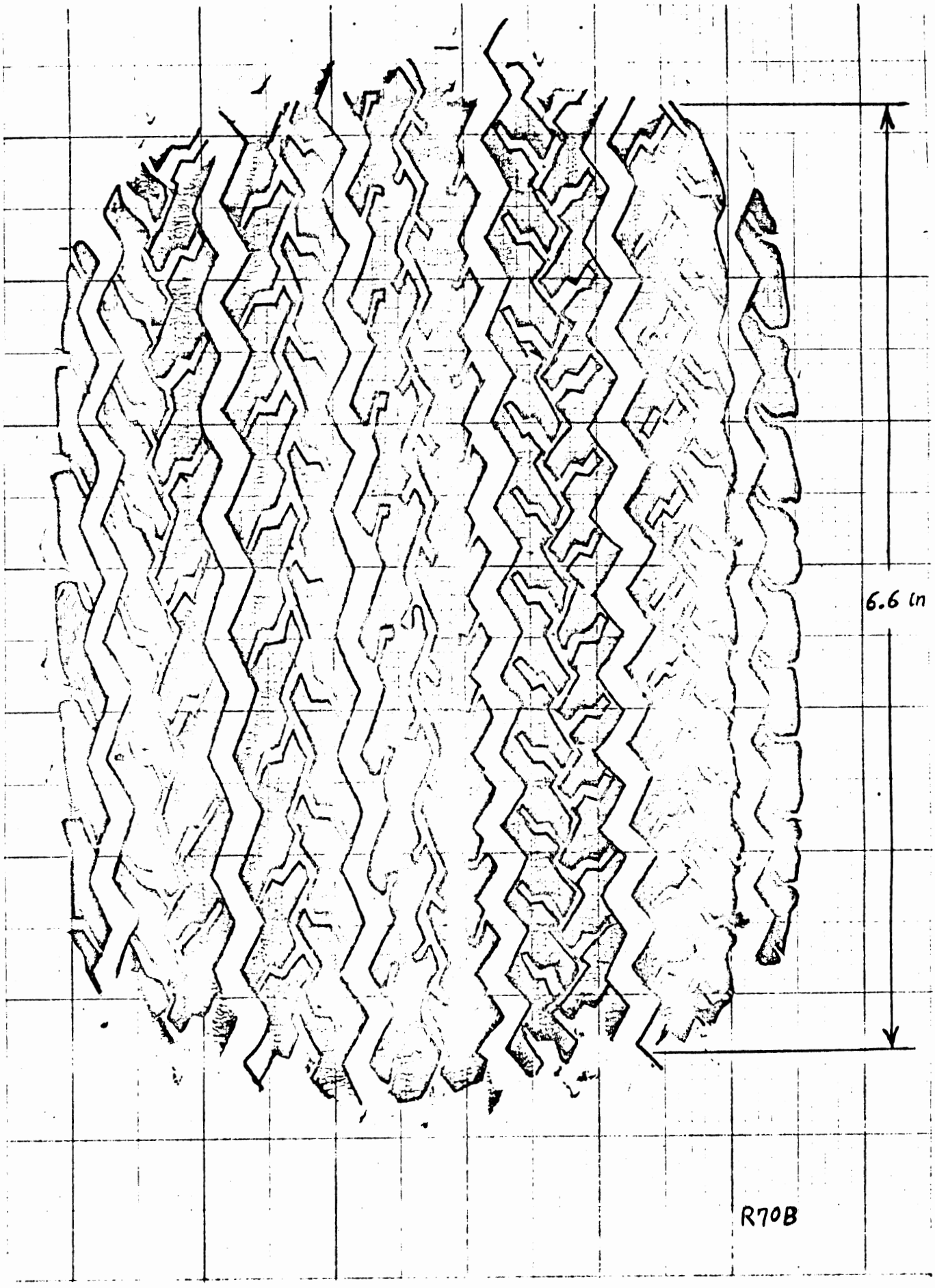

Figure E1 Inked tread footprint of a standing radial tire FR70-14 inflated to 24 psi and statically loaded at 1000 lb.

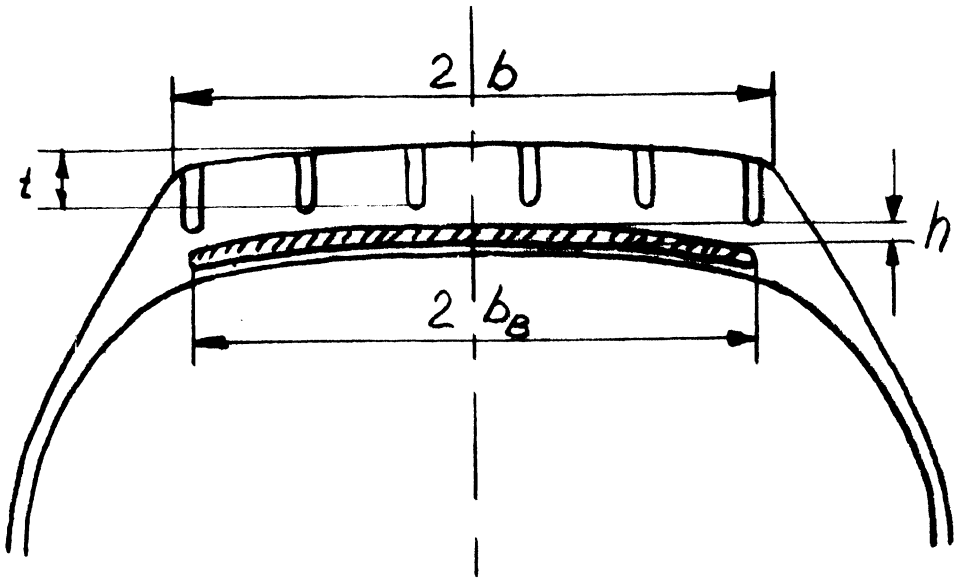

Belt Width	$2b_B$ = 14 cm
Width of Contact Patch	2b = 12 cm
Effective Width of Contact Patch (2b less grooves)	w_e = 9.2 cm
Depth of Groove (Average)	t = .9 cm
Circumference of Belt	2L = 198 cm

Figure E2. Cross-Section of Tire and Some Tire Dimensions Used in the Computations.

where K_c is the circumferential spring constant of the beam and 2L is the length of the circumference. The cross-section area, A, of the beam is

$$A = 2b_B \cdot h$$

The moment of inertia, I, for lateral bending of the beam is given by

$$I = 2 \cdot b_B^3 \cdot h/3 = b_B^2 A/3$$

This gives for E·I

$$E \cdot I = K_c \cdot 2L \cdot b_B^2/3$$

Measurements of the tire circumference at various inflation pressures have yielded a circumferential spring constant, K_c, of

$$K_c = 1.03 \cdot 10^5 \text{ N/m}$$

For E·I we now have an estimate

$$E \cdot I = 3.35 \cdot 10^2 \text{ Nm}^2$$

The tension, N, in the beam has not been accurately calculated, since large variations can be tolerated without noticeably affecting the deflection calculated by the model.

After comparing with [19] and [20], the following estimate is used

$$N = 5000 \text{ N}$$

Since no measurements of the foundation spring constant, K, have been made for the actual tire, an estimate is made based on data from [21] to yield

$$K = 1.5 \cdot 10^5 \text{ N/m}^2$$

The combined longitudinal carcass and tread spring rate, K_{CT}, has been obtained for the actual tire [22]. The value arrived at is

$$K_{CT} = 1000 \text{ lb/in} = 1.77 \cdot 10^5 \text{ N/m}$$

The relation between the spring constants for springs in series and the resultant constant for the combination reads as follows:

$$\frac{1}{K_{CT}} = \frac{1}{K_L} + \frac{1}{k_x \cdot L}$$

With known values of K_{CT} and the tread constant, k_x (given in the next section), the carcass constant, K_L, obtained is

$$K_L = 2.08 \cdot 10^5 \text{ N/m}$$

3. TREAD ELEMENT DATA

The tread stock has a measured Shore hardness of A = 62. Making use of data from Reference [23], this indicates a specific mass, γ, of

$$\gamma = 1.18 \text{ g/cm}^3$$

The tread thickness (depth of grooves), t, is taken to have an average value of

$$t = .9 \text{ cm}$$

The effective width of the tread (less the grooves) is taken to be

$$w_e = 9.2 \text{ cm}$$

This gives a cross-sectional tread area, A, of

$$A = 8.3 \text{ cm}^2$$

The mass, m_o, per unit of circumferential length is

$$m_o = \gamma \cdot A = 10g/cm = 1\ kg/m$$

This is a mass that is distributed along the height of the tread. The dynamic model of the tread assumes the mass to be concentrated at the top of the element. This requires a reduction of the mass with a factor $4/\pi^2$, taken from [23].

Hence, the mass, m, used in the calculations is

$$m = .4\ kg/m$$

The longitudinal and lateral spring constants were originally not known for the R70B tire and had, therefore, to be estimated from other sources.

From reference [24] can be obtained an average value for the lateral spring constant per unit of circumferential length of

$$k = 8.92\ N/mm^2$$

for a tread specimen with a width of 9.7cm. If the same pattern design is assumed for the R70B tire, the k-value above only has to be corrected for the actual tread width of 12.0cm. This gives us the spring constant

$$k_y = 11.1 \cdot 10^6\ N/m^2$$

During the course of development of the present model, measurements were started on the actual tread of tire R70B. Force-elongation curves were obtained for a 3 by 2.5 in. specimen from the central part of the contact patch. Tests were first tried with the specimen pressed to a safety walk clad surface with pressure ~30 psi. Sliding occurred, however, and the specimen had to be glued to the surface. The glued specimen was subject to the same normal pressure. There is the suspicion that the gluing affects the freedom of deflection of the contact area of the specimen to produce too high a force value. The magnitude of this amplification factor is, however, not known at this time.

Figure E3 shows the force deflection curves obtained. Measurements performed in the longitudinal and lateral direction of the specimen gave very nearly the same results.

The actual maximum deflections encountered by the elements in the model are of the order of .15 in. (4mm). As can be seen from the test data, the force-deflection curve is highly nonlinear for this range with a decreasing slope, i.e., decreasing local spring constant.

Due to lack of time, the model originally implemented, assuming a linear force deflection relation, was never changed to represent the actual nonlinear relation. Instead, a spring constant representing the conditions at the origin was used throughout. This gives rise to an exaggeration of obtained forces apparent from Figure E3.

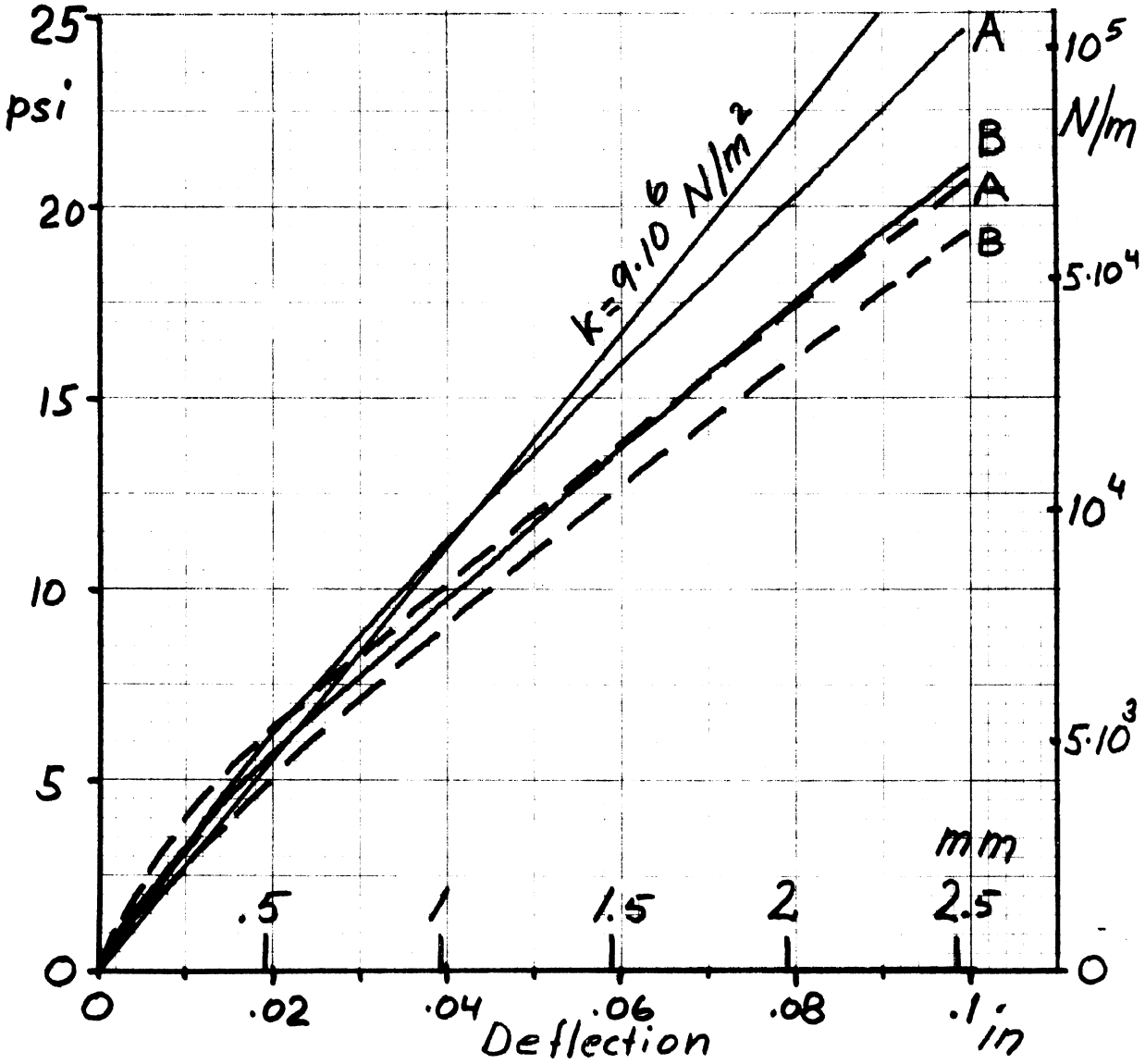

Direction of Deflection	Speed of Deflection in/min	
Longitudinal————	A: .1	B: .01
Lateral----------	A: .5	B: .05

Figure E3. Experimentally Obtained Curves for Shear Stress (left ordinate) or Total Tread Force Per Unit of Circumferential Length (right ordinate). The Slope Equivalent to the Spring Constant k = $9.10^6 N/m^2$ is also shown. The shear stress is measured in units of force per unit of gross contact area.

The spring constant at the origin computed from the test data is $k \approx 9 \cdot 10^6$ N/m^2. Because of the uncertainty of this value due to the gluing effect, the values $k_x = 9.1 \cdot 10^6$ N/m^2 and $k_y = 8.7 \cdot 10^6$ N/m^2 were chosen, since they give the same braking stiffness and cornering stiffness as obtained with the mobile tire tester [2].

For the damping constants we assume the same values in longitudinal and circumferential directions.

The damping coefficient, c, for rubber is highly dependent on the oscillation frequency. We, therefore, chose to use a value that is relevant to the natural frequency of the element.

The mass and spring constants above give a natural frequency through

$$f_n = \frac{1}{2\pi} \frac{k}{m}$$

of $f_n \sim 760$ Hz for longitudinal oscillations and $f_n \sim 745$ Hz for lateral.

From Reference [23], the following relations for a spring constant, k, and a damping constant, c, are taken.

$$k = \frac{E' \cdot A}{t} \qquad c = \frac{E'' \cdot A}{\omega_n \cdot t}$$

which gives

$$c = \frac{k}{\omega_n} \frac{E''}{E'} = k \frac{tg\delta}{\omega_n}$$

The loss tangent is taken to be

$$tg\delta \sim .44$$

So, with an average of f_n = 750 Hz,

$$\frac{tg\delta}{\omega_n} \sim \frac{.44}{2\pi \cdot 750} \sim .93 \times 10^{-4}$$

This results in

$$c = 8.2 \cdot 10^2 \text{ N} \cdot \text{s/m}^2$$

and we use this value for both c_x and c_y.

4. SUMMARY OF DATA USED IN THE COMPUTATIONS

4.1 General Tire Data.

Type:	FR70-14 on 6" rim
Inflation Pressure:	28 psi
Vertical Load:	F_z = 800 lb. (3560 N)
Corresponding Contact Patch Length:	2a = 5.25 in (13.3 cm)
Corresponding Contact Patch Width:	2b = 4.7 in (12.0 cm)
Beam Width:	b_B = 5.5 in (14.0 cm)
Circumferential Length:	2L = 78 in (198.0 cm)

4.2 Beam and Foundation Constants.

Stiffness: $E \cdot I = 3.35 \cdot 10^2 \ Nm^2$

Tension: $N = 5000 \ N$

Foundation Spring Constants:

- Lateral: $K = 1.5 \cdot 10^5 \ N/m^2$
- Longitudinal: $K_L = 2.08 \cdot 10^5 \ N/m$
- Circumferential: $K_c = 1.03 \cdot 10^5 \ N/m$

Beam Damping Coefficient: $C_B = .06$

Combined Foundation and Tread Element Longitudinal Spring Constant: $K_{CT} = 1.77 \cdot 10^5 \ N/m$

4.3 Tread Element Constants.

Mass: $m = .4 \ kg/m$

Spring Constant:

- Lateral: $k_y = 8.7 \cdot 10^6 \ N/m^2$
- Longitudinal: $k_x = 9.1 \cdot 10^6 \ N/m^2$

Damping Constant: $c_x = c_y = 8.2 \cdot 10^2 \ Ns/m^2$

4.4 Parameter Values for Analytical $\mu(V_S)$ Functions.

(See Appendix A for Definitions)

Parabola

$\mu_{P0} = .21$

$\mu_{P1} = 1.35$

Plateau

$\mu_{PT} = 1.11$

Hyperbola

$\mu_{H} = 1.4$

$\mu_{AS} = .7$

$V_{AS} = -.225$

APPENDIX F

NON-DIMENSIONAL QUANTITIES

The actual calculations have mostly been made with non-dimensional quantities.

For this, three reference units have been used: The reference velocity, W_{Ref}, the vertical load, F_z, and the length of the contact patch, PL = 2a.

The non-dimensional time, $\bar{t}$, will be defined as

$$\bar{t} = t \cdot W_{Ref}/PL$$

Now writing a moment integral, e.g., M_{zy}, at free rolling we have

$$M_{zy} = \int_{-a}^{+a} q_y' \cdot x \cdot dx$$

Non-dimensionalizing this, we write

$$\frac{M_{zy}}{F_z \cdot PL} = \bar{M}_{zy} = \int_{-1/2}^{+1/2} \frac{q_y'}{F_z} PL \cdot \bar{x} \cdot d\bar{x}$$

with

$$\bar{x} = x/PL$$

From this we define a reference force per unit of length

$$q_o = F_z/PL$$

for non-dimensionalization of forces per unit of length of contact.

Using the so defined reference units, we transform a general form of the equation of motion of an element into non-dimensional units

$$m\ddot{x} + c\dot{x} + kx = q$$

where m, c, k, and q are per unit length of circumference.

We now write

$$x = \bar{x} \cdot PL$$

$$\dot{x} = \frac{dx}{dt} = \frac{PL\ d\bar{x}}{PL/W_{Ref}\ d\bar{t}} = \dot{\bar{x}} \cdot W_{Ref}$$

$$\ddot{x} = \ddot{\bar{x}} \cdot W_{Ref}^2/PL$$

Dividing through by q_o brings the equation of motion into

$$m \cdot \left[W_{Ref}^2/(PL \cdot q_o)\right] \cdot \ddot{\bar{x}} + c \cdot \left[W_{Ref}/q_o\right] \cdot \dot{\bar{x}}$$

$$+ k \cdot \left[PL/q_o\right] \cdot \bar{x} = q/q_o$$

or

$$\bar{m} \cdot \ddot{\bar{x}} + \bar{c} \cdot \dot{\bar{x}} + \bar{k} \cdot \bar{x} = \bar{q}$$

where

$$\bar{m} = m \cdot W_{Ref}^2/(q_o \cdot PL) = m \cdot W_{Ref}^2/F_z$$

$$\bar{c} = c \cdot W_{Ref}/q_o$$

$$\bar{k} = k \cdot PL/q_o$$

$$\bar{q} = q/q_o$$

The values of the reference units used in this report are:

W_{Ref} = 70 mph = 31.3 m/s

F_z = 800 lb = 3560 N

PL = 5.25 in = .133 m

With the chosen reference values, the non-dimensionalizing quantities become

$q_o = F_z/PL = 3560/.133 = 2.68 \cdot 10^4$ [N/m]

$q_o/PL = 2.68 \cdot 10^4/.133 = 2.02 \cdot 10^5$ [N/m^2]

$q_o/W_{Ref} = 2.68 \cdot 10^4/31.3 = 856.0$ [Ns/m^2]

$q_o \cdot PL/W_{Ref} = 3560/31.3^2 = 3.64$ [Ns^2/m^2 = kg/m]

APPENDIX G

DIGITAL PROGRAMS AND ANALOG PATCHING DIAGRAMS

FORMIC[1]

Interactive Continuous Systems Integration and Function Generation FORTRAN Package

GENERAL

The FORMIC package consists of the main program FORMIC and the following subroutines: FORMCO, which is the command program that permits interaction at run times; FORMIN, which does the four step Runge-Kutta-Merson variable step integration; FUN, which calculates function values through linear interpolation of given breakpoints of one independent variable per function; LPPLOT, which performs on-line plots on the line printer.

The user supplies the subroutine DERIV, where derivatives are calculated and output and plot functions are specified. The user also applies FORMCO with data such as print and plot intervals, max and min values for integration time steps, and integration error criteria. He furthermore specifies names and values of those constants (parameters) he may want to change between runs. He also specifies in FORMCO headers for print outputs and names, scales, and zeros for plots.

Primary inputs to FORMCO are generally stored in a specified file on disk or DEC-tape and called into core by the user. These primary data can then be changed through the interactive property of FORMCO.

---

[1]Origin: Saab-Scania AB, Sweden

The package is at present designed for a total of 100 derivatives of state variables to be integrated; 20 functions of one independent variable each, with a total maximum of 200 given breakpoints; 100 constants accessible through FORMCO; 20 output variables and 20 plot variables.

Data are shared between different programs in the package and the user supplies subroutine(s) DERIV through a number of labeled COMMONs.

Block Diagram of the FORMIC Package

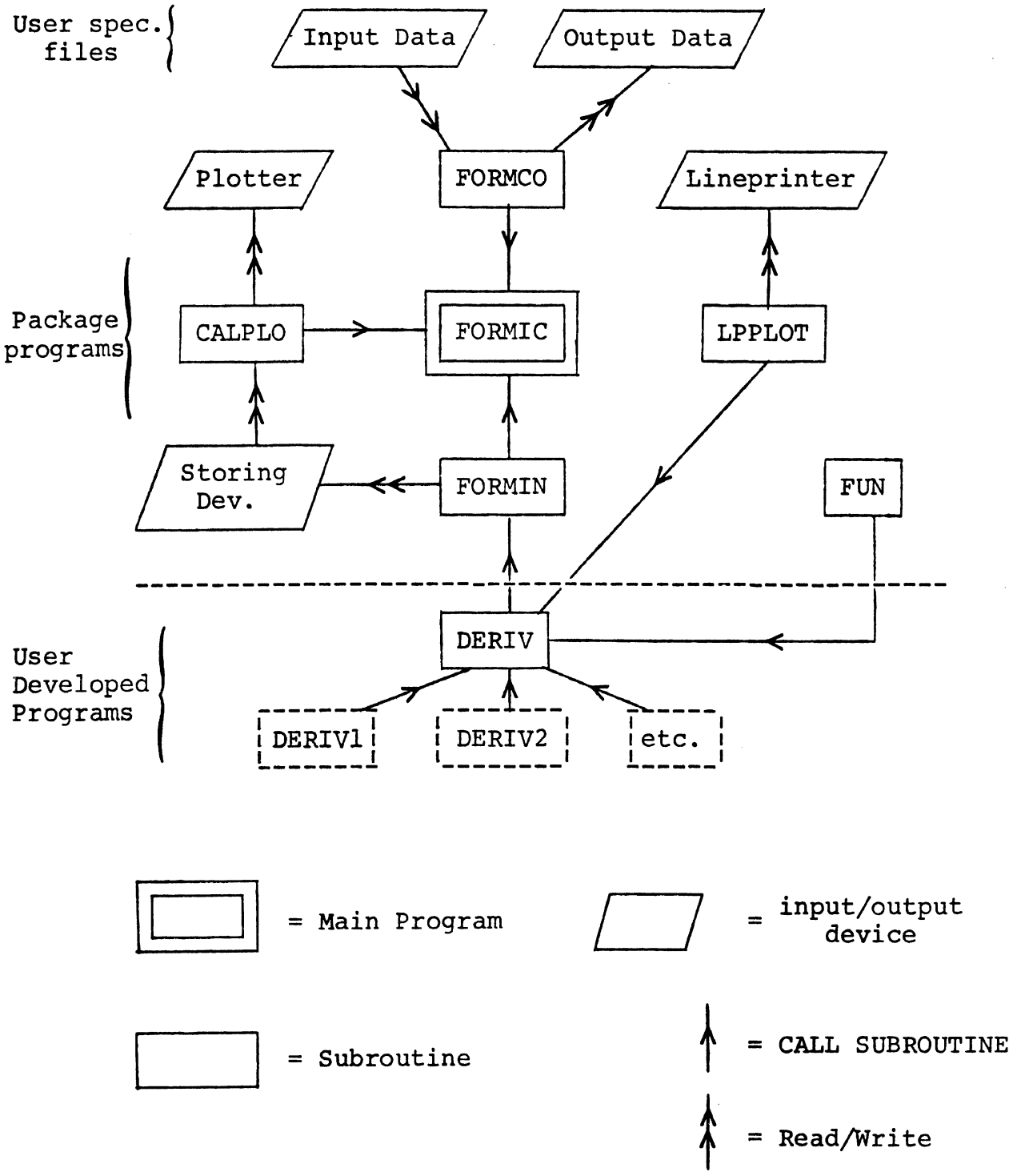

```
      C     PROGRAM HYBTIR,"DERIV" PART OF "FORMIC"
      C     SW 4 UP: ALFD FROM AD4
      C     SW 5 UP: NWW=2000 XSCA=0, FOR X-Y PLOTTING
      C     SW 6 DN: ALFD OR SX VARIABLE
      C     SW 7 DN: ALFD VARIABLE; UP: SX VARIABLE
      C     SW 8 DN: WRITE:NR,DVC,VCE,QPBY,VC,PXVC,TVC
      C     SW 9 DN: WRITE:NR,SX,FXS,ALFD,FYS,MZS,FZ,ALFP,HZ
      C     SW 10 UP: FX OUT  DN: AMP OUT
      C     SW 12 DN: TRANSIENT OPERATION
      C     SW 14 UP: FLEX CARCAS DN: RIDGID CARCAS
0001        SUBROUTINE DERIV(ISW)
0002        REAL MU1,MU2,MU,M,KY,MZ,MZ0,MZX,MZY,MUAS,MUH,MUP0,MUP1,MUPT,KX,
           +MZS,KC,KYS
0003        DIMENSION IPOT(19),IDATP(19),IDACG(4),IDATG(4),IPSCA(2),IDSCA(2)
0004        DIMENSION IDAC1(2),IDAT1(2),IDAC2(3),IDAT2(3),INT(8)
0005        DIMENSION IDAC3(8),IDAT3(8)
0006        DIMENSION B(2),C(2,2),G(20),DG(20),QPBY(20),DV(20),V(20),DVC(20)
           +,PXVC(20),PTVC(20),VC(20),TVC(20),TIM(2),DAY(3),DU(20),U(20)
           +,VCE(20)
0007        COMMON/OVERL/INIT
0008        COMMON/SWITC/IEND,IFIN,ISTEP
0009        COMMON/INTCO/DT,DTMAX,DTMIN,TMAX,EPSI
0010        COMMON/CONST/XSCA,VARI,ALFD,SX,HZ,ALFA,EI,CK,CN,PLIN,FZLB,
           +VMIL,CB,CTVC
      C     CONST IN FILE "HYBTIR.DAT"
0011        COMMON/COUNT/NINT
0012        COMMON/TIME/T
0013        DATA IPOT/3220,3222,3226,3305,3307,3312,3277,3324,3336,3245,3246,
           +3256,3302,3227,3275,3306,3027,3224,3316/,IDAC1/1156,1158/,
           +IPSCA/3304,3257/,
           +IDAC2/1165,1166,1167/,IDAC3/1152,1154,1155,1160,1161,
           +1162,1157,1159/,IDACG/1163,1164,1153,1156/,IADC/3216/,IADCA/3312/
0014        DATA PLK/.990/,VRMIL/70./,XF/1./,BM/.4/,BKY/8.7E6/,BCY/920./,
           +BKX/9.1E6/,BCX/920./,P302/.846/,MUP0/.21/,MUP1/.135/,MUPT/1.11/,
           +MUAS/.7/,MUH/1.4/,VAS/.225/,ANS/20./,BKC/2.08E5/
0015        GO TO(1000,2000,3000,4000,5000),ISW
0016  1000  NINT=0
0017        RETURN
0018  2000  CONTINUE
0019        CALL HYTST(1,3)
0020        CALL INITA(L,0)
0021        CALL LOAD(L)
0022        CALL LRUN(L)
0023        NX=XSCA+.5
0024        NX0=NX
0025        IF(NX-1)2010,2020,2030
0026  2010  NW=2000
0027        GO TO 2040
0028  2020  NW=200
0029        GO TO 2040
0030  2030  NW=20
0031  2040  CALL TSCAL(L,NX)
0032  2100  CONTINUE
0033        NS=ANS+.5
      C INITIALAZATION
```

```
0034            DO 2200 I=1,NS
0035            QPBY(I)=0.
0036            DV(I)=0.
0037            V(I)=0.
0038            DU(I)=0.
0039            U(I)=0.
0040            PTVC(I)=0.
0041            PXVC(I)=0.
0042            VCE(I)=0.
0043            TVC(I)=0.
0044            VC(I)=0.
0045     2200   DVC(I)=0.
0046            MZX=0.
0047            MZY=0.
0048            TP=0.
0049            ALFYIC=0.
0050            DALFM=0.
0051            DALMVR=0.
0052            VRALF=0.
0053            DALFIC=0.
0054            DALFIM=0.
0055            DDAMVR=0.
0056            AMP=0.
0057            YLIC=0.
0058            DYLM=0.
0059            DYLMVR=0.
0060            DYLIC=0.
0061            DDYLM=0.
0062            ISX0=0
0063            NR=0
0064            NE=1
        C COMPUTATION OF SCALEFACTORS
        C       10 LB MAKE 1 VOLT
        C       10 IN LB MAKE 1 VOLT
0065            SFX=FZLB*10.
0066            SFY=FZLB*10.
0067            SMZ=FZLB*PLIN*10.
        C COMPUTATION OF CONSTANTS
0068            PLM=PLIN*.0254
0069            P25000=25000.
0070            VREF=.447*VRMIL
0071            XF2=XF/2.
0072            X00=XF2
0073            XD=XF/NS
0074            DTOR=3.1416/180.
0075            ALFR=ALFD*DTOR
0076            W=VMIL/VRMIL
0077            VX=W*COS(ALFR)
0078            VCX=SX*VX
0079            VR=VX-VCX
0080            RV=1./VR
0081            VCY=W*SIN(ALFR)
0082            EPC=1./NS
0083            EPC10P=EPC*10.*P25000
0084            EPPL=EPC*PLM
0085            EP2=EPC/2.
```

```
                DT=EPC/VR
                CALL SSWTCH(12,J12)
                IF(J12.EQ.1)GO TO 2251
                DO 2250 I=1,NS
                TVC(I)=-W*SIN(ALFR)*CTVC
                PTVC(I)=TVC(I)
     2250       VCE(I)=TVC(I)*DT
     2251       CONTINUE
     C  COMPUTATION OF PARAMETERS
                FZM=FZLB*4.448
                Q0=FZM/PLM
                M=BM*VREF*VREF/FZM
                KY=BKY*PLM/Q0
                KYS=KY/NS
                KX=BKX*PLM/Q0
                CY=BCY*VREF/Q0
                CX=BCX*VREF/Q0
                KC=BKC/Q0
     C          PIVOTING MOTION
                C007=6.2832*PLM/VREF
                OMA2=HZ*C007
                DOMT=OMA2*DT*.5
                DALFA=ALFA*OMA2/57.2958
                DALAVR=DALFA/VR
                DDALFA=-DALFA*OMA2
                DDAAVR=DDALFA/VR
                OMA=3.1416*HZ*PLM/VREF/W
                SOMA=SIN(OMA)
                COMA=COS(OMA)
                SOMA2=SOMA*SOMA
                BET0=ALFA*DTOR
                SOMA1=OMA-SOMA*COMA
                AKL=7.6
                AMPK=.3333*AKL*BET0/OMA
     C          LATERAL MOTION
                YAL=0.
                DYLA=YAL*OMA2
                DYLAVR=DYLA/VR
                DDYLA=-DYLA*OMA2
                DDYAVR=DDYLA/VR
     C
     C  GREEN FUNCTION FOR LATERAL UNIT LOAD
                AK2=2.*CK
                A1=CN/(2.*EI)
                B1=CK/EI
                A1SQ=A1*A1
                C1SQ=B1-A1SQ
                IF(C1SQ.LE.0.)GO TO 2350
                C1=SQRT(C1SQ)
                AA=SQRT(SQRT(B1))
                D1=C1/A1
                TETA=ATAN(D1)/2.
                AR=AA*COS(TETA)
                BR=AA*SIN(TETA)
                AF=AR*PLK
                BF=BR*PLK
```

```
137           ABSQP=AR*AR+BR*BR
      C
138           EXPAF=EXP(AF)
139           EXNAF=EXP(-AF)
140           EPF=EXPAF+EXNAF
141           ENF=EXPAF-EXNAF
      C
142           CF=COS(BF)
143           SF=SIN(BF)
      C
144           CEPF=CF*EPF
145           SENF=SF*ENF
146           CENF=CF*ENF
147           SEPF=SF*EPF
      C
148           C(1,1)=AK2*(BR*SEPF+AR*CENF)/ABSQP
149           C(1,2)=AK2*(AR*SEPF-BR*CENF)/ABSQP
150           C(2,1)=AR*CENF-BR*SEPF
151           C(2,2)=AR*SEPF+BR*CENF
152           GO TO 2360
153     2350  SQBA=SQRT(1.-B1/A1SQ)
154           S1=SQRT(A1*(1.+SQBA))
155           S3=SQRT(A1*(1.-SQBA))
156           S1L=S1*PLK
157           S3L=S3*PLK
158           EX1=EXP(S1L)-EXP(-S1L)
159           EX3=EXP(S3L)-EXP(-S3L)
160           C(1,1)=AK2*EX1/S1
161           C(1,2)=AK2*EX3/S3
162           C(2,1)=S1*EX1

163           C(2,2)=S3*EX3
      C
164     2360  ANE=C(1,1)*C(2,2)-C(2,1)*C(1,2)
165           B(1)=C(2,2)/ANE
166           B(2)=-C(2,1)/ANE
      C       DEFLEXION AND SLOPE COMPUTED AT SECTION EDGE
167           DO 2500 I=1,NS
168           XX=EPPL*(I-1)-PLK+EPPL*.5
169           IF(C1SQ.LE.0.)GO TO 2400
170           AX=AR*XX
171           BX=BR*XX
172           EPX=EXP(AX)
173           ENX=EXP(-AX)
174           EP=EPX+ENX
175           EN=EPX-ENX
176           CEP=COS(BX)*EP
177           CEN=COS(BX)*EN
178           SEN=SIN(BX)*EN
179           SEP=SIN(BX)*EP
180           G(I)=FZM*(B(1)*CEP+B(2)*SEN)/PLM
181           DG(I)=FZM*(B(1)*(AR*CEN-BR*SEP)+B(2)*(AR*SEP+BR*CEN))
182           GO TO 2500
183     2400  E1P=EXP(S1*XX)
184           E1N=EXP(-S1*XX)
185           E3P=EXP(S3*XX)
```

```
                E3N=EXP(-S3*XX)
                G(I)=FZM*(B(1)*(E1P+E1N)+B(2)*(E3P+E3N))/PLM
                DG(I)=FZM*(B(1)*(S1*E1P-S1*E1N)+B(2)*(S3*E3P-S3*E3N))
     2500       CONTINUE
                CALL DATE(DAY)
                CALL TIME(TIM)
                WRITE(5,2900)DAY,TIM
     2900       FORMAT(1X,3A4,1X,2A4/)
                WRITE(5,2)EI,CK,CN,PLIN,FZLB,VMIL,CB,CTVC
     2          FORMAT(' EI=',1PE9.2,' CK=',1PE9.2,' CN=',1PE9.2,' PLIN=',1PE9.2,
                +' FZLB=',1PE9.2,' VMIL=',1PE9.2,' CB=',1PE9.2,' CTVC=',1PE10.3/)
                NSI=NS/20
                IF(NR.EQ.0)WRITE(5,1)(G(IG),IG=1,NS,NSI),(DG(IG),IG=1,NS,NSI)
     1          FORMAT(' G=',2(10(1X,1PE10.3)/),' DG=',2(10(1X,1PE10.3)/))
     3000       CONTINUE
                DVI=0.
                VI=0.
                QPBYI=0.
                IF(INIT.EQ.1)GO TO 3005
           C    CALCULATE AND INITIATE POTS AND DACS
                IDATP(1)=10000./(10.*M)
                IDATP(2)=10000.*CY/10.
                IDATP(3)=10000.*KY/50.
                IDATP(4)=IDATP(1)
                IDATP(5)=IDATP(2)
                IDATP(6)=10000.*KX/50.
                IDATP(7)=10000.*MUP0/10.
                IDATP(8)=10000.*MUP1
                IDATP(9)=10000.*MUPT
                IDATP(10)=10000.*MUAS
                IDATP(11)=10000.*MUH
                IDATP(12)=10000.*VAS
                IDATP(13)=10000.*P302
                IDATP(14)=10000.*1.25
                IDATP(15)=10000.*.2
                IDATP(16)=10000.*.2
                IDATP(17)=10000.*10./NS
                IDATP(18)=10000.*.05
                IDATP(19)=10000.*.05
                CALL STINA(L,IPOT,IDATP,1,1,19)
     3005       SCAX=1.
                IF(VCX.LT..1)SCAX=10.
                SCAY=1.
                IF(VCY.LT..1)SCAY=10.
                IDSCA(1)=10000./SCAX
                IDSCA(2)=10000./SCAY
                CALL STINA(L,IPSCA,IDSCA,1,1,2)
     3006       IDAT2(1)=10000.*VCX*SCAX
                IDAT2(2)=10000.*VCY*SCAY
                IDAT2(3)=10000.*VR
                CALL STARY(IDAC2,IDAT2,3)
                IDAT3(1)=10000.*X00
                DO 3010 I=2,8
     3010       IDAT3(I)=0.
                CALL STARY(IDAC3,IDAT3,8)
                IF(INIT.EQ.0)PAUSE 1
```

```
240           INIT=0
241     4000  CONTINUE
        C     COMPUTATION OF SECTION DATA
242           TVCS=TVC(NE)
243           NEP=NE+1
244           IF(NEP.GT.NS)NEP=NE
245           TVCSM=.5*(TVC(NE)+TVC(NEP))
246     4020  CALL SSWTCH(14,J14)
247           IF(J14.EQ.1)GO TO 4021
248           TVCS=0.
249           TVCSM=0.
250     4021  CONTINUE
251           IDAT3(1)=X00*10000.
252           XVCSM=-TVCSM*RV
253           IF(NR.NE.0)VI=VI+XVCSM*EPC10P
254           IDAT3(2)=VI
255           IF(NE.EQ.1)IDAT3(2)=0.
256           IDAT3(3)=DVI
257           TPVB=DDALVR*X00-DALFIM-DDYLM
258           IDAT3(4)=-TPVB*5000.
259           TVBIC=TVCS+VRALF-DALFIC*X00+DYLIC
260           IDAT3(5)=-TVBIC*50000.
261           IF(NE.EQ.1)IDAT3(3)=-IDAT3(5)
262           PVY=ALFYIC-DALMVR*X00+DYLMVR
263           IDAT3(6)=-(XVCSM-PVY)*P25000
264           IDAT3(7)=UI
265           IF(NE.EQ.1)IDAT3(7)=0.
266           IDAT3(8)=DUI
267           IF(NE.EQ.1)IDAT3(8)=0.
268           CALL STARY(IDAC3,IDAT3,8)
        C     RUN ANALOGUE
        C IC
269           CALL SETWD(0,2)
270           NWW=NW
271           CALL SSWTCH(5,J5)
272           IF(J5.EQ.2.AND.NX0.NE.0)GO TO 4090
273           NX0=NX
274           IF(J5.EQ.1)NX0=0
275           NWW=2000
276           IF(NE.EQ.1)NWW=20000
277           CALL TSCAL(L,NX0)
278     4090  CALL WAIT(NWW)
        C OPERATE
279           CALL SETWD(0,1)
280     5000  CONTINUE
281           CALL SSWTCH(0,J0)
282           IF(J0.EQ.2)GO TO 5001
283           INIT=1
284           RETURN
285     5001  IF(INIT.EQ.1)GO TO 2000
286           CALL SENSW(0,L)
287     5005  IF(ITEST(L,0,2).EQ.1)GO TO 5010
288           GO TO 5005
        C HOLD
        C     COMPUTATION OF PATCH DATA
289     5010  CALL SETWD(0,0)
```

```
0290            CALL RDSEQ(IADC,INT,8)
0291            DVI=INT(1)
0292            VI=INT(2)*PVY*EPC10P
0293            MZY=MZY+INT(4)
0294            QPBYI=INT(3)/50000.
0295            FZ0=FZ0+INT(5)
0296            DUI=INT(6)
0297            UI=INT(7)
0298            QPBXI=INT(8)
0299            FX0=FX0+QPBXI
0300            MZX=MZX-QPBXI*VC(NE)
0301            QPBY(NE)=QPBYI
0302            T=0.
0303            NE=NE+1
0304     5050   IF(NE-NS)5061,5061,5062
0305     5061   GO TO 5070
0306     5062   GO TO 5100
0307     5070   X00=XF2-EPC*(NE-1)
0308            DUM1=DV(NE)
0309            DUM2=V(NE)
0310            DV(NE)=DVI
0311            V(NE)=VI
0312            DVI=DUM1
0313            VI=DUM2
0314            DUM3=DU(NE)
0315            DUM4=U(NE)
0316            DU(NE)=DUI
0317            U(NE)=UI
0318            DUI=DUM3
0319            UI=DUM4
0320     5091   GO TO 5105
               C
0321     5100   X00=XF2
0322            CALL SSWTCH(12,J12)
0323            IF(J12.EQ.1)GO TO 5210
               C TRANSIENT OPERATION
               C      INCREMENT YAWING MOTION
0324            TP=TP+DT
0325            OMT=OMA2*TP
0326            SOMT=SIN(OMT)
0327            COMT=COS(OMT)
0328            SOMTM=SOMT+DOMT*COMT
0329            COMTM=COMT-DOMT*SOMT
0330            IF(ALFA.EQ.0.)GO TO 5205
0331            ALFYD=ALFA*SOMT
0332            IDATG(1)=(ALFD+ALFYD*4.)*500.
0333            ALFYIC=ALFYD*DTOR
0334            DALFM=DALFA*COMTM
0335            DALMVR=DALAVR*COMTM
0336            VRALF=VR*ALFYIC
0337            DALFIC=DALFA*COMT
0338            DALFIM=DALFIC+DALFM
0339            DDAMVR=DDAAVR*SOMTM
0340            AMP=AMPK*(SOMA1*SOMT+SOMA2*COMT)
0341     5205   IF(YAL.EQ.0.)GO TO 5102
               C      INCREMENT LATERAL MOTION
```

```
342           YLIC=YAL*SOMT
343           DYLM=DYLA*COMTM
344           DYLMVR=DYLAVR*COMTM
345           DYLIC=DYLA*COMT
346           DDYLM=DDYAVR*SOMTM
347           GO TO 5102
348      5210 TP=0.
349           ALFYIC=0.
350           DALFM=0.
351           DALMVR=0.
352           VRALF=0.
353           DALFIC=0.
354           DALFIM=0.
355           DDAMVR=0.
356           AMP=0.
357           YLIC=0.
358           DYLM=0.
359           DYLMVR=0.
360           DYLIC=0.
361           DDYLM=0.
362      5102 DVI=DV(1)
363           VI=V(1)
364           DUI=DU(1)
365           UI=U(1)
366           CALL SSWTCH(6,J6)
367           CALL SSWTCH(7,J7)
368           IF(J6.EQ.1)GO TO 5103
369           IF(J7.EQ.2)ALFD=VARI+ALFD
370           IF(J7.EQ.1)SX=VARI*.1+SX
371           GO TO 5104
372      5103 CONTINUE
373           CALL SSWTCH(4,J4)
374           IF(J4.NE.1)GO TO 5104
375           CALL RDSIN(IADCA,IALF)
376           ALFD=IALF*.01
377      5104 ALFR=ALFD*DTOR
378           IF(J7.EQ.1)VARG=SX*10000.
379           IF(J7.EQ.2)VARG=ALFD*500.
380           IF(J12.EQ.1)IDATG(1)=VARG
381           VX=W*COS(ALFR)
382           VCX=SX*VX
383           VR=VX-VCX
384           VCY=W*SIN(ALFR)
385           DT=EPC/VR
386           MZ=(MZX+MZY*.05)*.0002
387           FZ=FZ0*VR*.0002
388           FZ0=0.
389           FX=FX0*.0002
390           FX0=0.
391      5105 IF(NE.LE.NS)GO TO 4000
392           IF(VCX.LT..1.AND.SCAX.GT.2.)GO TO 5107
393           IF(VCX.GE..1.AND.SCAX.LT.9.)GO TO 5107
394           SCAX=1.
395           IF(VCX.LT..1)SCAX=10.
396           IDSCA(1)=10000./SCAX
397           CALL STIND(L,IPSCA(1),IDSCA(1))
```

```
0398     5107  IF(VCY.LT..1.AND.SCAY.GT.2.)GO TO 5108
0399           IF(VCY.GE..1.AND.SCAY.LT.9.)GO TO 5108
0400           SCAY=1.
0401           IF(VCY.LT..1)SCAY=10.
0402           IDSCA(2)=10000./SCAY
0403           CALL STIND(L,IPSCA(2),IDSCA(2))
0404     5108  IDAT2(1)=10000.*VCX*SCAX
0405           IDAT2(2)=10000.*VCY*SCAY
0406           IDAT2(3)=10000.*VR
0407           CALL STARY(IDAC2,IDAT2,3)
0408     5110  NE=1
0409           NR=NR+1
0410           FY=0.
0411           MZX=0.
0412           MZY=0.
0413           DO 5120 I=1,NS
0414     5120  FY=FY+QPBY(I)
0415           CBDT=CB/DT
0416           DO 5140 I=1,NS
0417           VCN=0.
0418           PXVCN=0.
0419           DO 5130 J=1,NS
0420           XX=I-J
0421           IX=1+ABS(I-J)+1
0422           VCN=VCN+G(IX)*QPBY(J)
0423           PXVCN=PXVCN+SIGN(DG(IX),XX)*QPBY(J)
0424     5130  CONTINUE
0425           DVC(I)=VCN-VCE(I)
0426           VC(I)=VCN
0427           PTVC(I)=PTVC(I)+CBDT*DVC(I)
0428           VCE(I)=VCN+PTVC(I)*DT
0429           F1=PTVC(I)
0430           IF(J12.EQ.1)F1=0.
0431           PXVC(I)=PXVCN
0432           TVC(I)=F1-VR*PXVCN
0433     5140  CONTINUE
0434           FYS=-FY*SFY
0435           VG2=FYS
0436           IDATG(2)=VG2
0437           CALL SSWTCH(10,J10)
0438           FXS=-FX*SFX
0439           VG3=AMP*SMZ
0440           IF(J10.EQ.1)VG3=FXS
0441           IDATG(3)=VG3
0442           MZS=(MZ+FX*FY/KC)*SMZ
0443           IDATG(4)=MZS
0444           CALL STARY(IDACG,IDATG,4)
0445           CALL SSWTCH(8,J8)
0446           CALL SSWTCH(9,J9)
0447           IF(J9.EQ.1)GO TO 5997
0448           FXS=FXS*.1
0449           FYS=FYS*.1
0450           MZS=MZS*.1
0451           WRITE(5,5998)NR,SX,FXS,ALFD,FYS,MZS,FZ,ALFP,HZ
0452     5998  FORMAT(' NR=',I3,' SX=',1PE10.3,' FXS=',1PE10.3,' ALF=',1PE10.3,
              +' FYS=',1PE10.3,' MZS=',1PE10.3,' FZ=',1PE10.3,' ALFP=',1PE10.3,
```

```
     +' HZ=',1PE10.3/)
5997  IF(J8.EQ.1)GO TO 6000
      WRITE(5,777)NR,(DVC(IG),IG=1,NS,NSI),(VCE(IG),IG=1,NS,NSI)
777   FORMAT(' NR=',I3,' DVC=',2(10(1X,1PE10.3)/)/' VCE=',2(10(1X,1PE10.
     +3)/))
      WRITE(5,5999)(QPBY(IG),IG=1,NS,NSI),(VC(IG),IG=1,NS,NSI),(PXVC(IG)
     +,IG=1,NS,NSI),(TVC(IG),IG=1,NS,NSI)
5999  FORMAT(' QPBY=',2(10(1X,1PE10.3)/)/' VC=',2(10(1X,
     +1PE10.3)/)/' PXVC=',2(10(1X,1PE10.3)/)/' TVC=',2(10(1X,1PE10.3)/))
6000  GO TO 4000
      END

ROUTINES CALLED:
HYTST , INITA , LOAD  , LRUN  , TSCAL , COS   , SIN
SSWTCH, SQRT  , ATAN  , EXP   , DATE  , TIME  , STINA
STARY , SETWD , WAIT  , SENSW , ITEST , RDSEQ , RDSIN
STIND , IABS  , SIGN

OPTIONS =/ON,/OP:3

BLOCK       LENGTH
DERIV   5437   (025172)*
OVERL   1      (000002)
SWITC   3      (000006)
INTCO   10     (000024)
CONST   28     (000070)
COUNT   1      (000002)
TIME    2      (000004)

**COMPILER ----- CORE**
   PHASE       USED  FREE
DECLARATIVES 01576 13248
EXECUTABLES  03503 11321
ASSEMBLY     03573 15891
```

```
      C     PROGRAM DIGTIR "DERIV" PART OF "FORMIC"
      C     SW 5 UP;DAC-TANSFERE TO CHART RECORDER
      C     SW 6 DN; ALFD OR SX VARIABLE
      C     SW 7 DN; ALFD VARIABLE; UP; SX VARIABLE
      C     SW 8 DN; WRITE;NR,DVC,VCE,QPBY,VC,PXVC,TVC
      C     SW 9 DN; WRITE;NR,SX,FXS,ALFD,FYS,MZS,FZ,ALFP,HZ
      C     SW 12 DN; TRANSIENT OPERATION
      C     SW 14 UP; FLEX CARCAS DN; RIDGID CARCAS
0001        SUBROUTINE DERIV(ISW)
0002        LOGICAL VS0
0003        REAL MU1,MU2,MU,M,KY,MZ,MZYI,MZX,MZY,MUAS,MUH,MUP0,MUP1,MUPT,KX,
           +MZS,KC,KYS
0004        DIMENSION B(2),C(2,2),G(20),DG(20),QPBY(20),DV(20),V(20),DVC(20)
           +,PXVC(20),PTVC(20),VC(20),TVC(20),TIM(2),DAY(3),DU(20),U(20)
           +,VCE(60)
0005        DIMENSION IDAC(7),IDAT(7)
0006        COMMON/SWITC/IEND,IFIN,ISTEP
0007        COMMON/INTCO/DT,DTMAX,DTMIN,TMAX,EPSI
0008        COMMON/CONST/DVS,VARI,ALFD,SX,HZ,ALFA,EI,CK,CN,PLIN,FZLB,
           +VMIL,CB,CTVC
      C     CONST IN FILE "DIGTIR.DAT"
0009        COMMON/COUNT/NINT
0010        COMMON/TIME/T
0011        COMMON/INTS/DVI,VI,QPBYI,MZYI,DUI,UI,QPBXI
0012        COMMON/DERS/DDVI,DVP,QPYI,DMZYI,DDUI,DUP,QPXI
0013        DATA PLK/.990/,VRMIL/70./,XF/1./,BM/.4/,BKY/8.7E6/,BCY/920./,
           +BKX/9.1E6/,BCX/920./,P302/.846/,MUP0/.021/,MUP1/.135/,MUPT/1.11/,
           +MUAS/.7/,MUH/1.4/,VAS/.225/,ANS/20./,BKC/2.08E5/
0014        DATA IDAC/1153,1155,1157,1159,1161,1163,1165/
0015        GO TO(1000,2000,3000,4000,5000),ISW
0016  1000  NINT=7
0017        IF(SX.EQ.0.)NINT=4
0018        RETURN
      C CONSTANTS
0019  2000  CONTINUE
0020        CALL SSWTCH(5,J5)
0021        IF(J5.EQ.2)GO TO 2100
0022        CALL HYTST(1,3)
0023        CALL INITA(L,0)
0024  2100  CONTINUE
0025        NS=ANS+.5
0026        DO 2200 I=1,NS
0027        QPBY(I)=0.
0028        DV(I)=0.
0029        V(I)=0.
0030        DU(I)=0.
0031        U(I)=0.
0032        PXVC(I)=0.
0033        PTVC(I)=0.
0034        VC(I)=0.
0035        DVC(I)=0.
0036        VCE(I)=0.
0037  2200  TVC(I)=0.
0038        NINT=7
0039        IF(SX.EQ.0.)NINT=4
```

```
0040            MZX=0.
0041            MZY=0.
0042            T=0.
0043            TP=0.
0044            ALFYIC=0.
0045            DALFM=0.
0046            DALMVR=0.
0047            VRALF=0.
0048            DALFIC=0.
0049            DALFIM=0.
0050            DDAMVR=0.
0051            AMP=0.
0052            YLIC=0.
0053            DYLM=0.
0054            DYLMVR=0.
0055            DYLIC=0.
0056            DDYLM=0.
0057            NR=0
0058            NE=1
          C COMPUTATION OF CONSTANTS
0059            PLM=PLIN*.0254
0060            VREF=.447*VRMIL
0061            CMUP0=10.*MUP0
0062            CMUP1=10.*SQRT(10.)*MUP1
0063            XF2=XF/2.
0064            X00=XF2
0065            XD=XF/NS
0066            DTOR=3.1416/180.
0067            ALFR=ALFD*DTOR
0068            W=VMIL/VRMIL
0069            SXV=SX
0070            VX=W*COS(ALFR)
0071            VCX=SXV*VX
0072            VR=VX-VCX
0073            RV=1./VR
0074            VCY=W*SIN(ALFR)
0075            EPC=1./NS
0076            EPPL=EPC*PLM
0077            EP2=EPC/2.
0078            DT=EPC/VR
0079            CALL SSWTCH(12,J12)
0080            IF(J12.EQ.1)GO TO 2251
0081            DO 2250 I=1,NS
0082            TVC(I)=-W*SIN(ALFR)*CTVC
0083            PTVC(I)=TVC(I)
0084       2250 VCE(I)=TVC(I)*DT
0085       2251 CONTINUE
          C COMPUTATION OF PARAMETERS
0086            FZM=FZLB*4.448
0087            Q0=FZM/PLM
0088            M=BM*VREF*VREF/FZM
0089            AM=1./M
0090            KY=BKY*PLM/Q0
0091            KYS=KY/NS
0092            KX=BKX*PLM/Q0
0093            CY=BCY*VREF/Q0
```

```
0094            CX=BCX*VREF/Q0
0095            KC=BKC/Q0
                C       PIVOTING MOTION
0096            C007=6.2832*PLM/VREF
0097            OMA2=HZ*C007
0098            DOMT=OMA2*DT*.5
0099            DALFA=ALFA*OMA2/57.2958
0100            DALAVR=DALFA/VR
0101            DDALFA=-DALFA*OMA2
0102            DDAAVR=DDALFA/VR
0103            OMA=3.1416*HZ*PLM/VREF/W
0104            SOMA=SIN(OMA)
0105            COMA=COS(OMA)
0106            SOMA2=SOMA*SOMA
0107            BET0=ALFA*DTOR
0108            SOMA1=OMA-SOMA*COMA
0109            AKL=7.6
0110            AMPK=.3333*AKL*BET0/OMA
                C       LATERAL MOTION
0111            YAL=0.
0112            DYLA=YAL*OMA2
0113            DYLAVR=DYLA/VR
0114            DDYLA=-DYLA*OMA2
0115            DDYAVR=DDYLA/VR
                C GREEN FUNCTION FOR LATERAL UNIT LOAD
0116            AK2=2.*CK
0117            A1=CN/(2.*EI)
0118            B1=CK/EI
0119            A1SQ=A1*A1
0120            C1SQ=B1+A1SQ
0121            C1=SQRT(C1SQ)
0122            AA=SQRT(SQRT(B1))
0123            D1=C1/A1
0124            TETA=ATAN(D1)/2.
0125            AR=AA*COS(TETA)
0126            BR=AA*SIN(TETA)
0127            AF=AR*PLK
0128            BF=BR*PLK
0129            ABSQP=AR*AR+BR*BR
                C
0130            EXPAF=EXP(AF)
0131            EXNAF=EXP(-AF)
0132            EPF=EXPAF+EXNAF
0133            ENF=EXPAF-EXNAF
                C
0134            CF=COS(BF)
0135            SF=SIN(BF)
                C
0136            CEPF=CF*EPF
0137            SENF=SF*ENF
0138            CENF=CF*ENF
0139            SEPF=SF*EPF
                C
0140            C(1,1)=AK2*(BR*SEPF+AR*CENF)/ABSQP
0141            C(1,2)=AK2*(AR*SEPF-BR*CENF)/ABSQP
0142            C(2,1)=AR*CENF-BR*SEPF
```

```
5            C(2,2)=AR*SEPF+BR*CENF
     C
4            ANE=C(1,1)*C(2,2)-C(2,1)*C(1,2)
5            B(1)=C(2,2)/ANE
6            B(2)=-C(2,1)/ANE
7            DO 2500 J=1,2
8            XJ=EPPL*.5
9            IF(J.EQ.2)XJ=0.
0            DO 2500 I=1,NS
1            XX=EPPL*(I-1)-PLK+XJ
2            AX=AR*XX
3            BX=BR*XX
4            EPX=EXP(AX)
5            ENX=EXP(-AX)
6            EP=EPX+ENX
7            EN=EPX-ENX
8            CEP=COS(BX)*EP
9            CEN=COS(BX)*EN
0            SEN=SIN(BX)*EN
1            SEP=SIN(BX)*EP
2            IF(J.EQ.1)G(I)=FZM*(B(1)*CEP+B(2)*SEN)/PLM
3            IF(J.EQ.2)DG(I)=FZM*(B(1)*(AR*CEN-BR*SEP)+B(2)*(AR*SEP+BR*CEN))
4    2500    CONTINUE
5            CALL DATE(DAY)
6            CALL TIME(TIM)
7            WRITE(5,2900)DAY,TIM
8    2900    FORMAT(1X,3A4,1X,2A4/)
9            WRITE(5,2)EI,CK,CN,PLIN,FZLB,VMIL,CB,CTVC
0    2       FORMAT(' EI=',1PE9.2,' CK=',1PE9.2,' CN=',1PE9.2,' PLIN=',1PE9.2,
          +' FZLB=',1PE9.2,' VMIL=',1PE9.2,' CB=',1PE9.2,' CTVC=',1PE10.3/)
1            NSI=NS/20
2            IF(NR.EQ.0)WRITE(5,1)(G(IG),IG=1,NS,NSI),(DG(IG),IG=1,NS,NSI)
3    1       FORMAT(' G=',2(10(1X,1PE10.3)/),' DG=',2(10(1X,1PE10.3)/))
4    3000    CONTINUE
5            DVI=0.
6            VI=0.
7            QPBYI=0.
8            MZYI=0.
9            DUI=0.
0            UI=0.
1            QPBXI=0.
2    4000    CONTINUE
3            DUP=DUI
4            DVP=DVI
     C POSITION IN SECTION
5            X=-VR*T
     C PRESSURE DISTRIBUTION 4, ORD, PARABOLA
6            X0=X00+X
7            QZ=20.*(.0625-X0*X0*X0*X0)
     C SLIDING VELOCITIES
8            VSX=VCX+DUI
9            VSXSQ=VSX*VSX
0            VSY=VCY+DVI
1            VS=SQRT(VSXSQ+VSY*VSY)
2            VS0=.FALSE.
3            IF(VS.GT.-DVS.AND.VS.LT.DVS)VS0=.TRUE.
```

```
0194            IF(VS0)GO TO 4010
0195            FMUP=CMUP1*SQRT(VS)+CMUP0
0196            FMUH=(MUH-MUAS)*VAS/(VS+VAS)+MUAS
0197            FMU=AMIN1(FMUP,FMUH,MUPT)
0198            QI=-QZ*FMU
0199            QZVS=QI/VS
0200            QXI=QZVS*VSX
0201            QYI=QZVS*VSY
0202            IF(T.NE.0.)GO TO 4022
0203    4010    TVCS=TVC(NE)
0204            NEP=NE+1
0205            IF(NEP.GT.NS)NEP=NE
0206            TVCSM=.5*(TVC(NE)+TVC(NEP))
0207    4020    CALL SSWTCH(14,J14)
0208            IF(J14.EQ.1)GO TO 4021
0209            TVCS=0.
0210            TVCSM=0.
0211    4021    CONTINUE
0212            XVCSM=-TVCSM*RV
0213            PVY=ALFYIC-DALMVR*X00+DYLMVR
0214            V1=XVCSM-PVY
0215            DV1=TVCS+VRALF-DALFIC*X00+DYLIC
0216            DV2=DDALVR*X00-DALFIM-DDYLM
0217            IF(NR.NE.0)VI=VI+XVCSM*EPC
0218            IF(NE.EQ.1)VI=0.
0219    4022    CONTINUE
        C DERIVATIVES
0220            V1=V1*X
0221            DV2=DV2*X
0222            QPYI=CY*(DVI-DV1-DV2)+KY*(VI-V1)
0223            QPXI=CX*DUI+KX*UI
0224            DMZYI=X0*QPYI
0225            IF(VS0)GO TO 4040
0226            DDUI=(QXI-QPXI)/M
0227            DDVI=(QYI-QPYI)/M
0228            GO TO 4050
0229    4040    QI0=-QZ*CMUP0
0230            IF(SX.EQ.0.)GO TO 4045
0231            DQXP=-QI0-QPXI
0232            DQXN=QI0-QPXI
0233            DDUI=0.
0234            IF(DQXN.GT.0.)DDUI=DQXN*AM
0235            IF(DQXP.LT.0.)DDUI=DQXP*AM
0236    4045    DQYP=-QI0-QPYI
0237            DQYN=QI0-QPYI
0238            DDVI=0.
0239            IF(DQYN.GT.0.)DDVI=DQYN*AM
0240            IF(DQYP.LT.0.)DDVI=DQYP*AM
0241    4050    CONTINUE
0242            CALL SSWTCH(5,J5)
0243            IF(J5.EQ.2)GO TO 4999
0244            IF(ISTEP.NE.0)GO TO 4999
0245            IDAT(1)=T*10000.
0246            IDAT(2)=VS*10000.
0247            IDAT(3)=VSX*10000.
0248            IDAT(4)=VSY*10000.
```

```
49          IDAT(5)=UI*100000.
50          IDAT(6)=(VI-V1)*100000.
51          IDAT(7)=X0*10000.
52          CALL STARY(IDAC,IDAT,7)
53          IF(NE.EQ.1.AND.T.EQ.0.)CALL WAIT(10000)
54    4999  RETURN
55    5000  CONTINUE
56          CALL SSWTCH(0,J0)
57          IF(J0.EQ.2)GO TO 5001
58          RETURN
59    5001  IF(T.EQ.0.)RETURN
60          VI=VI-PVY*EPC
61          MZY=MZY+MZYI
62          MZYI=0.
63          FX0=FX0+QPBXI
64          MZX=MZX-QPBXI*VC(NE)
65          QPBXI=0.
66          QPBY(NE)=VR*QPBYI
67          QPBYI=0.
68          T=0.
69          NE=NE+1
70    5050  IF(NE.GT.NS)GO TO 5100
71          X00=XF2-EPC*(NE-1)
72          DUM1=DV(NE)
73          DUM2=V(NE)
74          DV(NE)=DVI
75          V(NE)=VI
76          DVI=DUM1
77          VI=DUM2
78          DUM3=DU(NE)
79          DUM4=U(NE)
80          DU(NE)=DUI
81          U(NE)=UI
82          DUI=DUM3
83          UI=DUM4
84          RETURN
    C
85    5100  X00=XF2
86          CALL SSWTCH(12,J12)
87          IF(J12.EQ.1)GO TO 5210
    C       TRANSIENT OPERATION
    C       ICREMENT YAWING
88          TP=TP+DT
89          OMT=OMA2*TP
90          SOMT=SIN(OMT)
91          COMT=COS(OMT)
92          SOMTM=SOMT+DOMT*COMT
93          COMTM=COMT-DOMT*SOMT
94          IF(ALFA.EQ.0.)GO TO 5205
95          ALFYD=ALFA*SOMT
96          ALFYIC=ALFYD*DTOR
97          DALFM=DALFA*COMTM
98          DALMVR=DALAVR*COMTM
99          VRALF=VR*ALFYIC
00          DALFIC=DALFA*COMT
01          DALFIM=DALFIC+DALFM
```

```
0302            DDAMVR=DDAAVR*SOMTM
0303            AMP=AMPK*(SOMA1*SOMT+SOMA2*COMT)
0304     5205   IF(YAL.EQ.0.)GO TO 5102
                C      INCREMENT LATERAL MOTION
0305            YLIC=YAL*SOMT
0306            DYLM=DYLA*COMTM
0307            DYLMVR=DYLAVR*COMTM
0308            DYLIC=DYLA*COMT
0309            DDYLM=DDYAVR*SOMTM
0310            GO TO 5102
0311     5210   TP=0.
0312            ALFYIC=0.
0313            DALFM=0.
0314            DALMVR=0.
0315            VRALF=0.
0316            DALFIC=0.
0317            DALFIM=0.
0318            DDAMVR=0.
0319            AMP=0.
0320            YLIC=0.
0321            DYLM=0.
0322            DYLMVR=0.
0323            DYLIC=0.
0324            DDYLM=0.
0325     5102   DVI=DV(1)
0326            VI=V(1)
0327            DUI=DU(1)
0328            UI=U(1)
0329            CALL SSWTCH(6,J6)
0330            CALL SSWTCH(7,J7)
0331            IF(J6.EQ.1)GO TO 5103
0332            VAR=VAR+VARI
0333            IF(J7.EQ.2)ALFDV=VAR+ALFD
0334            IF(J7.EQ.1)SXV=VAR/100.
0335            GO TO 5106
0336     5103   VAR=0.
0337     5104   ALFDV=ALFD
0338            SXV=SX
0339     5106   ALFR=ALFDV*DTOR
0340            VX=W*COS(ALFR)
0341            VCX=SXV*VX
0342            VR=VX-VCX
0343            RV=1./VR
0344            VCY=W*SIN(ALFR)
0345            DT=EPC*RV
0346     5110   NE=1
0347            NR=NR+1
0348            MZ=(MZX+MZY)*VR
0349            FX=FX0*VR
0350            FX0=0.
0351            FY=0.
0352            MZX=0.
0353            MZY=0.
0354            DO 5120 I=1,NS
0355     5120   FY=FY+QPBY(I)
0356            CBDT=CB/DT
```

```
      DO 5140 I=1,NS
      VCN=0.
      PXVCN=0.
      DO 5130 J=1,NS
      XX=I-J
      IX=IABS(I-J)+1
      VCN=VCN+G(IX)*QPBY(J)
 5130 PXVCN=PXVCN+SIGN(DG(IX),XX)*QPBY(J)
      DVC(I)=VCN-VCE(I)
      VC(I)=VCN
      PTVC(I)=PTVC(I)+CBDT*DVC(I)
      VCE(I)=VCN+PTVC(I)*DT
      F1=PTVC(I)
      IF(J12.EQ.1)F1=0.
      PXVC(I)=PXVCN
      TVC(I)=F1-VR*PXVCN
5140  CONTINUE
5150  CONTINUE
      FX=FX*FZLB
      FY=FY*FZLB
      MZ=MZ*FZLB*PLIN
      CALL SSWTCH(8,J8)
      CALL SSWTCH(9,J9)
      IF(J9.EQ.1)GO TO 5997
      WRITE(5,5998)NR,SX,FXS,ALFD,FYS,MZS,FZ,ALFP,HZ
5998  FORMAT(' NR=',I3,' SX=',1PE10.3,' FXS=',1PE10.3,' ALF=',1PE10.3,
     +' FYS=',1PE10.3,' MZS=',1PE10.3,' FZ=',1PE10.3,' ALFP=',1PE10.3,
     +' HZ=',1PE10.3/)
5997  IF(J8.EQ.1)GO TO 6000
      WRITE(5,777)NR,(DVC(IG),IG=1,NS,NSI),(VCE(IG),IG=1,NS,NSI)
777   FORMAT(' NR=',I3,' DVC=',2(10(1X,1PE10.3)/)/' VCE=',2(10(1X,1PE10.
     +3)/))
      WRITE(5,5999)(QPBY(IG),IG=1,NS,NSI),(VC(IG),IG=1,NS,NSI),(PXVC(IG)
     +,IG=1,NS,NSI),(TVC(IG),IG=1,NS,NSI)
5999  FORMAT(' QPBY=',2(10(1X,1PE10.3)/)/' VC=',2(10(1X,
     +1PE10.3)/)/' PTVC=',2(10(1X,1PE10.3)/)/' DVC=',2(10(1X,1PE10.3)/))
6000  RETURN
      END

ROUTINES CALLED:
SSWTCH, HYTST , INITA , SQRT  , COS   , SIN   , ATAN
EXP   , DATE  , TIME  , AMIN1 , STARY , WAIT  , IABS
SIGN

OPTIONS =/ON,/OP:3

BLOCK       LENGTH
DERIV   4528    (021540)*
SWITC   3       (000006)
INTCO   10      (000024)
CONST   28      (000070)
COUNT   1       (000002)
TIME    2       (000004)
INTS    14      (000034)
DERS    14      (000034)
```

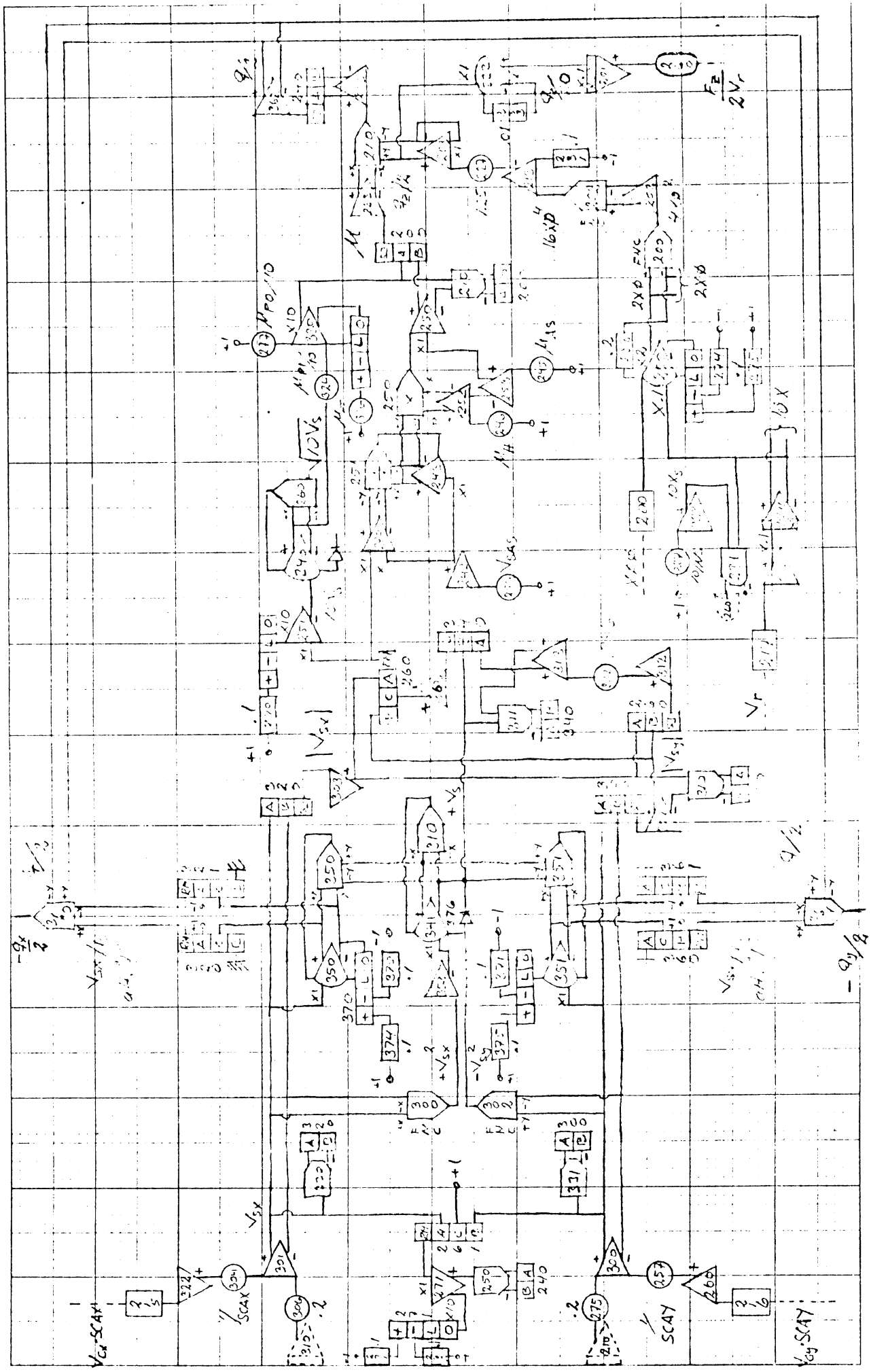

Patching Diagram 1. Computed Functions: Vertical Pressure Intensity q_z; Sliding Velocities V_{sx}, V_{sy}, V_{si}; Friction Coefficient μ; Friction Forces q_x, q_y.

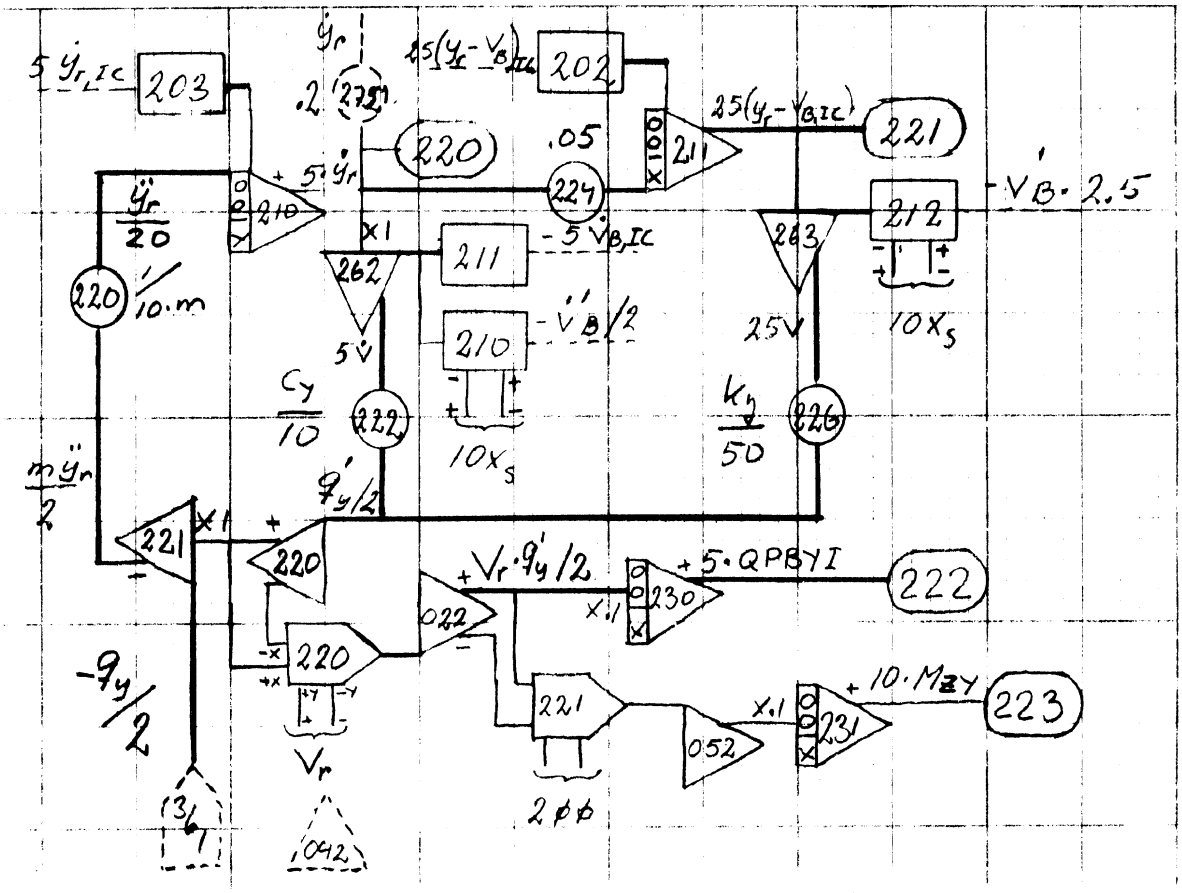

Patching Diagram 2. Lateral Element Dynamics.

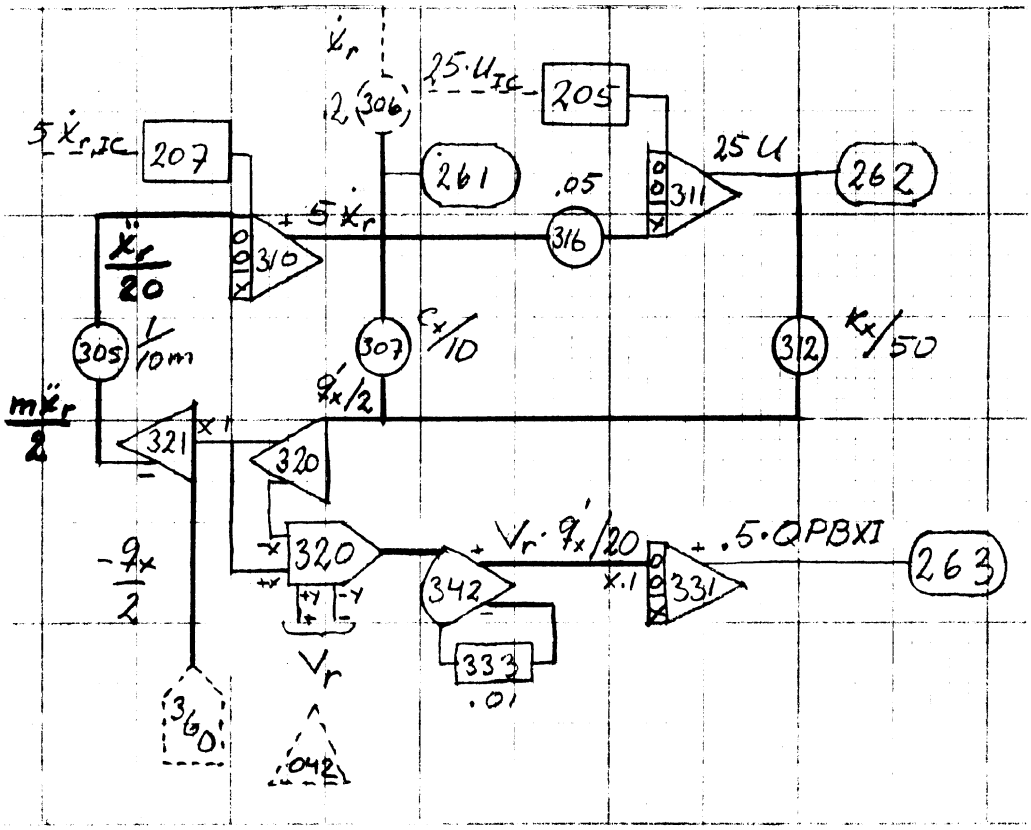

Patching Diagram 3. Longitudinal Element Dynamics.

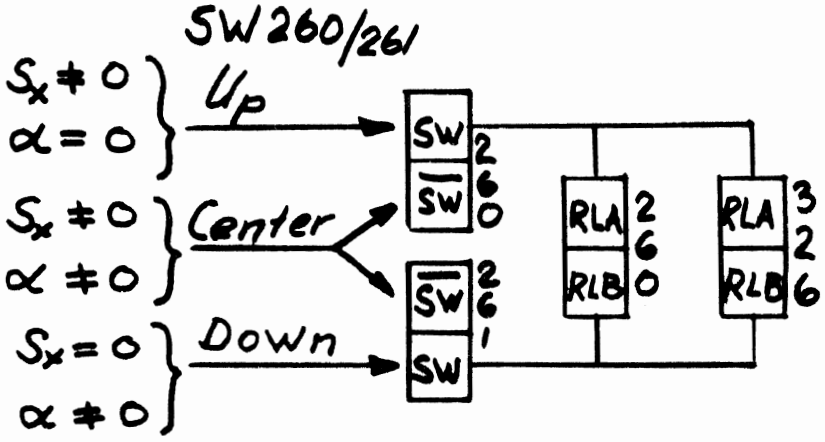

Alternative patchings through the use of Switch 260/261 are used to enhance the accuracy when $\alpha = 0$ or $S_x = 0$.

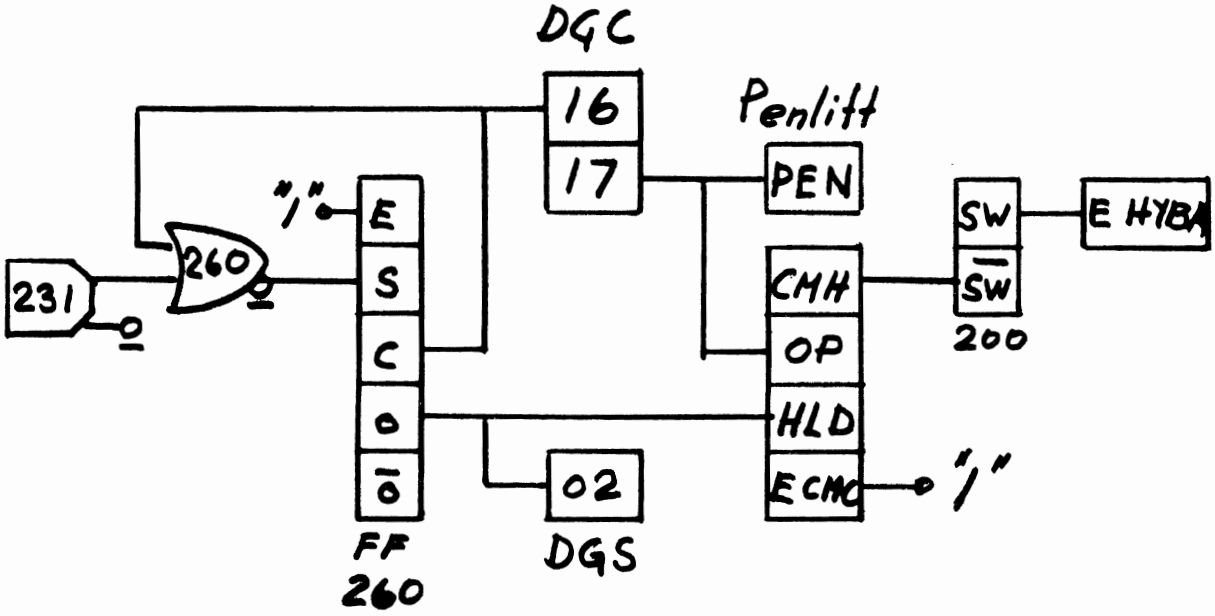

Patching for communication analog <–> digital.
Switch 200 gives manual run interrupts.

Patching Diagram 4. Logic Patchings.